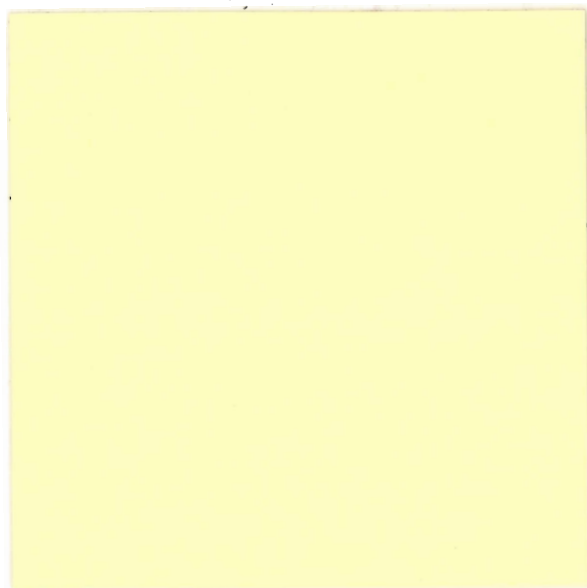


REGIONAL GEOLOGY, GEOCHRONOLOGY AND METALLOGENY  
OF THE COASTAL CORDILLERA OF CHILE  
BETWEEN 25°30' and 26° SOUTH

by

CARLOS E. ULRIKSEN

Submitted in partial fulfillment  
of the requirements for the degree of  
Master of Science at Dalhousie University,  
Halifax, Nova Scotia, August, 1979



DALHOUSIE UNIVERSITY

Date September 1st, 1979

AUTHOR Carlos E. Ulriksen

TITLE Regional Geology, Geochronology and Metallogeny of the Coastal  
Cordillera of Chile between 25° 30' and 26° South.

DEPARTMENT OR SCHOOL GEOLOGY

DEGREE MSc CONVOCATION Fall YEAR 1979

Permission is herewith granted to Dalhousie University to circulate and to have copied for non-commercial purposes, at its discretion, the above title upon the request of individuals or institutions.



Signature of Author

THE AUTHOR RESERVES OTHER PUBLICATION RIGHTS, AND NEITHER THE THESIS NOR EXTENSIVE EXTRACTS FROM IT MAY BE PRINTED OR OTHERWISE REPRODUCED WITHOUT THE AUTHOR'S WRITTEN PERMISSION.

To Perla and  
Carola Andrea, Ingrid Karen

Regional Geology, Geochronology and Metallogeny  
of the Coastal Cordillera of Chile  
Between 25°30' and 26° South

by C. E. Ulriksen

ABSTRACT

Geological mapping at a scale of 1:100,000 of an area over 3,000 square kilometres, the examination of 165 mineral occurrences and ore deposits, and 13 new K/Ar and 4 new  $^{40}\text{Ar}/^{39}\text{Ar}$  dates form the basis for this thesis.

Paleozoic rocks metamorphosed to greenschist grade, folded into WNW-ESE trending folds and intruded by post-tectonic Permian (259 Ma  $^{40}\text{Ar}/^{39}\text{Ar}$ ) granitoids constitute the crystalline basement of the Cifuncho-Cerro del Pingo study area. The Andean Orogen was overprinted onto this basement and onto remnants of relatively undeformed Permo-Triassic volcanic and sedimentary formations.

In the western part of the area, a marine, fossiliferous and partially volcanic Lower Jurassic (Hettangian to Sinemurian) sequence, intruded by a Lower Jurassic (186 Ma  $^{40}\text{Ar}/^{39}\text{Ar}$ ) granitoid pluton is unconformably overlain by over 3,000 m of mafic to silicic volcanics of Middle to Late Jurassic age. The above formations were intruded by small porphyry plutons (undated) and by swarms of mafic dykes during the Late Jurassic (142 Ma, K-Ar whole rock).

East of the Atacama Fault System that divides the area



(ii)

marine to continental sediments and volcanics were deposited during the Early Cretaceous (Neocomian) and were intruded by granitoid plutons during Early to early Late Cretaceous times (124 Ma to 96 Ma).

The major longitudinal Atacama Fault System has affected all formations. Over 3,000 m of vertical displacement (west block down) can be deduced for pre-Cretaceous times and the fault has displaced Neogene gravels. Slickensides indicate some late component of strike-slip motion.

Dyke swarms and the tectonic style of the study area attest to a prevailing extensional regime which was probably imposed by subduction-related tectonism since the Jurassic. Compressive tectonism is mainly a Late Tertiary phenomenon at this latitude.

A Lower Jurassic metallogenic unit (Au, Ag, Co, Cu, Pb, Zn) occurs mainly nearest to the coast, and is followed inland by veins and disseminations of Cu of probable Middle to Upper Jurassic age. A Lower Cretaceous metallogenic unit (Fe, apatite, Cu, Mn, barite) occurs in the east and is genetically associated with Cretaceous magmatism and in part structurally related to the Atacama Fault System. Cenozoic ore deposits occur farther inland outside the area.

This work confirms both the existence of an Early Jurassic magmatic episode and the eastward younging of magmatic and metallogenic units previously suggested for a more southerly transect of the Central Andes.

## Acknowledgements

The present thesis has been completed with the generous help, support and understanding of a number of institutions and people to which the author is much in debt. The Instituto de Investigaciones Geológicas gave me permission to do this thesis, and allowed me to travel to Halifax (N.S.). I am extremely grateful to Dr. Marcos Zentilli for his supervision, guidance, criticism, funding and stimulating discussions which have given me the opportunity to address geological problems with a sense of curiosity.

I also wish to thank Dr. Peter Reynolds for his help, advice and encouragement in the study of the isotope geology; for the use of his geochronology facilities at Dalhousie University and for critically reading the manuscript. Appreciation is also extended to Wendy Clay, who patiently provided technical assistance.

I would like to thank Dr. R. A. Jamieson and Dr. A. L. Sangster (St. Joseph Exploration) for critically reading the manuscript and suggesting many improvements.

I am grateful to the Instituto de Investigaciones Geológicas, especially to Mr. Carlos Huete and Mr. Jaime Behm, who made this cooperative project possible; and, to the Department of Geology of Dalhousie University for financial support in the form of a Graduate Student Fellowship.

All the persons at the Department of Geology, and especially my fellow students of the "Penthouse", are thanked for providing a stimulating and lively environment for learning and research. Funds for laboratory work have been provided by the National Science and Engineering Council of Canada through grants to Dr. M. Zentilli and to Dr. P. H. Reynolds.

## TABLE OF CONTENTS

	Page
Title Page	
Abstract	i
Acknowledgements	iii
Table of Contents	v
List of Figures	viii
List of Tables	xi
I Introduction	1
- General Statement	1
- Previous Work	9
- Previous Knowledge	11
- Mineralization	12
- Purpose and Scope	15
- Methods	19
- Organization of the Thesis	20
II Regional Geology	24
Stratigraphy	
1. Stratified Rocks	24
A. Paleozoic Rocks	
Las Tortolas Formation	24
Distribution	27
Lithology	27
Structural Relationships	30
Depositional Environment	31
Age and Correlation	32
Rhyolite Conglomerate Unit	33
Distribution	33
Lithology	33
Structural Relationships	37
Depositional Environment	37
Age and Correlation	38

B. Mesozoic Rocks	
The Triassic Cifuncho Formation	39
Distribution	39
Lithology	40
Structural Relationships	40
Depositional Environment	41
Age and Correlation	41
The Jurassic Rocks	
Pan de Azucar Formation	45
Distribution	48
Lithology	48
Structural Relationships	53
Depositional Environment	54
Age and Correlation	54
Posada Hidalgos Formation	59
Distribution	59
Lithology	62
Structural Relationships	64
Depositional Environment	65
Age and Correlation	66
La Negra Formation	67
Distribution	67
Lithology	72
Structural Relationships	73
Depositional Environment	73
Age and Correlation	74
The Cretaceous Aeropuerto Formation	75
Member 1	76
Distribution	76
Lithology	79
Structural Relationships	79
Member 2	80
Distribution	80
Lithology	81
Structural Relationships	81
Depositional Environment	82
Age and Correlation	82
Tertiary and Quaternary Sediments	85

2.	Igneous Rocks	89
	Paleozoic Granitic Rocks	90
	Age	94
	Mesozoic Rocks	94
	Jurassic Intrusive Rocks	95
	Age	101
	Cretaceous Intrusive Rocks	101
	Dioritic Rocks	102
	Granodioritic Rocks	102
	Adamellitic Rocks	105
	Age	105
	Minor Intrusive Rocks	106
	Structural Geology	106
	A. Folding	107
	B. Unconformities	108
	C. Faults	119
	Atacama Fault System	119
	1. The Eastern Branch	119
	2. Central Branches	120
	3. Aguada de Chépica Fault	121
	4. The Taltal Fault	122
	Age of the Faults	122
III	Geochronology	125
	Previous Dates	125
	Method	134
	Results and Discussion	134
	Paleozoic Dates	147
	Mesozoic Dates	152
IV	Mineralization and its Relationship to the Geological Evolution: Metallogeny	163
	Mineralization in Paleozoic Rocks	163
	Jurassic Metallogenic Subprovince	174
	Cretaceous Metallogenic Subprovince	176
	Geological Evolution	180
	Conclusions	184
	References	186
	Appendix I	198
	Appendix II	220

## LIST OF FIGURES

	Page
1.1 Location of the study area south of the port of Taltal, Chile	4
1.2 The Cifuncho-Cerro del Pingo region, the study area (shaded)	6
1.3 Physiographic regions of part of northern Chile and Argentina	8
1.4 Geological map of the Taltal Region (Cifuncho-Cerro del Pingo), from Mapa Geologico de Chile, 1968	14
1.5 Mines and mineral occurrences in the Cifuncho-Cerro del Pingo area (in pocket)	17
2.1 Satellite image (ERTS, Band 5, 24 Mar 73)	23
2.2 Distribution map of the Las Tortolas Formation (shaded)	29
2.3 Regional map of the area (in pocket)	
2.4 Distribution map of the Rhyolite Conglomerate Unit (RCU), (shaded)	36
2.5 Distribution map of the Cifuncho Formation (shaded)	43
2.6 Correlation columns for the Cifuncho Formation and the Rhyolite Conglomerate Unit	47
2.7 Distribution map of the Pan de Azucar Formation (shaded)	50
2.8 Correlation columns for the Pan de Azucar Formation	58
2.9 Distribution map of the Posada Hidalgos Formation (shaded)	61
2.10 Correlation columns for the Posada Hidalgos Formation	69

2.11	Distribution map of the La Negra Formation (shaded)	71
2.12	Distribution map of the Aeropuerto Formation (shaded)	78
2.13	Correlation columns for the Aeropuerto Formation	84
2.14	Distribution of studied plutonic samples in the APQ classification diagram	87
2.15	Distribution map of Paleozoic granitic intrusions (shaded)	92
2.16	Distribution map of Jurassic intrusions (shaded)	97
2.17	Distribution map of Cretaceous intrusions (shaded)	99
2.18	Paleozoic rocks, bedding planes	110
2.19	Triassic rocks, bedding planes	112
2.20	Lower Jurassic rocks (Pan de Azucar Formation), bedding planes	114
2.21	Lower Jurassic rocks (Posada Hidalgos Formation), bedding planes	116
2.22	Lower Jurassic rocks (La Negra Formation), bedding planes	118
3.1	Geographic distribution of previous geochrono- logical dates of northern Chile	132
3.2	Localities of the dated samples	139
3.3	A histogram of the new dated samples (above) and previous dates (below) in northern Chile	141
3.4	A Map of the Taltal-Copiapo area showing the belts of granitic rocks	144
3.5	Partial compilation of radiometric dates from the study area and northern Chile	146



3.6	A graph representing the relationship between the apparent ages of the plutons and their distance perpendicular to the axis of the Peru-Chile Trench	149
3.7	Stepwise degassing release curves for sample 4 (Paleozoic granodiorite)	151
3.8	Stepwise degassing release curves for sample 12 (Lower Cretaceous porphyry)	156
3.9	Stepwise degassing release curves for sample 1 (Lower Cretaceous diorite)	159
3.10	Stepwise degassing release curves for sample 6 (Lower Cretaceous diorite)	161
4.1	Distribution of mineral occurrences and mines (in pocket)	173
4.2	Distribution of mineral occurrences and mines; metallogenic subprovinces (in pocket)	173b
4.3	Stratigraphic column of the study area (synoptic chart)	183

## LIST OF TABLES

	Page
2.1 Table of Formations	25
2.2 Chemical Analyses of the Dated Rocks	88
2.3 Approximate Modes of Typical Paleozoic Granitic Rocks	93
2.4 Approximate Modes of Typical Diorites	100
2.5 Approximate Modes of Granodiorites	103
2.6 Approximate Modes of Miscellaneous Rocks	104
3.1 Compilation of Previous Isotopic Age Data of Northern Chile	127
3.2 Radiometric Data for the Plutonic Rocks, Cifuncho-Cerro del Pingo Area	135
3.3 Analytical Data for $^{40}\text{Ar}/^{39}\text{Ar}$ Incremental Heating	136
4.1 List of Mineral Deposits, Cifuncho del Pingo Area	164

## CHAPTER 1

### INTRODUCTION

#### General Statement

The Pacific margin of South America, and especially the Central Andes, is emerging as a classic instance of interaction of continental and oceanic lithosphere. The Central Andes is a volcano-plutonic orogen constructed along a convergent or consuming plate margin between the continental edge of the American plate and the subducting Nazca Plate.

On the basis of field work, stratigraphic methods and geochronology of igneous rocks, this thesis attempts to shed light upon the procession of sedimentary, magmatic and metallogenic events that have taken place in the Taltal area in the coastal cordillera of northern Chile. Controversial hypotheses regarding the existence of a Jurassic plutonic event, the migration of the magmatic fronts with time and the type and age of the earliest displacement of a major longitudinal fault system are tested within the context of this thesis.

#### Location of the Area and Geographical Setting

The area selected for this study is located on the coast of northern Chile between latitudes  $25^{\circ}30'$  and  $26^{\circ}$  south and

longitudes  $70^{\circ}$  and  $70^{\circ}45'$  west (Figures 1.1 and 1.2). The area comprises 3,164 square kilometres and lies in the 2nd region, Antofagasta Province, comprising the Cifuncho and Cerro del Pingo (1:100,000 scale) map sheets.

The nearest town, located to the north of the study area, is Taltal (population 20,000). Taltal is linked to the rest of the country by the Pan-American Highway and by regular bus services to Santiago (1082 km) and Antofagasta (330 km).

Within the study area, numerous gravel or dirt roads branch from the Pan-American Highway and give access to the coastal zone and more inland localities. Four-wheel drive vehicles are needed to reach some localities and small mines. Water is scarce.

Three nearly parallel morphological units running north-south characterize the physiography of northern Chile (Figure 1.3): the high Cordillera de los Andes, comprising the Alta Cordillera on the east, the lower Cordillera de la Costa (or coastal cordillera) on the west and a series of intervening intermontane depressions commonly grouped as the Valle Longitudinal or longitudinal depression. The area under study comprises the Cordillera de la Costa and part of the Valle Longitudinal.

The coastal cordillera varies in width from 50-70 km and has moderate elevations, generally between 1000-2500 m. It

FIGURE 1.1 Location of the study area,  
south of the port of Taltal, Chile.

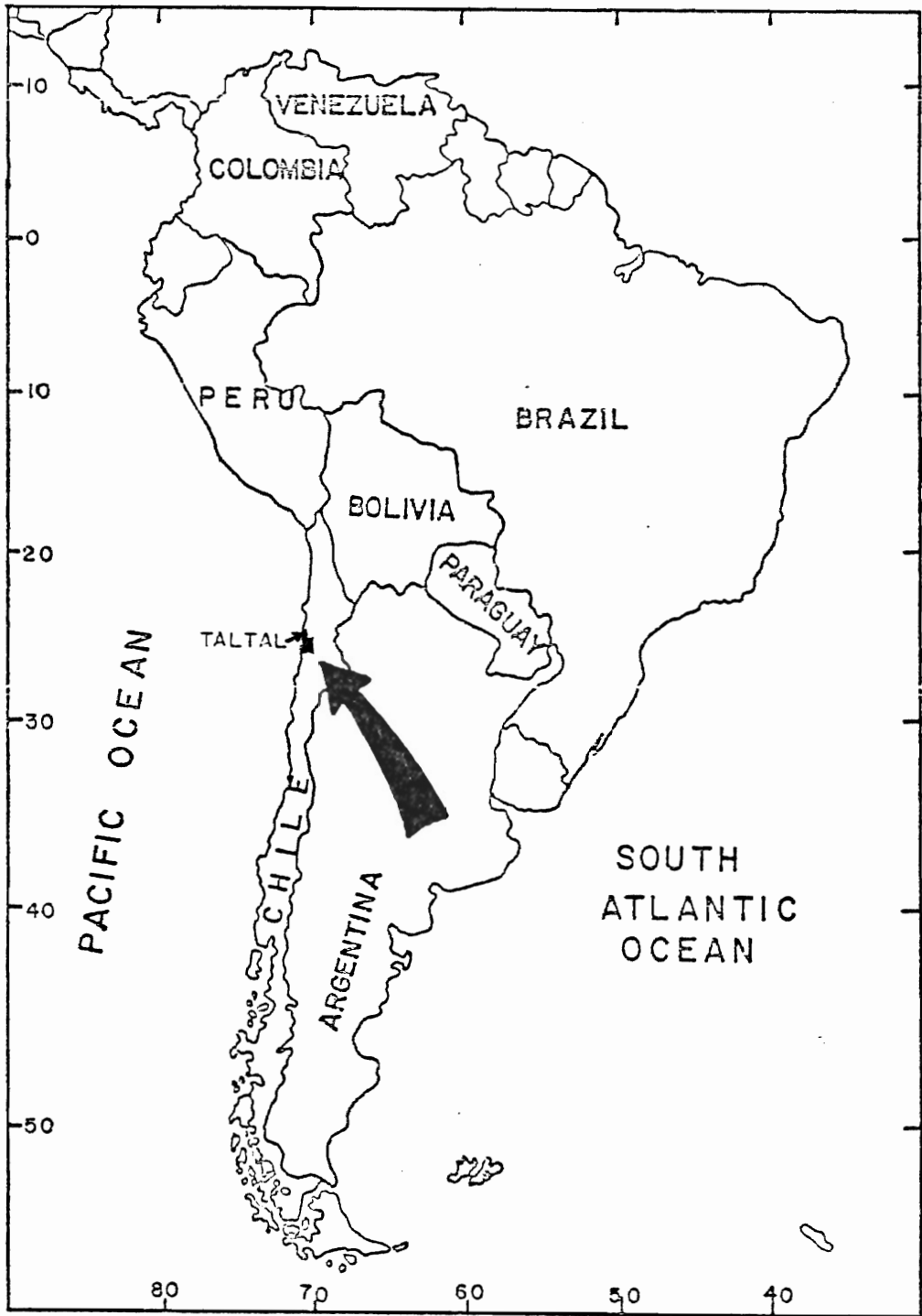


FIGURE 1.2 The Cifuncho - Cerro del Pingo region,  
the study area (shaded).

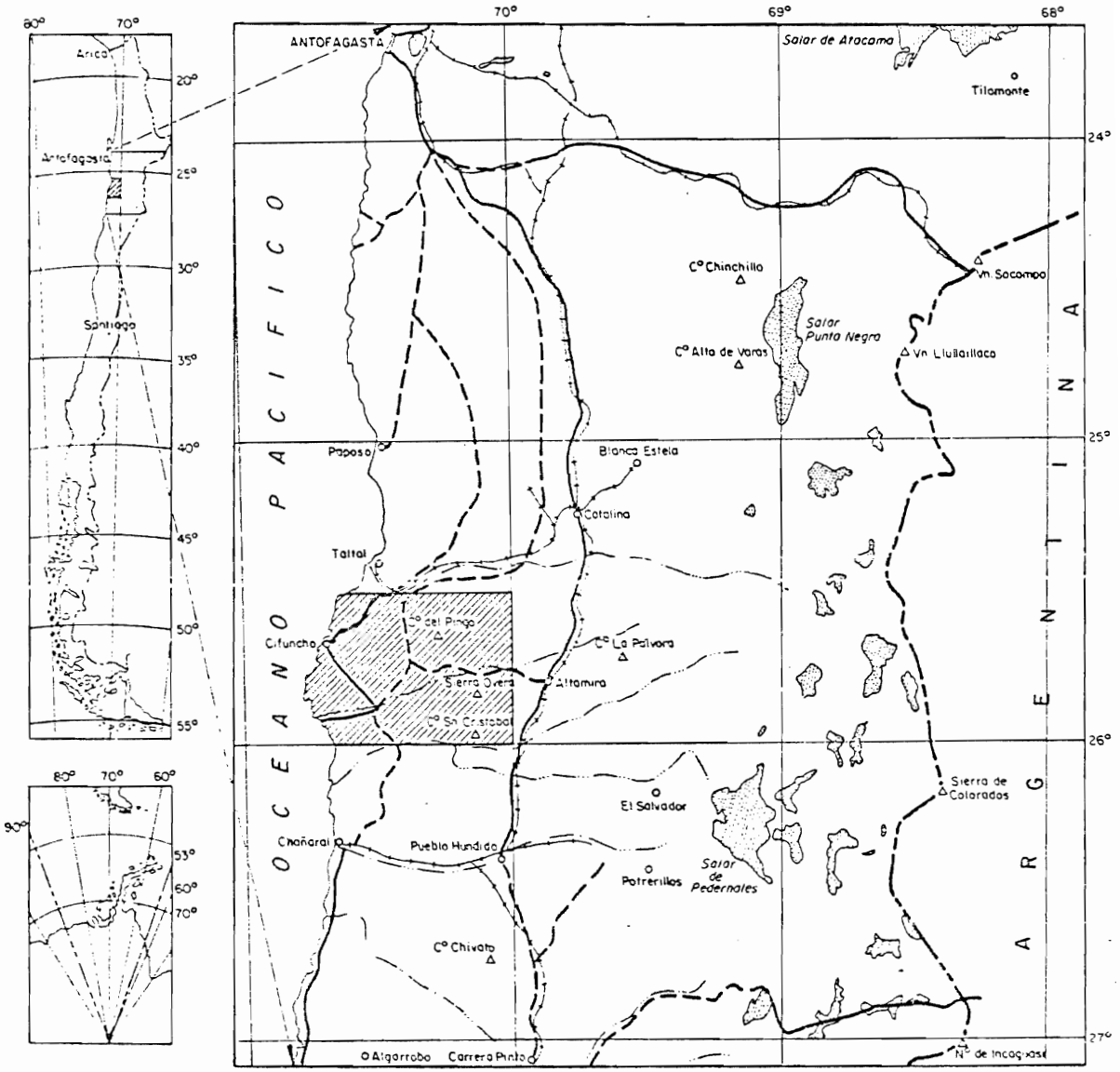




FIGURE 1.3 Physiographic regions of part of  
northern Chile and Argentina (after Zentilli, 1974).



is segmented into numerous fault blocks, its eastern margin being either abrupt or transitional. It shows an arid-cycle, old-age topography that has been disturbed by faulting.

The intermontane depressions of the Valle Longitudinal slope towards the west and abut against the eastern margin of the coastal cordillera delimiting imperfectly-drained desert basins, locally termed llanos or pampas characterized by a surface layer of caliche, rich in soda nitrate and other salts.

The climate in the area under study has strong regional and local variations. There is a transitional increase in the overall meagre precipitation toward the south and also from west to east.

The coastal area has a high relative humidity (avge. 70%), overcast skies and moderate temperature (annual mean over 17°C) (Fuenzalida, 1965). Vegetation is practically non-existent, except along the coast, near Pan de Azúcar gully where there is some vegetation with cactus plants predominating.

#### Previous Work

The first comprehensive account on the regional geology of the Taltal segment of the Andes was that of Darapsky (1900) who recognized volcanic and plutonic rocks and marine Jurassic formations.

Brüggen (1950), delineated the volcanic and marine rocks between Taltal and Chañaral along with the granodioritic plutons.

Zeil (1960), recognized Paleozoic and Mesozoic beds and put forward evidence for an early Jurassic transgression along the coastal Cordillera. He distinguished Paleozoic and Mesozoic plutons situated respectively along the coastal cordillera and further inland.

Ortiz (1960) measured and described stratigraphic sections of Triassic to Jurassic age in the Cifuncho area.

Groeber (1960) summarized the regional geology of the area under study based essentially on descriptions by L. Sundt and J. San Roman (1909) and J. Muños Cristi (1950). Groeber reported Paleozoic rocks, Jurassic fossiliferous marine rocks and volcanic formations.

An intensive geologic reconnaissance mapping from the northernmost part of Chile reaching to Copiapó area was done by García (1967). He reported the regional geology of the area as constituted by Paleozoic and Mesozoic metamorphic, plutonic, volcanic and sedimentary rocks. He described and named several geological formations and integrated them into a general geological model.

Miller (1970) discusses the structure and metamorphism of the Paleozoic rocks along the coastal cordillera of northern to central Chile.

### Previous Knowledge

Most of the geological information available at the beginning of this project was summarized in the Geological Map of Chile, scale 1:1,000,000, published by the Instituto de Investigaciones Geologicas (IIG), in 1968. A part of this map is presented in Figure 1.4.

The main belt of outcrops of Paleozoic rocks follows the coast along the whole length of the area. To the southwest of Taltal, a felsic plutonic complex considered Permo-Carboniferous (Levi et al., 1963) intrudes low grade metamorphic slates and quartzites.

Triassic sediments occur in scattered outcrops. In the Quebrada Cifuncho, the Permian granite is unconformably overlain by the Cifuncho formation (Ruiz et al., 1965; Bowes et al., 1966) of probable Triassic age. The Jurassic is represented by an almost continuous belt of outcrops along the coastal cordillera. The rocks range in age from Lower Jurassic (fossiliferous marine sediments with volcanic intercalations) to Upper Jurassic volcanic rocks.

The granitic rocks of the area have been generally subdivided into Paleozoic, Jurassic-Cretaceous and Cretaceous provinces. The ages were assigned on the basis of two alpha-lead age determinations on zircons (Levi et al., 1963) and tenuous supporting structural and stratigraphic evidence.

The small numbers of age determinations were clearly insufficient for an understanding of the complex geology of a region with widespread mineralization associated with a variety of rocks.

The Atacama Fault (Figures 1.4 and 2.3) represents one major structural feature of the Circum-Pacific region. It has been considered analogous to large regional transcurrent faults such as the San Andreas Fault of California or the Alpine Fault of New Zealand (St. Amand and Allen, 1960; Allen, 1962, 1965; Arabasz, 1971). Arabasz (1971) mapped the fault from Copiapó to Antofagasta, did geophysical (micro-seismic) measurements and discussed the tectonic significance of this major regional structure.

The plate tectonic setting of the area has been discussed by several authors (e.g. Baranzagi and Isacks, 1976; Hanus and Vanek, 1978; James, 1978; Schweller and Kulm, 1978; Kulm, Schweller and Masias, 1977; Megard and Philip, 1976). The relationships between mineral deposits and plate tectonics have been considered by Strong, (1974); Mitchell and Garson, (1976); Mitchell, (1976); Sillitoe, (1976).

#### Mineralization

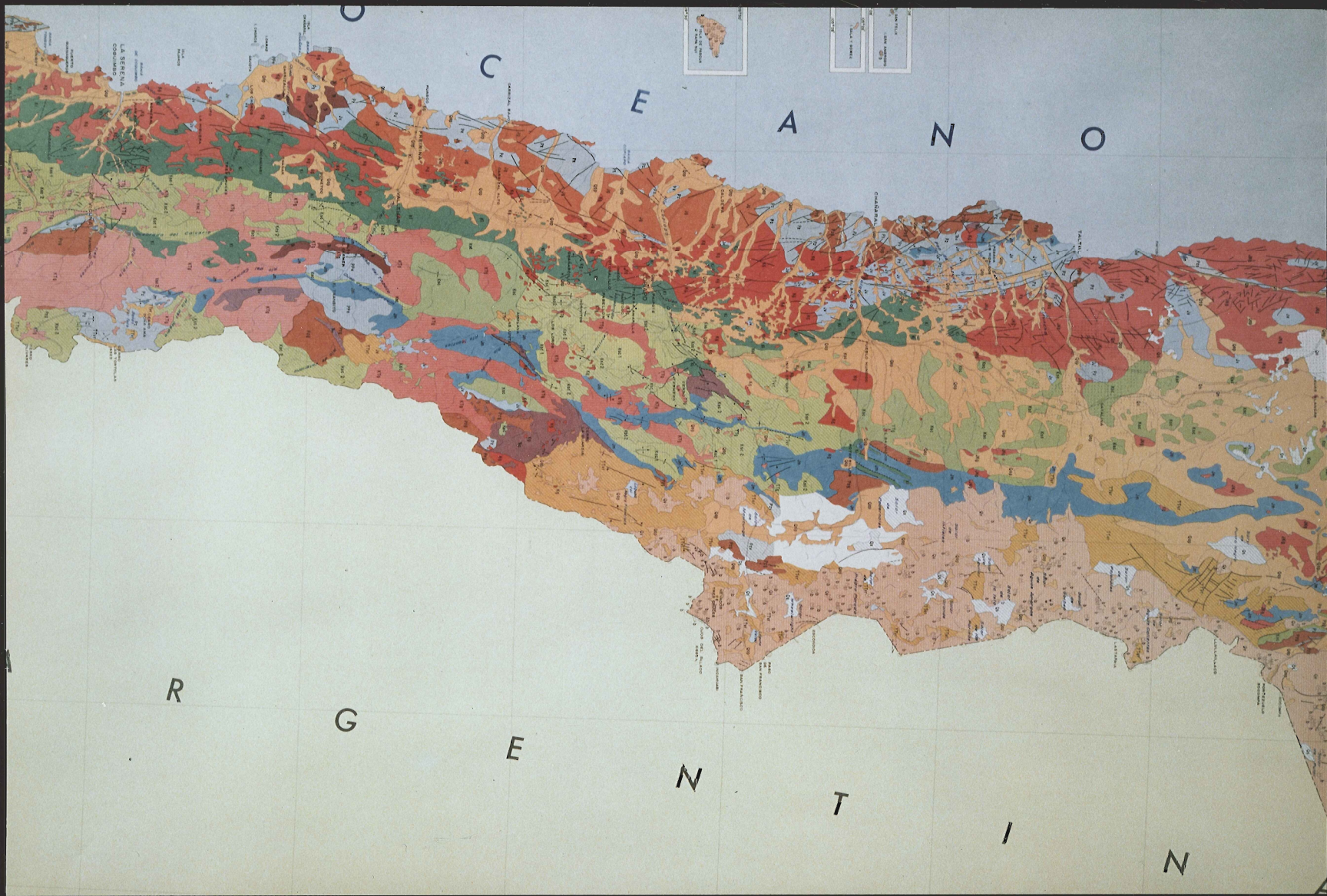
Active mining and prospecting have taken place along the coast and on the central part of the study area. Wherever a mineral showing is found there is evidence that someone has dug, trenched and sampled.

FIGURE 1.4 Geological map of the Taltal Region (Cifuncho-Cerro Del Pingo), from Mapa Geológico De Chile, 1968.

Approximate scale 1:3,500,000.

LEGEND		
COLOUR ON PHOTOGRAPH	SYMBOL	ROCK UNIT
Dark red brown	Pzg	Paleozoic intrusive.
Grey solid	Pz	Paleozoic metasediments.
Grey cross-hatched	Pv	Paleozoic volcanic.
Mauve	Trc	Triassic continental, volcanic and sediments.
Red brown	Jg	Jurassic intrusive.
Blue	Jm	Marine Jurassic.
Light blue	Jv	Jurassic volcanic.
Dark green	Ki	Cretaceous continental and marine.
Rose	Kg	Cretaceous intrusives.
Light green	Ksc	Undifferentiated Upper Cretaceous and Lower Tertiary continental sediments.
Pink cross-hatched	Ktg	Tertiary intrusive.
Dark yellow cross-hatched	TTvr	Tertiary volcanic and continental rocks.
Beige cross-hatched	Qv	Quaternary volcanic rocks.







In the study area the metallic mineralization appears to be spatially associated almost exclusively with Mesozoic plutonic, volcanic and marine rocks. A few of these, copper, gold, silver, cobalt, and iron prospects and mines (Figure 1.5) have been described by Serrano and Ortiz (1962) and Bowes et al. (1966). The age of this potentially significant mineralization is uncertain, and is the subject of Chapter 4 of this thesis. Southeast of the area, Tertiary porphyry copper deposits have been mined at the El Salvador and Potrerillos mines.

#### Purpose and Scope

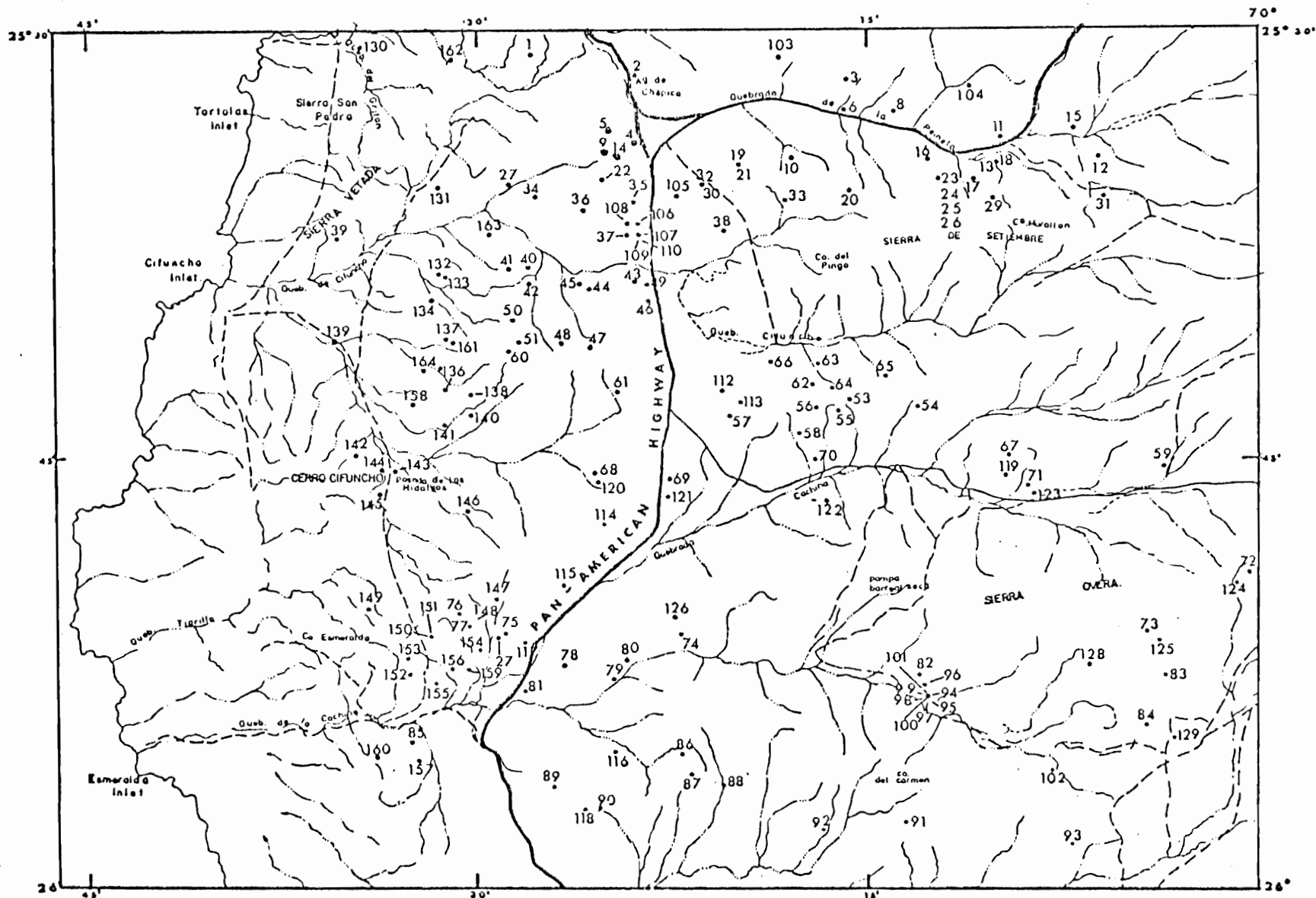
The Cifuncho-Cerro del Pingo area contains the key to verify several hypotheses on the evolution of the continental margin proposed recently for the Copiapo region situated further south, near latitude 27°S.

The existence of a Lower Jurassic batholith along the coastal cordillera of northern Chile has been a matter of dispute since it was proposed, on the basis of K/Ar studies by Farrar et al. in 1970. Geologists familiar with the area have insisted that no such Jurassic magmatic episode exists but that the dates of the above authors reflect uplift ages, reheating of Paleozoic plutons by a Cretaceous magmatic episode, or insufficient data (James, 1971; Stewart et al., 1974).

This thesis provides stratigraphic and geochronologic evidence for the existence of this Lower Jurassic plutonism.

FIGURE 1.5 Mines and mineral occurrences in the  
Cifuncho-Cerro del Pingo area.

Numbers refer to Table 4.1



Furthermore, Farrar et al. proposed that at latitude  $27^{\circ}\text{S}$ - $28^{\circ}\text{S}$  igneous foci migrated with time forming narrow longitudinal belts of decreasing ages with increasing distance from the present coast line. However, Arabasz (1971) mapped supposedly Tertiary plutons in the coastal cordillera of the Cifuncho-Cerro del Pingo area, and this would have meant that the eastward migration of Farrar et al. would break down north of latitude  $26^{\circ}$ , and this would have important implications for metallogenic interpretations. This thesis confirms the extension of the age belts to at least latitude  $25^{\circ}$ - $26^{\circ}\text{S}$ . Arabasz (1971) proposed that the major Atacama Fault, which is still active at present, had started its motion in Mid-Late Cretaceous times. The Cifuncho-Cerro del Pingo area provided a place to test this hypothesis. The thesis work has documented a much earlier pre-Cretaceous vertical movement for the Atacama Fault.

Several authors (e.g. Zentilli, 1974; Sillitoe, 1976; Clark et al., 1976) have proposed a zonation of the mineralization related spatially and genetically to the longitudinal belts of granitoids defined by Farrar et al. (1970). This mineralization, these authors contend, formed during successive discrete metallogenic episodes, becoming progressively younger from west to east, giving rise to a series of longitudinal belts or metallogenic sub-provinces. The study area provided the possibility to test this model and to confirm the extension

of the metallogenic sub-provinces to at least latitude  $25^{\circ}$ - $26^{\circ}$ S. The present project necessitated the mapping of the different stratigraphic units to determine their field relationships; inspection of over 150 mineral occurrences; collection of fossils for paleontological determinations and dating of key igneous rocks using K/Ar and  $40\text{ Ar}/39\text{ Ar}$  methods.

The regional scale of the problems whose solution was attempted have not permitted the completion of detailed studies of any kind.

This research is a contribution to the Regional Geology Project carried out by the Instituto de Investigaciones Geológicas (IIG), Chile.

#### Methods

A critical revision of the geological literature was undertaken, using published reports and also unpublished maps and reports, mainly from the IIG library. Field work leading to this thesis was started during 1969-1971, while the writer was resident geologist for the Instituto de Investigaciones Geológicas (IIG) in Antofagasta, and completed in 1977.

The field work involved a preliminary photogeological interpretation followed by geological mapping in the field using vertical aerial photographs (scale 1:60,000) and the data were then transferred to topographic base maps

(sheets No. 2530-7030 Cifuncho and No. 2530-7000 Cerro del Pingo; scale 1:100,000, Inst. Geográfico Militar, Chile).

Samples for geochronology were collected by the author, by M. Zentilli and a few by field parties of the IIG. Thin sections were prepared for most specimens. Those selected for dating were crushed, ground and sieved. The largest size fraction containing free mica or hornblende was selected for mineral separation. The samples were dated by K/Ar and  $^{40}\text{Ar}/^{39}\text{Ar}$  methods. The sample preparation and the geochronology methods and principles are explained in detail in Chapter 3 and in Appendix 1.

#### Organization of the Thesis

In this thesis, the author first describes the regional geology of the Cifuncho-Cerro del Pingo area, attempting to clarify the geological development of the region (Chapter 2). Information gathered during the present project, geochronological data and published information (to 1978) have been incorporated into the discussion.

Chapter 3 discusses the results of the geochronological investigations of the intrusive rocks. These results are essential for the understanding of the Paleozoic and Mesozoic stratigraphy and provide useful information for the overall geological history of the area.

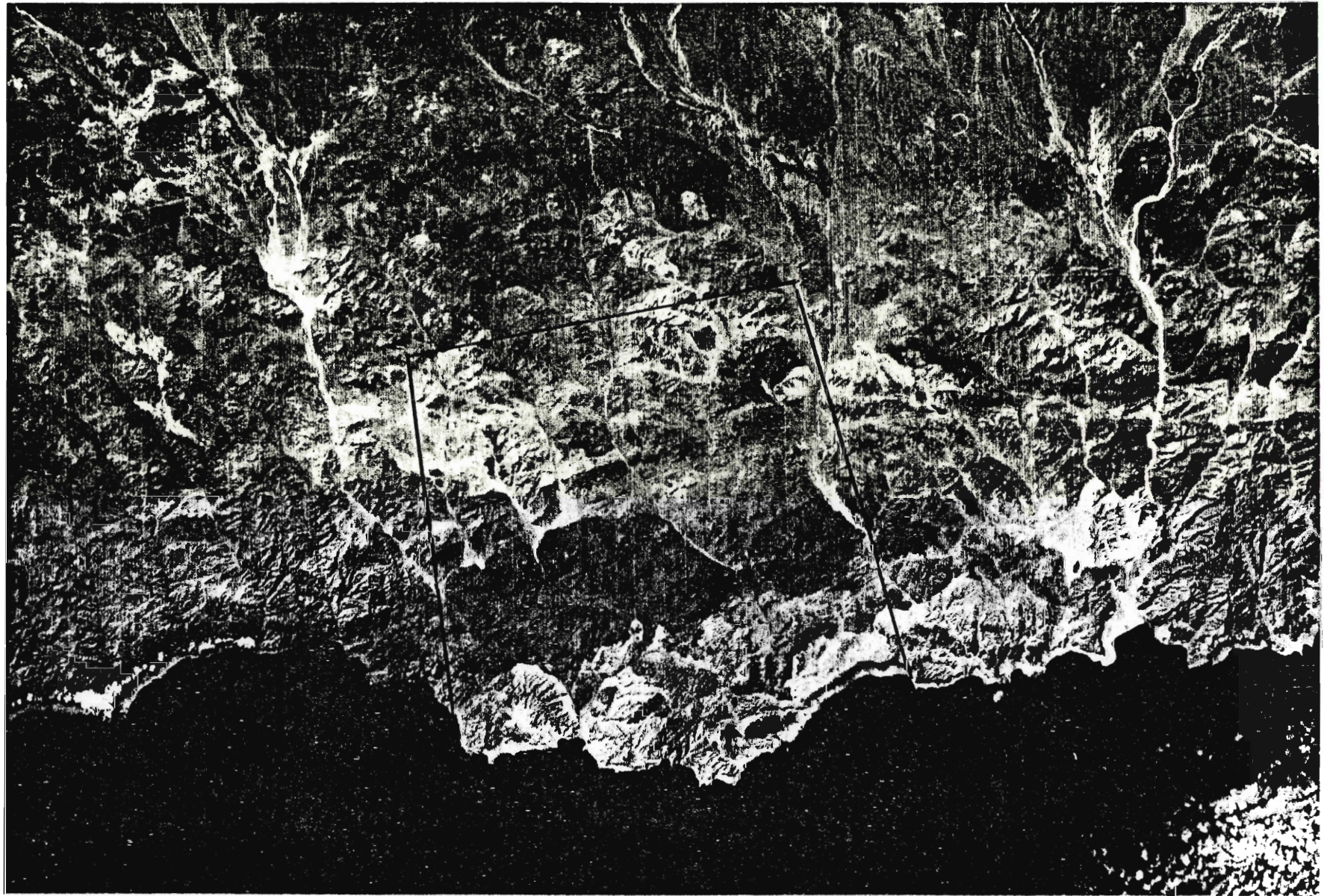
Chapter 4 is a brief discussion of the geological evolution of the Cifuncho-Cerro del Pingo area together with the principal mineral deposits and their relationships to the sedimentary, volcanic and plutonic rocks and to the metallogenic epochs.

FIGURE 2.1 Satellite image (ERTS, Band 5, 24 MAR 73)

Approximate scale 1:750,000.

Note the expression of the Atacama Fault.





## CHAPTER II

### REGIONAL GEOLOGY

The rocks exposed in the study area are marine and continental sedimentary, volcanic, and metamorphic rocks with ages ranging from Paleozoic to Quaternary. These rocks have been intruded by plutonic bodies ranging in age from Permian to Late Cretaceous. The continental and marine sedimentary rocks and volcanics deposited in the Tertiary and Quaternary periods are not well represented in the area. The Atacama Fault Zone and its numerous branches are the major structural features and represent an important control for the distribution of ore mineralization.

Folding and unconformities reflecting important tectonic events occurred during the geological evolution of the Cifuncho-Cerro del Pingo area. A Table of Formations is shown in Table 2.1.

#### Stratigraphy

##### 1. Stratified Rocks

###### A. Paleozoic Rocks

###### Las Tórtolas Formation

A unit approximately 1000 m thick of meta-sedimentary rocks, with variable lithology (quartzites, slates, phyllites, mica

TABLE 2.1

## TABLE OF FORMATIONS

ERA	PERIOD or EPOCH	FORMATION and THICKNESS (m)	LITHOLOGY
Cenozoic	Quaternary and Tertiary		Alluvial deposits; eolian sand deposits.
		Unconformity	
Mesozoic	Upper Cretaceous or Lower Cretaceous	Batholith	Granodiorite, adamellite; quartz-monzodiorite.
		Intrusive contact	
	Lower Cretaceous	Aeropuerto Formation 2500 - 3000	Conglomerate, sandstone, limestone, andesite, volcanic sandstone.
		Unconformity	
Middle Jurassic		La Negra Formation 3000 +	Andesite; minor sandstone and tuff
		Unconformity	
		Sierra Esmeralda pluton	Dioritic rocks (hornblende and/or biotite).
		Intrusive contact	

	Lower Jurassic	Posada Hidalgos Formation 1021	Sandstone, shale, andesite breccia, limestone and conglomerates.
		Unconformity	
		Pan de Azucar Formation 761	Shale, sandstone, limestone conglomerate.
		Unconformity	
	Upper Triassic	Cifuncho Formation 400	Sandstone, conglomerate, shale and limestone.
		Unconformity	
Paleozoic	Permian to Lower Triassic	Rhyolite Conglomerate Unit 164 †	Rhyolite, sandstone.
		Unconformity	
	Middle Permian	Cifuncho Batholith	Granodiorite, leucogranite, adamellite.
		Intrusive contact	
	Lower Permian to Middle Devonian	Las Tortolas Formation 1000 †	Quartzite, slate, mica-schist, metalimestone.



schists) is widespread in the western part of the area (Figure 2.2) and also outcrops north of Cerro del Pingo gully ( $25^{\circ}39'S-70^{\circ}38'W$ ). Because of the lack of a suitable type section exposing both contacts of the unit, there is some uncertainty concerning the stratigraphic position, and the strong folding does not permit an accurate measurement of its thickness; accordingly, this unit is herewith informally named the Las Tórtolas Formation, after Las Tórtolas inlet where the best known outcrops occur (Figure 2.3).

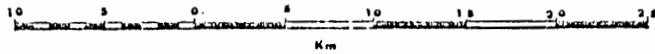
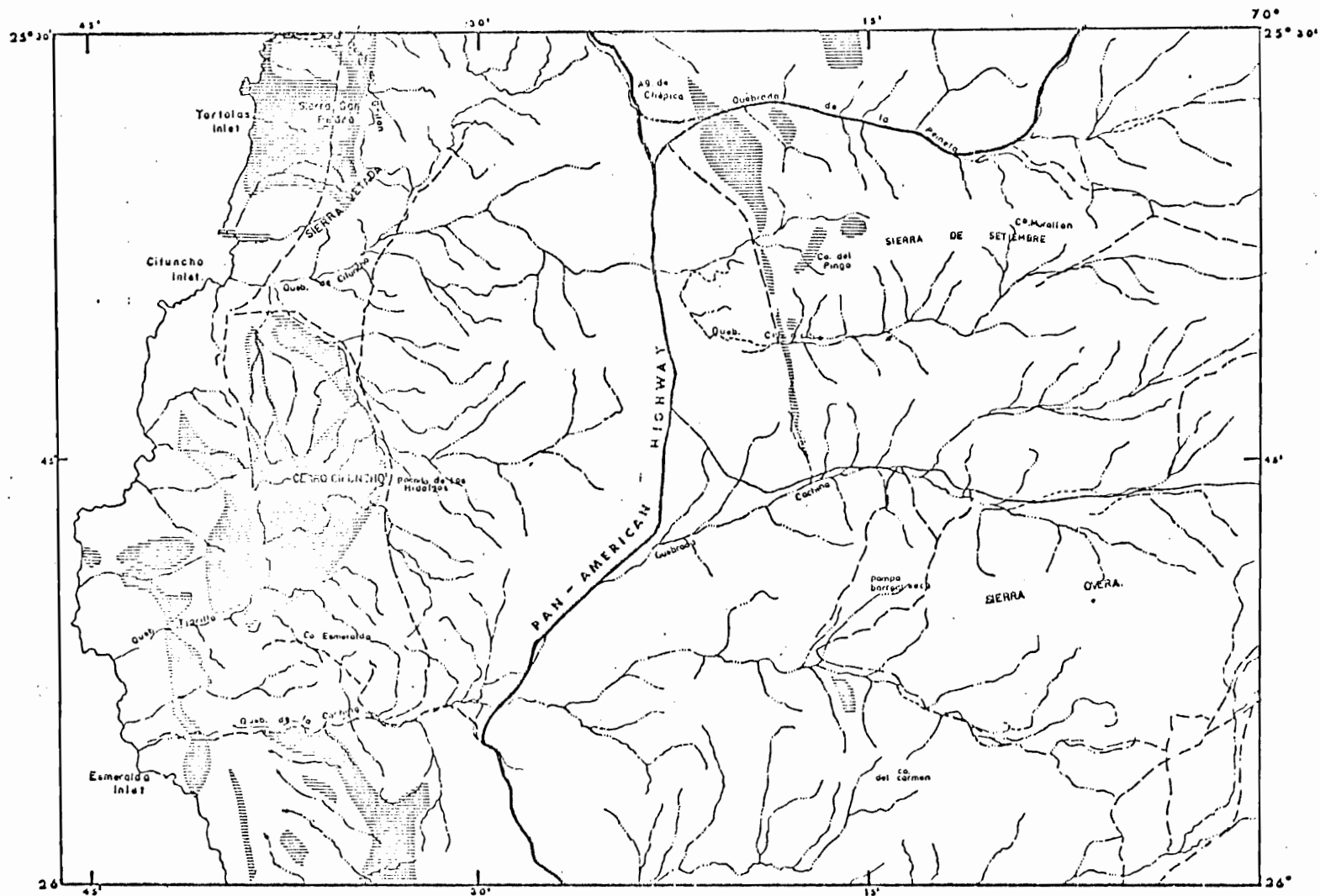
#### Distribution

The outcrops of the Las Tórtolas Formation occur predominantly in the western part of the area, along the present coastline. The formation also outcrops on the northern side of Cerro del Pingo ( $25^{\circ}31'S-70^{\circ}20'W$ ) gully and along the eastern branch of the Atacama Fault Zone, on the northwestern side of Sierra del Carmen (Figure 2.2). This unit has also been recognized south of the study area (Mercado, 1977; Naranjo, 1978).

#### Lithology

The Las Tórtolas Formation is composed of quartzites, slates, phyllites and schists, with the intensity of metamorphism varying from place to place. These rocks appear to be the metamorphic equivalents of sandstones, greywackes, shales and mudstones.

FIGURE 2.2 Distribution map of  
the Las Tórtolas Formation (shaded).



The main lithologic elements are quartzites of pale brownish grey colour, fine- to medium-grained chloritic slates and schists of grayish green, pale to dark greenish gray colour, gray to black laminated phyllites and meta-sandstones grading to meta-graywacke. A meta-limestone layer intercalated near the top (?) of the sequence was observed south of La Cachina gully ( $25^{\circ}56'S-70^{\circ}33'W$ ). Dykes of andesitic basaltic composition cross-cut the formation along the whole area.

#### Structural Relationships

The intense folding of these rocks contrasts with the much less intense folding of the Mesozoic rocks. Miller (1970) measured several fold axes with a general northwest-southeast trend which are in agreement with the author's observations (see below).

The lower contact of the Las Tórtolas Formation was not observed because it is intruded by a granitic body in which the rocks appear as "roof pendants". The upper contact was observed on Cerro del Gritón and Cerro de Cifuncho ( $25^{\circ}32'S-70^{\circ}33'W$ ,  $25^{\circ}45'S-70^{\circ}38'W$ ) (Figure 2.3) where a fault separates the Las Tórtolas Formation from a basal conglomerate of the Cifuncho Formation and Posada Hidalgos Formation. On the north side of La Cachina gully ( $25^{\circ}56'S-70^{\circ}33'W$ ) however, a basal, red weathering volcanic unit is exposed which rests with slight angular unconformity on metamorphosed rocks of the Las Tórtolas Formation.



The rocks supported a previous regional metamorphism (Abukuma-type, Miller, 1970) and as a consequence of the granitoid intrusion, an overprinted contact metasomatism. Sericite, chlorite and Biotite were formed during the metamorphism and near the contact with the granitoid, andalusite was found (Zeil, 1960). Detailed discussion of the metamorphism is beyond the scope of this thesis.

#### Depositional Environment

No detailed sedimentological analysis of the Las Tórtolas Formation has been undertaken, but the environment of its deposition can be inferred from its lithology: the monotony of parts of the sequences, good stratification, alternation of meta-sandstones and slates, ripple marks, grooves, load casts, etc. appear to suggest deposition under water, the depth of which cannot be estimated. The presence of fetid meta-limestone in the sequence suggests the existence of organic-rich basins with restricted circulation. There is scant supporting evidence, however, for the interpretations of this sequence as a flysch (cf. Reutter, 1974) or for a sedimentation in a paralic basin (cf. Vicente, 1975) or for a "marine sedimentation" suggested by Chong (1977). Furthermore the presence of fossil plants in the sequence (see below, Miller, 1970) may indicate that at least some of the strata were deposited subaerially or in a deltaic environment.

## Age and Correlation

The only fossil found in the Las Tórtolas Formation was collected at La Cachina gully and is a plant, Lophoctenium comosum Reinhold Richter (Miller, 1970) which in Germany is considered to be Middle Devonian in age. On the basis of petrographic and structural evidences, the same author (1973) reasserted the same age.

Along the coast and in the central part of the area, the Las Tórtolas Formation is intruded by a granodiorite belonging to an extensive plutonic body that yielded a K/Ar biotite age of  $267 \pm 8$  Ma (Quirt, 1972; Zentilli, 1974) and a Pb/ $\alpha$  zircon age of  $354 \pm 40$  Ma (Levi et al., 1963). A Permian (?) intrusive phase is hence suggested. Stratigraphic and isotopic evidences taken together suggest an age between Permian and Middle Devonian.

Different authors (Cecioni, 1960; Ortiz, 1960; García, 1967) have correlated the unit now defined as the Las Tórtolas Formation with the El Toco Formation (Harrington, 1961; García, 1967) located in the coastal cordillera, north of Antofagasta (Lat.  $23^{\circ}$ S). This correlation is based purely on lithological similarities. In that area Wetzel (1927) collected a fossil tree identified by Gothan as Dadoxylon sp. On this basis Wetzel assigned an Upper Paleozoic age to the sequence.

### "Rhyolite Conglomerate" unit

A well exposed unit at least 164 m thick of rhyolites, rhyolitic Breccias and coarse sandstone interbeds underlies Triassic rocks along the western part of the area (Figures 2.3 and 2.4).

This unit was tentatively correlated by Corvalán (1965) with the Cifuncho Formation of Triassic age (see below). However, the lithology and the style of folding of this unit are clearly different and this correlation is therefore not tenable. For the purpose of this thesis, this unit is informally named the "rhyolite conglomerate" unit abbreviated herewith as RCU.

### Distribution

The outcrops of the RCU are restricted to the western part of the area (Figure 2.4) between La Cachina gully and Cifuncho gully. They show a relatively continuous distribution and can be easily identified in the field by their brown-red colour.

### Lithology

The most distinctive feature of the RCU is the great homogeneity of its rock types; it consists of brown-red sandstones with interbeds 2-3 m thick of conglomerates with well-rounded pebbles and cobbles of quartz and granite, in a matrix of brown

quartz-rich sand. Towards the top the unit tends to be angular conglomerate. A type-section is described (see below) 2 km north of Aguada Jacinto Diaz (Figure 2.3). This unit has a minimum thickness of 164 m and a maximum of 600 m.

Type Section of Rhyolite Conglomerate Unit (RCU)

Unit	Description	Thickness (m)
1	Rhyolite, yellow-red, poorly defined stratification; abundance of limonite veins. Towards the bottom, there are lenses of conglomerate interbeds (0.5-5 m), rounded clasts size 1 to 5 cm, composed of quartzites and porphyry	32
2	Rhyolitic breccia, gray-green, fragments of 2 cm	25
3	Volcanic rhyolitic Breccia, gray-green, fragments ranging between 2-15 cm; locally up to 30 cm; highly weathered and with abundant limonite	82
4	Rhyolite, gray-green in fresh surface, yellow to yellowish-white in weathering surface; the weathering zones are shaly; brecciated toward the top, blocks 10-20 cm in size.	25
		164 m

Under the microscope the rhyolite shows a porphyritic texture and a pilotaxitic groundmass. Phenocrysts (0.2-3 mm) include plagioclase ( $An_{0-10}$  to  $An_{10-45}$ ), and amphibole altered to chlorite and calcite.

FIGURE 2.4 Distribution map of the  
Rhyolite Conglomerate Unit (RCU), shaded.



The matrix contains veinlets of calcite and limonite (after Levi et al., 1960 and the author's personal observations).

#### Structural Relationships

The RCU is folded into gentle anticlines and synclines with axes approximately north-south and its structural style contrasts with that of the intensely deformed Las Tórtolas Formation.

The lower contact of the RCU can be observed on the east flank of Cerro de Cifuncho and on the west flank of Cerro Buena Esperanza (Figure 2.3), where it rests unconformably over the Las Tórtolas Formation. On the east flank of Cerro de Cifuncho, however, the contact between both formations is a fault. The upper contact can be observed 2 km north of Aguada Jacinto Díaz (Figure 2.3) where the basal units of the Jurassic sequence rest with slight angular discordance over the RCU. The thickness of the RCU diminishes in the middle zone of outcrops and increases toward the south and north (i.e. south side of Cifuncho gully, north side of La Cachina gully).

#### Depositional Environment

The shaly, weathered interbeds between the volcanic units and the presence of coarse conglomerates suggest a subaerial,

fluvial environment of deposition for this formation. The lithology and the character of the sedimentary structures correspond to a flood plain association which can be regarded as a mixed load deposit (e.g. Reineck and Singh, 1975) developed in a point bar sub-environment.

#### Age and Correlation

The lithology of the RCU is very similar to the base of the overlying Cifuncho Formation (see below). Nowhere in the mapped area were any fossils found in this unit, so the only available criteria that would suggest the relative age of this unit are the lithology and structural relationships.

The unit is not metamorphosed and on the north side of La Cachina gully, it is intruded by a diorite belonging to an extensive plutonic body that yielded a K/Ar biotite age  $189 \pm 8$  Ma (Zentilli, 1974) (see below) and thus the formation is older than Lower Jurassic. Pebbles of sandstones, shales, and limestones are not present, indicating that local Triassic rocks were not a source of the conglomerate. The rhyolite pebbles could have originated from the local Jurassic rocks but had that been the source, limestones and calcareous sediments would be expected also. The regional lithologic considerations and the structural relations lead the author to assign the continental rhyolite conglomerate unit to the Upper Permian or Triassic.



The RCU can be correlated on the basis of lithologic and structural relations with other Middle to Upper Triassic formations outcropping in several places outside the study area. For example, in the Limón Verde-Moctezuma area (Lat.  $22^{\circ}40'S$ ) Harrington (1961) described a sequence of greenish gray rhyolitic flows and tuff, 200 m thick, overlain by fossiliferous Triassic horizons (Norian. In Caracoles (Lat.  $23^{\circ}20'S$ ) he also mentioned the same Norian-Lower Jurassic sequence overlain by marine Bajocian Beds. García (1967) named that unit the Agua Dulce Formation. At Sierra de Varas (Lat.  $24^{\circ}S-25^{\circ}30'S$ ), Chong (1977) describes a sequence of acidic volcanic and continental beds, 2000 m thick. These rocks have been dated as Upper Triassic, on the basis of plant fossils.

#### B. Mesozoic Rocks

##### The Triassic Cifuncho Formation

The Cifuncho Formation was defined by García (1967), at the Cifuncho gully (Lat.  $25^{\circ}39'S$ ), 6 km east of Cifuncho inlet, as a sequence of conglomerates, sandstones, shales and thin layers of limestones. This sequence has been observed only in the type locality and in the southernmost part of the area.

##### Distribution

The Cifuncho Formation outcrops west of Sierra Buena Esperanza (Lat.  $25^{\circ}40'S$ ) and 2.5 km of the south side of Cifuncho

gully (Figures 2.3 and 2.5), at west and north of Sierra Esmeralda (Lat.  $25^{\circ}50'S$ ), north side of La Cachina gully (Figure 2.3).

García (1967) does not give a thickness for this formation; a thickness of 164 m, however, was estimated by Corvalán (1965). The present author estimates a maximum thickness of 400 m for this formation according to measurements performed in the area, but lateral variations were observed.

#### Lithology

In his definition García (1967) describes "red brown layers of conglomerates in the lower part and toward the upper part white gray layers of quartz sandstones, conglomerates and gray-greenish finely laminated shales with thin lenses of light brown limestones".

The conglomerates consist of rounded clasts of granite (10%), quartzite and phyllites (80%), and quartz and volcanic (rhyolite?) rocks (10%); the matrix is a coarse sandstone of quartz, feldspar and granite fragments.

The sandstones consist essentially of quartz, feldspars, granite fragments and lithic aphanitic clasts. Shales and limestones appear toward the top of the formation.

#### Structural Relationships

The Cifuncho Formation forms a gentle anticline with a NE trend. The lower contact of the formation was observed west of

Sierra Esmeralda where it rests with angular and erosional discordance over the rhyolite conglomerate unit (Figures 2.3 and 2.5). In the type locality the base lies beneath the modern sediments of the gully. The upper contact is an angular discordance which separates it from the basal conglomerate of the overlying Jurassic formation.

#### Depositional Environment

The presence of feldspathic to subfeldspathic sandstones, pebbles and cobble conglomerates, shales and limestones suggests deposition in an alluvial fan (e.g. Reineck and Singh, 1975). These deposits could have developed in a tectonically active area by a sudden change in the slope of the alluvial fan.

#### Age and Correlation

The lithology of the upper part of the Cifuncho Formation is distinctly different from the underlying rocks, showing a change from continental to marine deposition. The formation contains pebbles of quartzites, phyllites, rhyolite and Paleozoic granite, indicating that the Paleozoic formations were the source of both conglomerate and sandstone. Fossil trunks of cordaites type determined by G. Cecionias species Dadoxylon (Permo-Carboniferous) (García, 1967) have been found in the area. However, Zentilli (1974) suggested that the fossil in question could be Araucarioxylon, of Triassic age, which is indistinguishable from Dadoxylon trunks alone. On the basis of

FIGURE 2.5 Distribution map of the  
Cifuncho Formation (shaded).



the lithology, stratigraphic position and fossil content, the Cifuncho Formation has been assigned an Upper Triassic-Lower Triassic age (Zeil, 1960); a Rhaetian age (Corvalan, 1965); an Upper Paleozoic age (Ruiz et al., 1965); or an Upper Triassic age (García, 1967].

The Cifuncho Formation and the underlying formations have been intruded by numerous andesitic dykes and sills of different thicknesses. However, a similar pattern of dykes occurs in the overlying Jurassic rocks.

In summary, regional lithologic considerations and the structural relationships lead the present author to assign the Cifuncho Formation to the Middle or Upper Triassic.

Several formations outcropping outside the study area can be correlated with the Cifuncho Formation on the basis of the lithology and structural relations (e.g. see Figure 2.19).

The classical locality and sequence for the continental Triassic is Sierra La Ternera, located in the pre-cordillera of Copiapo (Lat.  $27^{\circ}07'S-69^{\circ}43'W$ ). The continental sediments contain plant remains that have been dated as Rhaetian by Solms-Laubach and Steinmann (1899] and coal horizons which were worked on a small scale, but have no present commercial value.

In the pre-cordillera of Copiapó (Rio Turbio-Ramadas; Las Juntas), Segerstrom (1968] described various sedimentary sequences as Upper Triassic. At Alto del Carmen (Lat.  $28^{\circ}45'S$ )

fossiliferous marine and continental sediments outcrop. Brüggem (1950) assigned them to the Upper Triassic. Later, Zeil and Ichikawa (1958) and Barthel (1958) dated the sequence as being Lower-Middle Anisian and Upper Anisian.

East of the study area, outcrops of rocks assigned to Middle to Upper Triassic have been described by Tobar (1977) on the eastern margin of Sierra Castillo ( $26^{\circ}12'S-69^{\circ}24'W$ ).

#### The Jurassic Period

##### Pan de Azúcar Formation

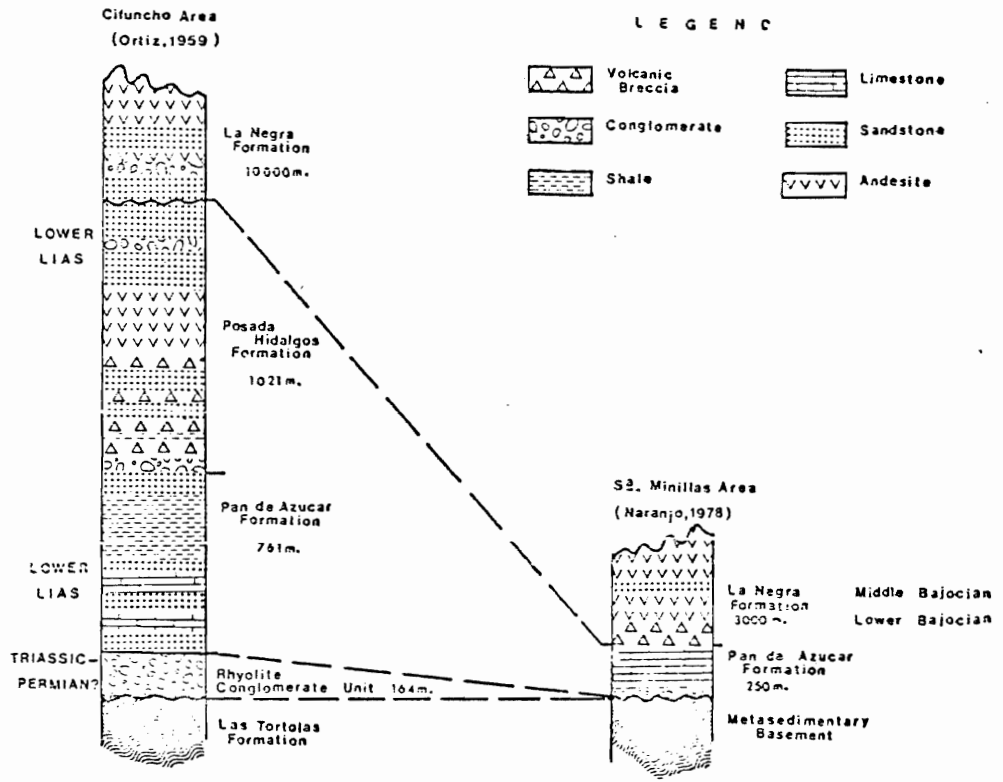
The outcroppings in Pan de Azúcar gully, 4 km west of Las Bombas, were grouped by García (1959) as the Pan de Azúcar Formation. There was no description of a type section, nor were the boundaries placed.

Ortiz (1959, 1960) described a sequence of limestones, shales and sandstones that outcrops in the Posada Hidalgos gully as belonging to the Pan de Azúcar Formation. Corvalán (1965) issued a columnar section of it. Recently, Naranjo (1978) defines as Pan de Azúcar Formation a sequence of marine, clastic sedimentary rocks outcropping in Sierra Minillas (Copiapó).

For the purpose of this thesis, the definition of Ortiz (1960) will be followed.

FIGURE 2.6 Correlation columns for the Cifuncho Formation  
and the Rhyolite Conglomerate Unit.





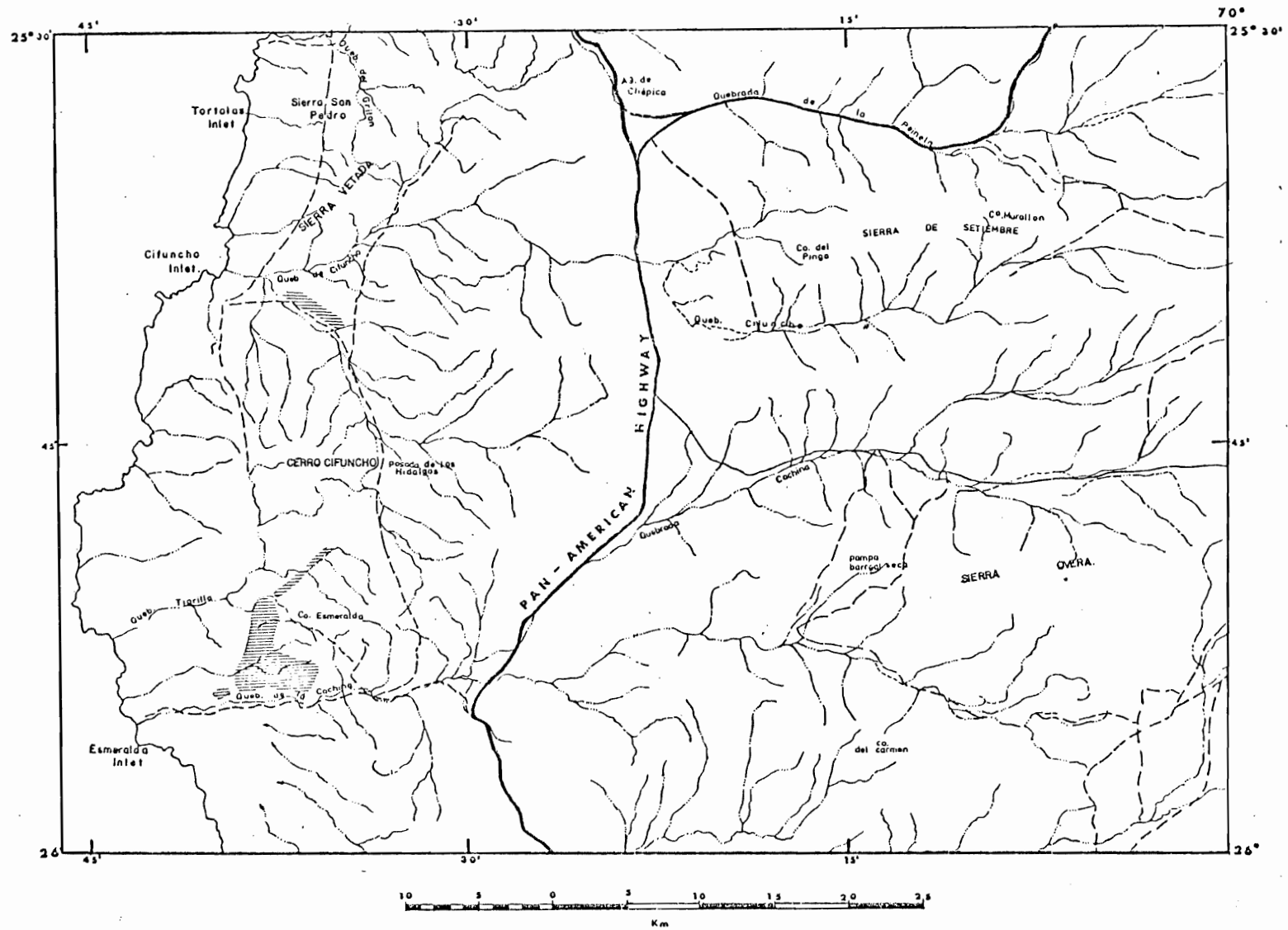
### Distribution

The outcrops of Pan de Azúcar Formation appear to be restricted to the western part of the study area (Figures 2.3 and 2.7) Between La Cachina gully and Cifuncho gully, in a continuous band. Its continuity has been recognized outside the study area (Naranjo, 1968).

### Lithology

The sequence is composed of predominantly gray greenish, reddish conglomerate, green yellowish sandstones, dark brown limestones, green yellow-dark shales and gray greenish to gray yellowish conglomeratic sandstones.

FIGURE 2.7 Distribution map of the  
Pan de Azúcar Formation (shaded).



Two km north of Aguada Jacinto Díaz (Figure 2.3) the following sequence can be observed from top to bottom:

Unit	Description	Thickness (m)
1	Sandstone, green yellowish, medium to coarse grained; poorly stratified; green shale intercalated; highly weathered. It contains 3 concordant "veins" of black chalcedony (chert?). Thin, lenticular layers of fine conglomerate composed of clasts of quartzite, granite and porphyry at the bottom.	53
2	Limestone, white (brown dark on fresh surface), thinly bedded; thin lenticular fine conglomerates at the bottom, yellow shales at the top, both as intercalations. Scarce fossil fragments poorly preserved within the limestone.	14
3	Sandstone, white yellowish, brown yellowish, medium to fine grained; well stratified beds of 20-30 cm thick. Locally these are coarse grained and show some lithic fragments.	76
4	Shale, whitish, dense; silicified. Scarce ammonites.	5
5	Shale, green yellowish (gray-white on fresh surface); fissile on surface. Ovoid shaped concretions of 20 cm diameter at depth.	20
6	Alternation of beds medium grained sandstone with beds 20-30 cm thick, yellow orange of well bedded limestone.	19
7	Alternation of beds of green shale with beds of well stratified limestone.	78
8	Sandstone, yellow orange, coarse grained ranging to conglomerate with fragments of gray shale.	42
9	Limestone, well bedded, 20 cm thick. At the bottom a black limestone with abundance of fossils.	56

Unit	Description	Thickness (m)
10	Calcareous shale, gray yellowish, compact, fissile on weathered surfaces.	15
11	Calcareous sandstone, gray dark, coarse grained to conglomeratic; scarce fossils.	0.1
12	Calcareous shale, yellow; fissile on weathered surface with scarce interbeds of black, coarse grained, sandstone with beds 50 cm thick; abundant ammonites at the top.	9
13	Calcareous shale, black, yellow with interbeds of calcareous, coarse grained sandstone, 10-20 cm thick, with beds of calcareous conglomeratic sandstones. Occasionally, the sandstone contains remains of carbonaceous material. This unit contains three layers of thin, fossiliferous shale, located at 8, 14 and 22 m from the bottom of the unit.	25
14	Shale, gray white; well bedded; numerous calcareous concretions, white (ranging between 0.40 m - 1.20 m), oval to spherical. In the middle of this unit there is a bed of yellow calcareous fissile shale, 9 m thick; scarce fossils at the bottom.	16
15	Alternation of yellow gray white, calcareous, fissile shale, with yellow greenish, compact shale. Scarce fossils.	46
16	Shale, yellow, calcareous, fissile with intercalations of medium grained quartz sandstone; flow and load cast.	37
17	Shale, red purple, fissile.	5
18	Shale, yellow, calcareous. Abundance of fossils at the bottom and at the top.	5
19	Shale, yellow, calcareous, fissile with intercalations of gray, fine grained sandstone. At the top of this unit there are two beds of black fossiliferous shale with carbonaceous remains.	36

Unit	Description	Thickness (m)
20	Shale, yellow, calcareous, fissile, intercalations of white limestone, 20 cm thick. This unit contains 5 fossiliferous beds of 1-2 m thick located at 7, 19, 24, 28 and 32 m from the bottom of the unit.	39
21	Sandstone, gray yellow, medium to coarse grained (locally conglomerate) poorly bedded; 20-30 cm thick. Intercalations of limestone, shale and fine sandstone with fossils. The fossiliferous beds are located at 2, 21, 31, 41 and 82 m from the bottom of the unit.	92
22	Conglomerate, brown white, clasts of 3-4 cm; andesitic (?) composition. Intercalations of coarse grained sandstone, 10-100 cm thick. Locally ripple marks can be observed.	73
TOTAL		761

### Structural Relationships

The Pan de Azúcar Formation is locally strongly folded (disharmonic folds) making it easy to distinguish from the overlying formations. With the exception of local faults, no major faults have been seen that affect the sequence greatly. The lower contact of the formation was observed in the type locality and west of Cerros Buena Esperanza (Figure 2.3). There are outcrops of a basal greenish, reddish conglomerate lying unconformably on limestone and sandstone of the Cifuncho Formation. The upper contact was observed west of Cerros Buena Esperanza

(Figure 2.3) where a fault separates the Pan de Azucar Formation from the La Negra Formation (see Below).

#### Depositional Environment

On the basis of its lithology and its sedimentary structures the Pan de Azucar Formation reflects a marine deposition by turbidity currents. The marine transgression continued during this time, reworking the Triassic sediments and increasing the depth of the Basin, accompanied by submarine (?) volcanic effusions.

#### Age and Correlation

The marine sediments of the Pan de Azucar Formation contain abundant fossils, in different states of preservation. The collected fossiliferous material was studied and classified by Corvalán (1960, 1970), who reports the following taxa:

Arietites

Charmasseiceras

Arnioceras

Oxytoma

Psiloceras (Franziceras)

Pseudaetomoceras

Kammerkaroceras

Pecten



Commenting on the age indications of this collection, Corvalan stated that "Psiloceras (Franziceras), Pseudaetomoceras and Kammerkaroceras are restricted to the Hettangian". In addition "the genus Arietites, Charmasseiceras and Arnioceras and some Pelecypods belonging to Oxytoma genus are common in the Sinemurian, and the genus Charmasseiceras and Arnioceras are restricted to this stage".

Zeil (1960) collected from the following localities:

a. Westward of Quebrada Tigrillos

Arnioceras cf. semicostatum (Young and Bird)

Arnioceras cf. laevissimum (Quenstedt)

Schlotheimia (Charmasseiceras) sp. Juv.

Paltechioceras? sp.

Meleagrinnella? ("Pseudomonotis") substriata (Munster)  
von Zieten

Arnioceras sp.

Arnioceras cf. ceratitoides (Quenstedt)

b. At Esmeralda Mine

Arnioceras cf. semicostatum (Young and Bird)

Arnioceras cf. ceratitoides (Quenstedt)

Arnioceras sp. Juv.

Schlotheimia (schl.) cf. donar (wahner) pachygaster (Suttner)

The fossils were identified by K. W. Barthel of the Bayerischen Staatssammlung für Palaeontologie und Historische Geologie (München). The collection demonstrates the presence of the Hettangian and Sinemurian stages.

In summary, the fossil fauna and the structural relations lead one to consider the Pan de Azúcar Formation to be of Hettangian-Sinemurian age.

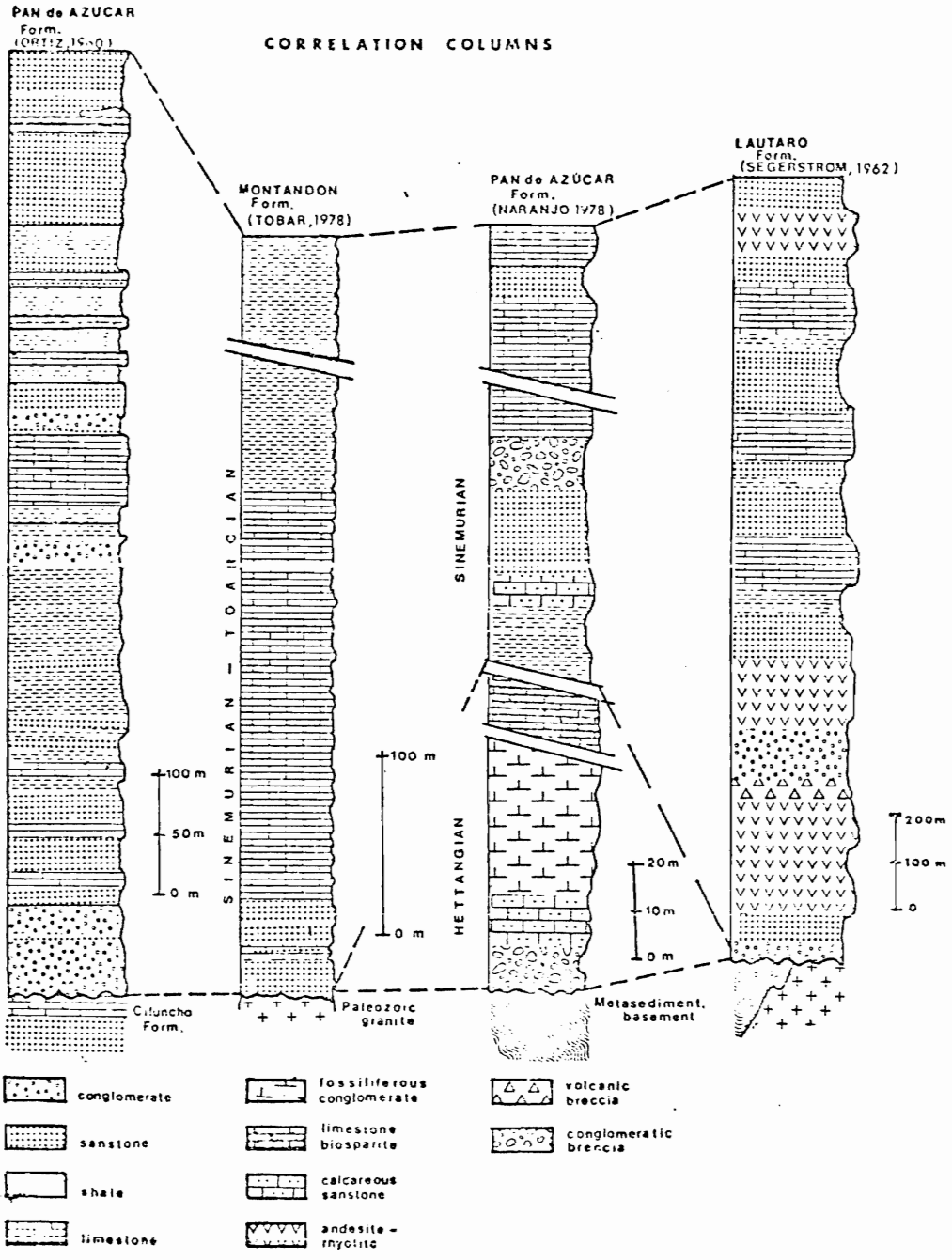
Several formations outcropping outside the study area can be correlated with the Pan de Azúcar Formation. A thick section of Jurassic strata, largely marine, is exposed continuously along the Domeyko range through Salvador and Potrerillos and continuing south. The extent is over 450 km between Antofagasta and Atacama provinces.

The Pan de Azúcar Formation is correlated with the El Profeta Formation of Chong (1977), which outcrops between Lat.  $24^{\circ}$  and  $25^{\circ}$ S. There the formation consists of volcanic (rhyolite) and marine (limestone) sediments with an abundant fossil fauna studied and classified by Chong (1977) and Von Hillebrandt (1973). The formation has a very wide span from Hettangian to Tithonian.

Southeast of the study area, Segerstrom (1959) described the Liassic Lautaro Formation, whose type locality is Tranque Lautaro ( $27^{\circ}53'S-70^{\circ}W$ ) located some 195 km south of El Salvador. There the formation consists of volcanic rocks (Sinemurian), marine sediments (Pliensbachian) and andesitic lavas (Lower Toarcian) (Figure 2.8).

At Montandon Station ( $26^{\circ}23'S-69^{\circ}25'W$ ) and along Quebrada Asientos ( $26^{\circ}24'S-69^{\circ}22'W$ ) a sequence of fossiliferous marine strata known as the Montandón Formation (Tobar, 1977) is exposed.

FIGURE 2.8 Correlation columns for the  
Pan de Azucar Formation.



It consists of sandstones alternating with sandy fossiliferous limestones, arkose, sandy conglomerate (Pliensbachian); black limestone intercalated with Black calcareous shale (Toarcian); limestone and shale (Bajocian).

#### Posada Hidalgos Formation

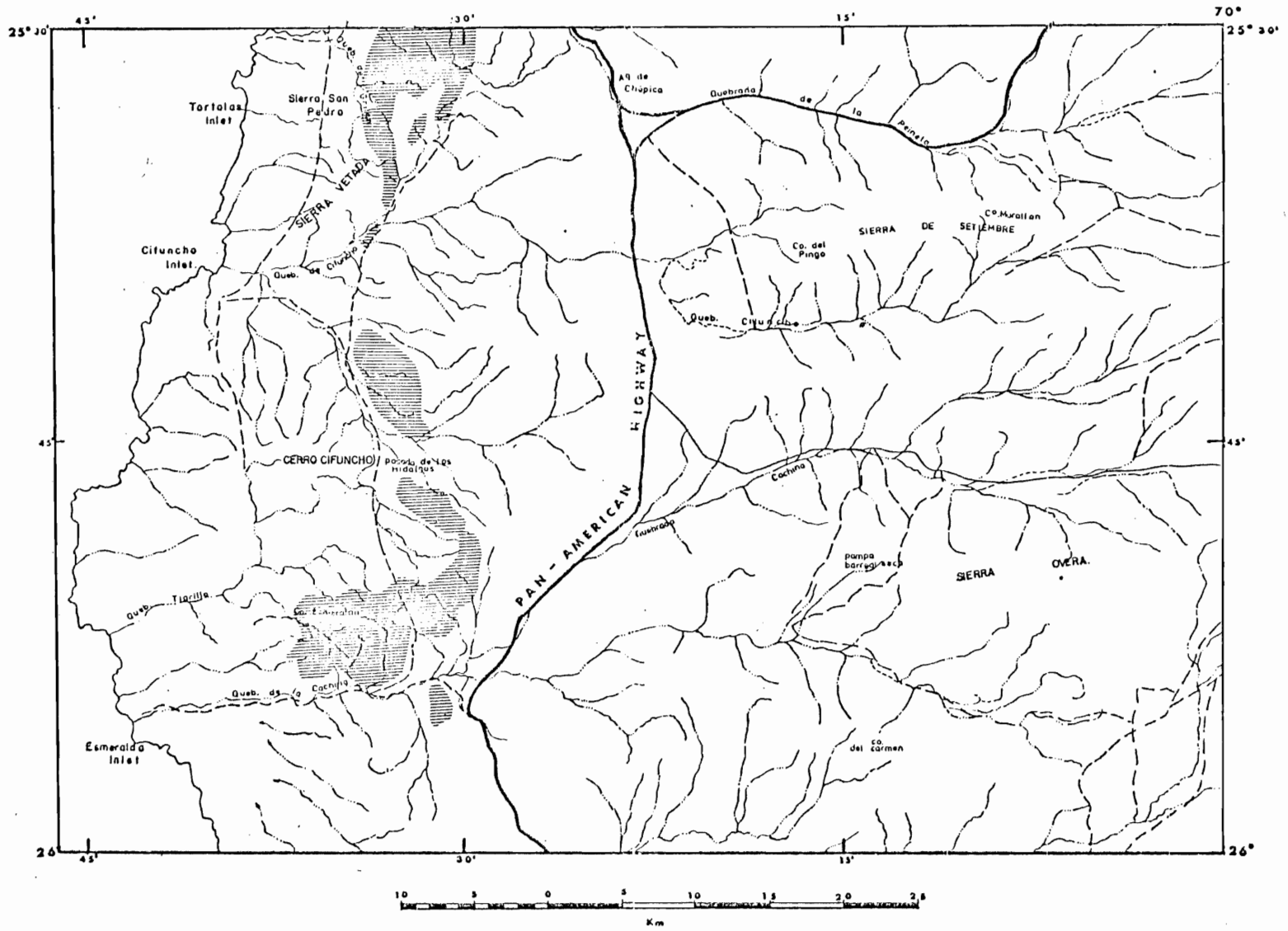
The Posada Hidalgos Formation was defined by Ortiz (1960) in Posada Hidalgos gully, east of Sierra Cifuncho, 2 km north of Aguada Jacinto Díaz (Figure 2.3). There crops out a sequence 1000 m thick of breccias, conglomeratic breccias, rhyolites, sandstones, shales and limestones. It is widespread along the western side of the study area (Figure 2.9).

Although Corvalán (1960) proposed to consider only the Posada Hidalgos Formation divided in two members: Pan de Azucar (lower) and Posada Hidalgos (upper), on the basis of the lithologic characteristics and structural relationships, the same author (1965) refers to them as formations. In agreement with García (1960) and Ortiz (1960), the present author considers that both units fill the requirement of distinctive lithology, unappability, etc. to be considered formations.

#### Distribution

The Posada Hidalgos Formation is well exposed in a narrow area extending from La Cachina gully to outside the north border of the study area (Figure 2.9). Intrusive bodies interrupt the continuity of the sequence.

FIGURE 2.9 Distribution map of the  
Posada Hídalgos Formation (shaded).



## Lithology

The formation consists of red brown, coarse, medium, and fine conglomerate with quartzite, granite, rhyolite, phyllite and sandstone clasts in a sandstone matrix; gray, green, dark brown, brown, red, coarse to fine sandstone; intercalations of red, dark gray fossiliferous shale, gray fossiliferous limestone; intercalations of dark brown, rhyolitic conglomerates; breccia. The type section 2 km north of Aguada Jacinto Díaz is from top to bottom:

Unit	Description	Thickness (m)
1	Rhyolitic breccia and conglomerate breccia, dark brown, fine grained, massive intercalations of reddish, fine, well stratified sandstone, 20 cm thick, and poorly sorted flow breccia. Toward the top it changes to a normal lava flow. Under the microscope the rhyolite shows a porphyritic texture and a cryptocrystalline to pilotaxitic groundmass. The phenocrysts are plagioclase ( $An_{0-10}$ ), altered to clay minerals, sericite and calcite.	398
2	Rhyolite, gray bluish, yellow greenish; massive. Under the microscope it shows a porphyritic texture and a pilotaxitic groundmass. The phenocrysts are plagioclase ( $An_{0-10}$ ), altered to clay, sericite, chlorite and calcite.	183
3	Limestone, gray-yellowish, beds of 20-30 cm thick, containing feldspar fragments. Abundant fossils.	6
4	Sandstone, gray-greenish; fine-grained; fragments of silicified tree trunks.	4
5	Rhyolite breccia, dark brown; clasts of 20-25 cm; no bedding.	79.5
6	Rhyolitic breccia, yellow-greenish at the bottom, brown-white at the top. Similar to unit 1.	8



Unit	Description	Thickness (m)
7	Tuff, gray-greenish, partially brecciated; scarce intercalations of green purple shale, 5-10 cm thick.	48
8	Intercalations of gray-white reddish sandstone, locally conglomerate, with ripple marks, and gray greenish shale.	4
9	Intercalations of yellow-grayish limestone, calcareous sandstone and yellow greenish sandstone, medium to coarse grained. Local thin intercalations of purple shales. Abundant fossils.	10
10	Limestone (calcareous sandstone?), dark yellow; abundant flora and fauna fossils.	1
11	Sandstone, yellow greenish, medium to coarse grained.	16
12	Rhyolite breccia, dark brown.	13
13	Intercalations of gray-greenish sandstone, fine grained and gray-greenish sandstone, coarse grained.	5
14	Rhyolite, brown-yellow; lateral variations to rhyolitic breccia. Local intercalations of feldspathic sandstone.	47
15	Shale, yellow-grayish, feldspar fragments, fragments of silicified tree trunks and fossil fauna.	1.5
16	Sandstone, gray-greenish, medium to coarse grained, abundant fossils.	2.5
17	Sandstone, gray-greenish, fine grained, calcareous. Fossil fauna.	12
18	Sandstone, yellow-green, medium to coarse grained; abundant fossils.	7
19	Sandstone, green-gray, coarse grained; abundant flora and fauna fossils.	10

Unit	Description	Thickness (m)
20	Shale, yellow; compact, abundant flora and fauna fossils; sandstone, green gray; medium grained.	6.5
21	Sandstone, green gray; medium to coarse grained; calcareous. Flora and fauna fossils.	10
22	Sandstone, green gray, fine grained.	3
23	Shale, yellow, abundant fauna and flora fossils.	5
24	Sandstone, green gray; medium to coarse grained; abundant fossil plants.	2.2
25	Sandstone, gray greenish; medium to coarse grained; locally conglomeratic; thickly bedded; intercalations of dark brown shales, 10 cm thick.	27
26	Volcanic conglomerate.	1
27	Sandstone, green grayish, fine to medium grained; locally conglomeratic.	79
28	Sandstone, green, coarse grained; intercalations of rhyolitic conglomerate.	32
TOTAL		1021.2

### Structural Relationships

The Posada Hidalgos Formation shows open folding with wide synclines and anticlines, except where the formation is intruded by plutonic bodies (i.e. Sierra Esmeralda, Figure 2.3). Faults and minor intrusions affect the sequence, producing silification and carbonatization in some places (i.e. west of Sierra Buena Esperanza, Figure 2.3).

According to Ortiz (1960) the lower contact of the formation is "abnormal" because the breccias of the bottom of the sequence rest over different units of the Pan de Azúcar Formation. The regional mapping showed a gentle angular discordance between the underlying Pan de Azúcar Formation and the Posada Hidalgos Formation.

The upper contact of the Posada Hidalgos Formation is an angular discordance separating this formation from the overlying La Negra Formation (see below). South of Cifuncho gully a fault separates both formations. The Pan de Azucar and Posada Hidalgos Formations have been intruded by a small number of dikes of andesite (basaltic andesite?) presumably related to the flows of La Negra Formation (see below). In Sierra Esmeralda and south of Cifuncho gully both formations are intruded by dioritic plutons (see below).

#### Depositional Environment

The lithologic characteristics and the faunal content suggest a marine deposition (sandstone, shale, limestone) by turbidity currents (cross bedding, ripple marks, graded bedding). The presence of rhyolitic volcanic breccia suggests volcanic activity (submarine?) with flows of rhyolite and andesite. Perhaps the source of this material was close to the area of deposition and this presumably shows the first manifestation of the volcanism which would later attain a wider development.

## Age and Correlation

The Posada Hídalgos Formation contains a relatively abundant marine fauna and plants in different stages of preservation. The fossil content was studied by Corvalán (1960, 1970) who reported the following taxa:

Vola alata (v. Buch) Bayle et Coq.

Rhynchonella

Pleurotomaria

Cardinia

Trygonia

Gastropod molds

Pecten

Vegetal debris

Montlivaultia

Rhynchonella

Pholadomya

Arietites

Astarte

Plagiostoma

Tree trunk well preserved

Commenting on the age indications of this collection, Corvalán stated that the "most representative genera would be Vola-alata (v. Buch), Bayle et Coquand, Cardinia, Trygonia, Pholadomya, Pecten, Plagiostoma, Pleurotomaria, Rhynchonella,

Montlivaultia and Arietites". The faunal association indicates Upper Sinemurian, and would represent the end of the late Liassic epoch (Lotharingian) and perhaps the base of the middle Liassic (Pliensbachian). Several formations outcropping outside the study area can be correlated with the Posada Hidalgos Formation. Sinemurian and Pliensbachian marine fossiliferous sediments are described by Chong (1977) in the Domeyko Range (25°30'S-27°30'W) and by Tobar (1977) along the Asientos gully (Montandón Formation) (see Figure 2.10).

#### La Negra Formation

The most extensive stratified rocks in the study area represent a volcanic-clastic sequence developed in the Early Jurassic through the Lower Cretaceous.

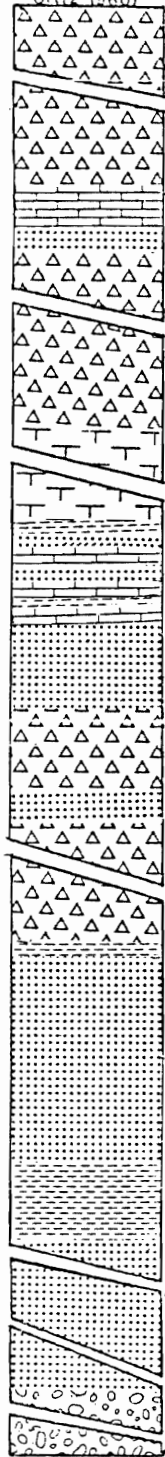
The La Negra Formation was defined by García (1967) in Quebrada La Negra, 6 km south of Antofagasta, and comprises a thick sequence (10,000 m) of andesite flows and breccias with intercalations of red clastic continental beds. The sequence is continuous from south of Iquique (Lat. 20°S) to Copiapó (Lat. 27°S).

#### Distribution

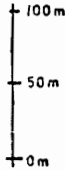
The La Negra Formation crops out in a wide band along the central part of the study area (Figures 2.3 and 2.11) in a north-south trend. It extends farther south, in areal continuation and is part of a continuous belt of outcrops

FIGURE 2.10 Correlation columns for the  
Posada Hidalgos Formation.

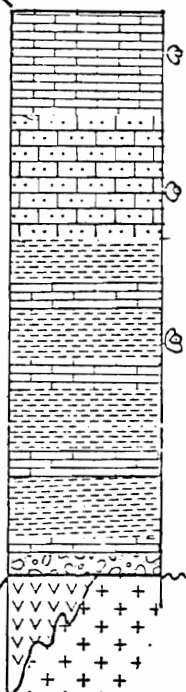
Posada Hídalgos Form.  
(Ortiz, 1960)



Pan de Azúcar  
Form.



Montandon Form  
(García, 1957)



(750m)

LEGEND

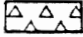
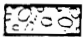
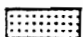
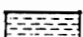
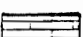
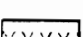
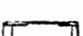
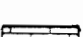


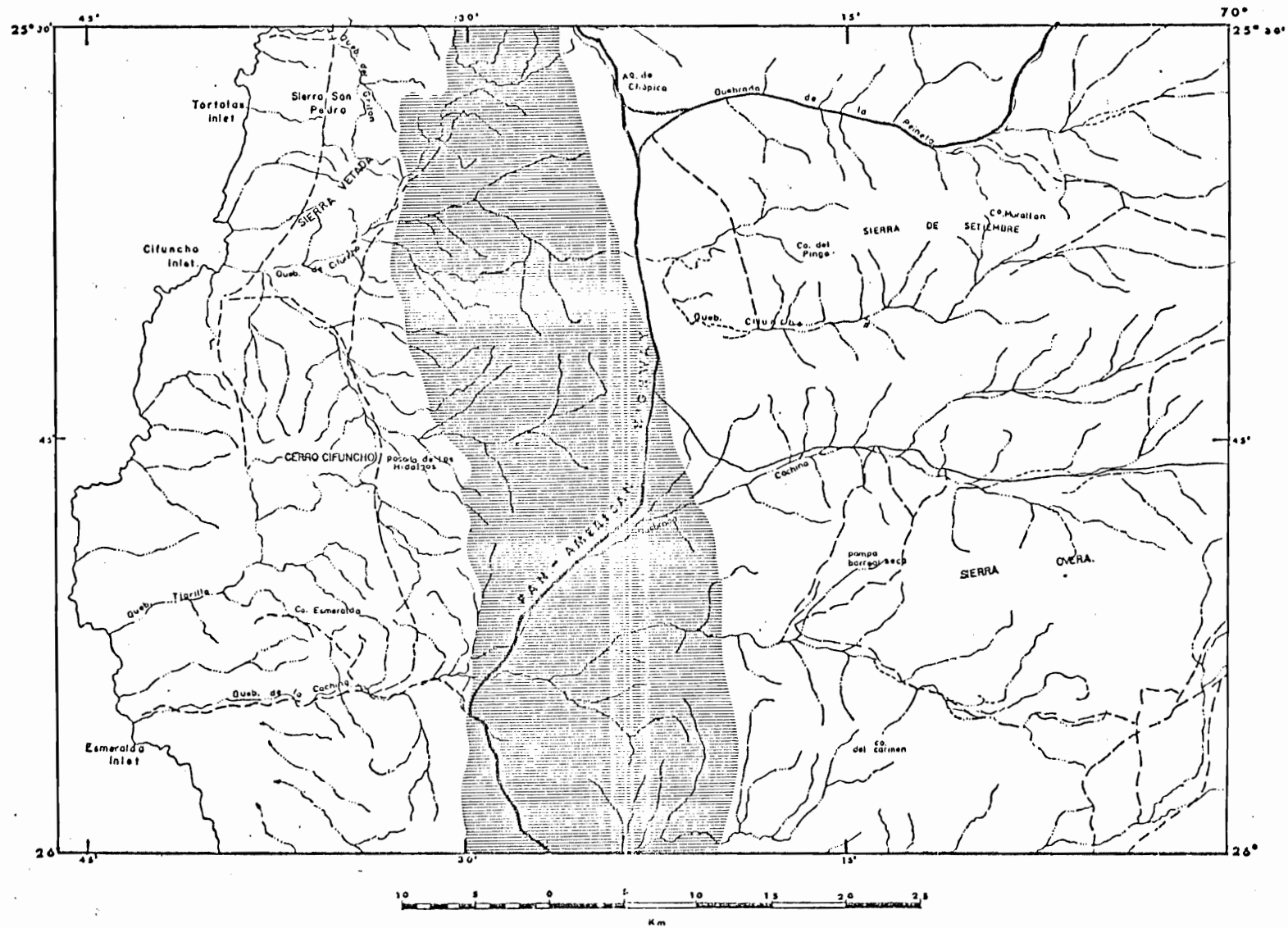
-  Volcanic Breccia
-  Conglomerate
-  Sandstone
-  Shale
-  Limestone
-  Rhyolite - Andesite
-  Tuff
-  Sandy Limestone
-  Fossil Fauna
-  Fossil Flora

FIGURE 2.11 Distribution map of the  
La Negra Formation (shaded).





extending along the coastal cordillera for over 500 km between Iquique and Copiapo.

### Lithology

The La Negra Formation comprises mainly dark-coloured, massive, andesite flows, flow Breccias, agglomerates and tuffs, with intercalations of reddish brown sandstones and a thin conglomeratic bed at the bottom. Various dykes and sills intrude the sequence, increasing its thickness. The rocks are predominantly andesites with local intercalations of basaltic andesite or basalt and consist of dark-grayish olive, porphyritic labradorite andesite, maroon to reddish brown porphyritic (augite-labradorite) andesite; maroon to purple porphyritic (andesine) andesite. The texture ranges from porphyritic (size 0.2-1 mm) to coarsely porphyritic (size 5 mm to cm); the phenocrysts are andesine to labradorite plagioclase and clinopyroxene; modal percentage analysis of them shows labradorite ( $Au_{62-68}$ ) 50-55%; labradorite ( $Au_{50-67}$ ) 3-35%; augite 3-5%; labradorite ( $Au_{56-69}$ ) 30-35%; epidote and chlorite after clinopyroxene 1-2%.

The groundmass is mainly hyalopilitic, intersertal or intergranular and consists of plagioclase laths and microlites with interstitial opaque grains, epidote, chlorite, devitrified glass and carbonate. The lava flows contain intercalations of gray-white to red-yellowish ignimbrite, probably of rhyolitic composition.

### Structural Relationships

The La Negra Formation is a volcanic sequence constituted by a succession of andesite flows of 2-10 m thickness and massive andesite in monoclinial arrangement. The lower contact is an angular and erosional unconformity with the underlying Posada Hidalgos Formation. It was observed northeast of Sierra Esmeralda; there a dark brown basal conglomerate rests over sandstones with fossil fauna. South of La Cachina gully, the formation overlies the Las Tortolas Formation (Paleozoic). Northward, south of Cifuncho gully, a fault separates this sequence from the underlying Posada Hidalgos Formation (Figure 2.3).

The upper contact was not observed because the sequence is cut in the east by the Atacama Fault, along the whole area.

### Depositional Environment

The great regularity and extent of the lava flows, the absence of preserved volcanic structures, the numerous andesitic dykes cutting the Mesozoic formations and the intercalations of sandstone, suggest a subaerial environment with explosive episodes (ignimbrites) near the source of the andesites; another possibility is that the material was transported from an area of volcanic activity, perhaps located farther east.

South of the study area the formation has intercalations of fossiliferous limestones suggesting a marine deposition with

submarine andesite lava flows.

This variation in the lithology suggests that during the marine transgression the area was a topographic high, though probably very close to sea level.

#### Age and Correlation

The lithology of the La Negra Formation is very similar to the sequence described by Naranjo (1978) south of the study area, but nowhere in the mapped area were any fossils found; the only available criteria that would suggest the age are the lithology and structural relations. The unit lies with marked angular unconformity over marine sediments of the Posada Hidalgos Formation (Sinemurian-Pliensbachian) and metamorphic rocks of the Las Tórtolas Formation. Toward the top the sequence is interrupted by the Atacama Fault Zone. Thus the formation can be assigned only a post Sinemurian-Pliensbachian age and a pre-Neocomian age in the study area.

The formation is intruded by small bodies of porphyritic diorite but radiometric dating has not been done due to the altered nature of the plutonic rocks.

The La Negra Formation is correlated with the volcanic sequence outcropping near Antofagasta (García, 1967), whose type locality is the La Negra Station. There the formation consists of ca. 10,000 m of continuous porphyritic, amygdaloidal andesitic flows with intercalations of porphyritic breccia and red, coarse

grained sandstone. This unit is overlain with angular unconformity by Caleta Coloso Formation (Neocomian, García 1967; Barremian, Harrington, 1961; Kimmeridgian, Tobar, 1966).

The closest outcrops of Jurassic volcanic rocks in areal continuation with those of the mapped area are south of the study area, in Sierra Minillas ( $26^{\circ}06'S-70^{\circ}18'W$ ). There the formation consists of andesites, andesitic breccias and intercalations of marine sedimentary rocks with abundant fossil fauna (Bajocian).

The La Negra Formation is correlated with the Callovian Potrerillos Formation of Tobar (1977), whose type locality is 5 km west of Montandón Station ( $26^{\circ}23'S-69^{\circ}25'W$ ).

In summary, in the study area it is difficult to assign an absolute age to the La Negra Formation; more detailed studies are necessary.

#### The Cretaceous Aeropuerto Formation

During the field work, two formations were distinguished, essentially based on lithologic characteristics: the Aeropuerto Formation and the Teresa Colmo Formation. However both formations appear to correspond to the same lithostratigraphic unit. The Teresa Colmo Formation is intruded by a Cretaceous plutonic body (see below) and the Aeropuerto Formation does not show a clear relationship with the intrusion because of the Atacama Fault Zone that affects the formation, but both belong to the

same depositional environment.

A well exposed sequence, at least 2500-3000 m thick, of conglomerates, sandstones, limestones and andesites overlying volcanic Jurassic rocks is informally named, for the purpose of this thesis, the Aeropuerto Formation and comprises two members spatially separated by the Cretaceous batholith.

#### Member 1

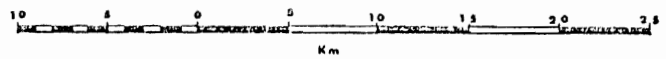
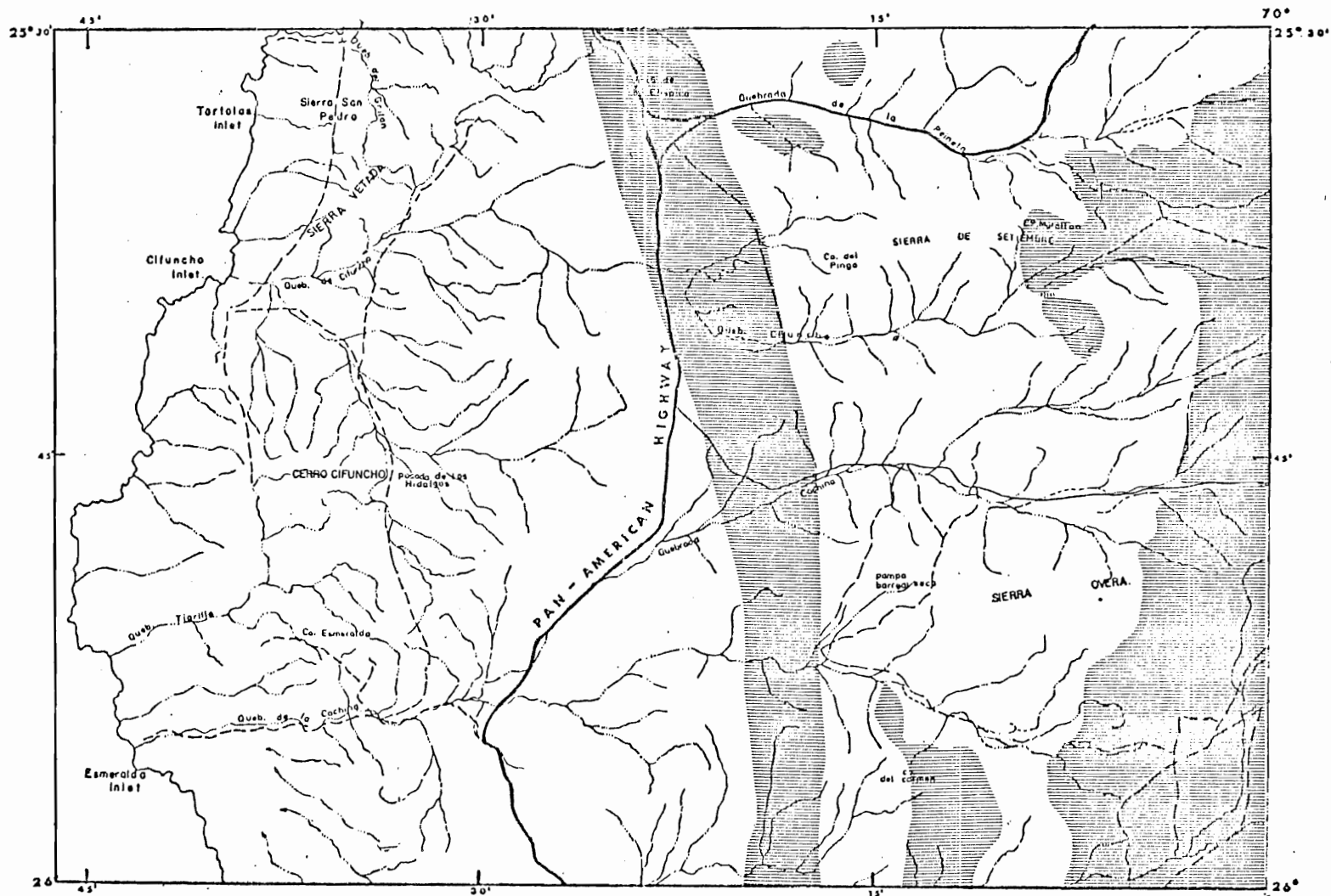
A unit between 1500-2000 cm thick of predominantly conglomerates, sandstones, limestones and andesites is widespread in the central part of the study area, north of La Peineta gully, south of Pan de Azúcar gully (Figures 2.3 and 2.12).

Because the lack of a suitable type section exposing both contacts of the unit and the scarce number of outcrops do not allow its thickness to be measured, this unit is informally named the Aeropuerto Formation member 1, after the Taltal airport where the best known outcrops are situated.

#### Distribution

The outcrops of member 1 appear to be restricted to the central part of the area in a northwest trend, between the Atacama Fault and La Isleña Fault. The outcrops can be followed along the whole area and to the north and south beyond its boundaries. Another area of outcrops is located between the Sierra del Pingo and Quebrada de la Peineta (Figure 2.3).

FIGURE 2.12 Distribution map of the  
Aeropuerto Formation (shaded).





They show a subcontinuous distribution and can be identified by their violet-gray and maroon colour.

### Lithology

The most distinctive features of member 1 are the rounded shape of its outcrops and its homogeneity. It consists of dark maroon, coarse conglomerates containing cobbles and boulders of granite, diorite, granodiorite, quartz pebbles; maroon, coarse to medium grained sandstones consisting mainly of rounded quartz and feldspar grains, violet-gray to maroon conglomeratic breccia consisting of andesitic clasts in a matrix volcanic sandstone, and yellow fossiliferous (Exogyra), mineralized limestones. Andesites are intercalated in different levels of the sequence and toward the top of the formation.

Southward, the thickness of member 1 decreases, partially due to the granitoid intrusion that affects it. In La Peineta gully outcrop violet-gray and maroon, fine grained sandstones (arkosic) and maroon to olive-gray breccias with an argillaceous to sandy matrix containing heterogeneous clasts of quartzite, argillite, angular clasts of a chert-like rock and coarse pebbles and cobbles of heterogeneous granitic rocks. They unconformably overlie Paleozoic rocks.

### Structural Relationships

The outcrop area is characterized by a flat topography, limited by the Atacama Fault Zone. The lower contact was

observed west of Taltal airport where a small outcrop of conglomerates and sandstones exists. It is separated from the lower volcanic rocks of the La Negra Formation by the Aguada de Chépica Fault. The upper contact is the Isleña Fault where it is in structural contact with Paleozoic rocks and Mesozoic granitoids. This contact can be observed along the whole area, trending north-south to northeast.

Most of the sequence shows open folding; limestone and sandstone, however, are more folded (i.e. Unión mine) forming synclinal and anticlinal structures. Conspicuous fault slices of limestone occur in the central part of the Atacama Fault Zone, between Taltal airport and La Cachina gully.

#### Member 2

Along the eastern border of the area under study, outcrops a sequence 1000 m thick composed predominantly of conglomerates, breccias and sandstones with intercalations of andesites.

Because the lack of a suitable type section exposing both contacts of the unit and the extensive plutonic body intruding it do not allow the thickness to be measured, this unit is informally named member 2 (Teresa Colmo), after the Teresa Colmo mine where it has its best development.

#### Distribution

The outcrops of member 2 are distributed along the eastern border of the area, from Pan de Azucar gully to La Peineta gully;

at the east side of Sierra Overa, Sierra Providencia and Sierra Murallon (Figures 2.3 and 2.12]. Some patches outcrop at the Sierra Murallon, as a roof-pendant on the granitic intrusion.

### Lithology

Member 2 consists of dark red coarse conglomerates with boulders and cobbles of andesite in a red volcanic sandstone matrix; red medium grained sandstone with graded bedding; dark red to reddish brown medium grained conglomerate intercalated with sandstones, with interbeds of gray-purple andesites and beds of red sandstones.

The andesites show a high magnetite content and near the contact with the granitic intrusion its content increases where they are affected by contact metamorphism.

### Structural Relationships

The lower sections of member 2 appear much affected by the granitic intrusion, so that lower contact of the formation was not observed. West of Pampa Sierra Overa an intrusive contact can be seen, where patches of andesite appear in the granitic intrusion.

The upper contact does not outcrop in the study area; it appears to be covered by Cenozoic (?) deposits which fill the plain.

### Depositional Environment

The conglomerates, sandstones, limestones and volcanic breccias and conglomerates suggest a shallow-water deposition with subaerial episodes.

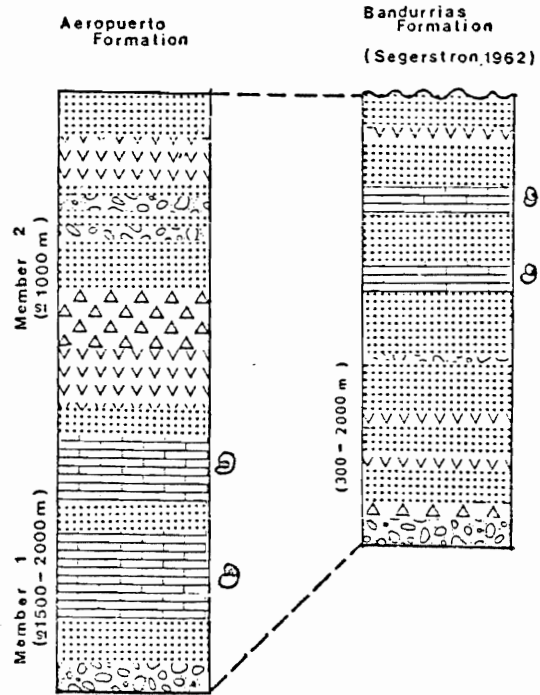
### Age and Correlation

The Aeropuerto Formation does not contain enough fossils to permit a more accurate definition of its age; the only fossils are pelecypod remains of Exogyra, sp. which do not allow a precise age determination because their range includes both the Triassic and Cretaceous Periods.

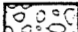

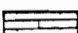
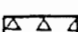
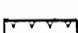

The Aeropuerto Formation is intruded by an extensive plutonic body extending in a north-south trend. The isotopic dating of samples of this intrusion suggest a Lower Cretaceous age (Hauterivian-Aptian) (see below). A sample of andesite of member 1 of the formation yielded a Lower Cretaceous age (Valanginian-Hauterivian) (see below). Thus, the formation can be assigned only a post-Triassic age and a pre-Hauterivian-Aptian age.

The Aeropuerto Formation can possibly be correlated with the continental, Lower Cretaceous Caleta Coloso Formation of Garcia (1967); with the volcanic rocks and marine sediments of the Lower Cretaceous Bandurrias Formation of Segerstrom (1968) and Tobar (1977) (see Figure 2.13) and with the continental Upper Jurassic-Lower Cretaceous Estratos de los Cerros Florida Formation of Naranjo (1978).

FIGURE 2.13 Correlation columns for the  
Aeropuerto Formation.



**LEGEND**

-  Conglomerate
-  Sandstone
-  Limestone
-  Volcanic Conglomerate
-  Andesite
-  Fossil Fauna

### Tertiary-Quaternary Sediments

Different types of unconsolidated to poorly consolidated clastic deposits crop out in the study area. They occur along the coastal platform and in the arid inland desert as well. Most of them are easily recognizable both in the field and on aerial photographs but the scale of mapping (1:100,000) is not large enough to represent them.

Four basic types of unconsolidated deposits were differentiated during the mapping:

1. Tertiary-Quaternary Alluvium: they correspond to primarily basin deposits, pediment gravels, older alluvium, coalescing colluvium and younger alluvium that occurs in inland basins and on older erosion surfaces. Locally they include eolian sand. These deposits correspond to several phases (I-IV) of the landscape evolution of the Atacama Desert (Mortimer, 1973) and they are assigned to the Eocene-Holocene.
2. Quaternary stream channel deposits: they correspond to stream gravel and sand filling youthful seaward-draining canyons.
3. Quaternary marine terrace deposits.
4. Quaternary non-marine deposits: they correspond to accumulation of debris, consisting of alluvial fans, talus cones, colluvium, landslide material and debris-flow material spread over the coastal platform both during and after marine terracing.

## Igneous Rocks

Plutonic rocks and related hypabyssal intrusive rocks underlie much of the study area and the adjacent ones. Significant intrusive events are recorded during the Paleozoic (Permian-Devonian) and Mesozoic (Jurassic to Cretaceous). The plutonic rocks intrude sequences of Paleozoic sedimentary rocks and several sequences of Mesozoic sedimentary and volcanic rocks. They reach their greatest areal extent in the eastern part of the mapped area (Figure 2.3). They range in size from sills, dikes, and small stocks to batholiths, the latter with outcrops of hundreds of square kilometers. They tend to be elongate with long axes parallel to the north-south tectonic trend of the Andes. Most of the dated rocks are from the central part of the area because they are closely related to the tectonic development and because some of the plutons they represent seem to be genetically related to mineral deposits.

Detailed petrological discussions are beyond the scope of this thesis; for the purpose of description, however, a number of whole rock chemical analyses were made. Table 2.3 shows the chemical analyses of the dated igneous rocks and in Figure 2.14 they are classified in the Streckeisen diagram.

Subdivisions of the plutonic rocks are not represented on the map because of the scale (1:100,000); during the field mapping, however, a subdivision of the rocks was possible in well-exposed localities.



FIGURE 2.14 Distribution of studied plutonic samples  
in the APQ classification diagram.

Numbers refer to Table 2.2.

1.-Quartz-rich granitoids.

2.-Tonalite.

3.-Granodiorite.

4.-Monzodiorite/monzogabbro.

5.-Diorite/gabbro/anorthosite.

6.-Monzonite.

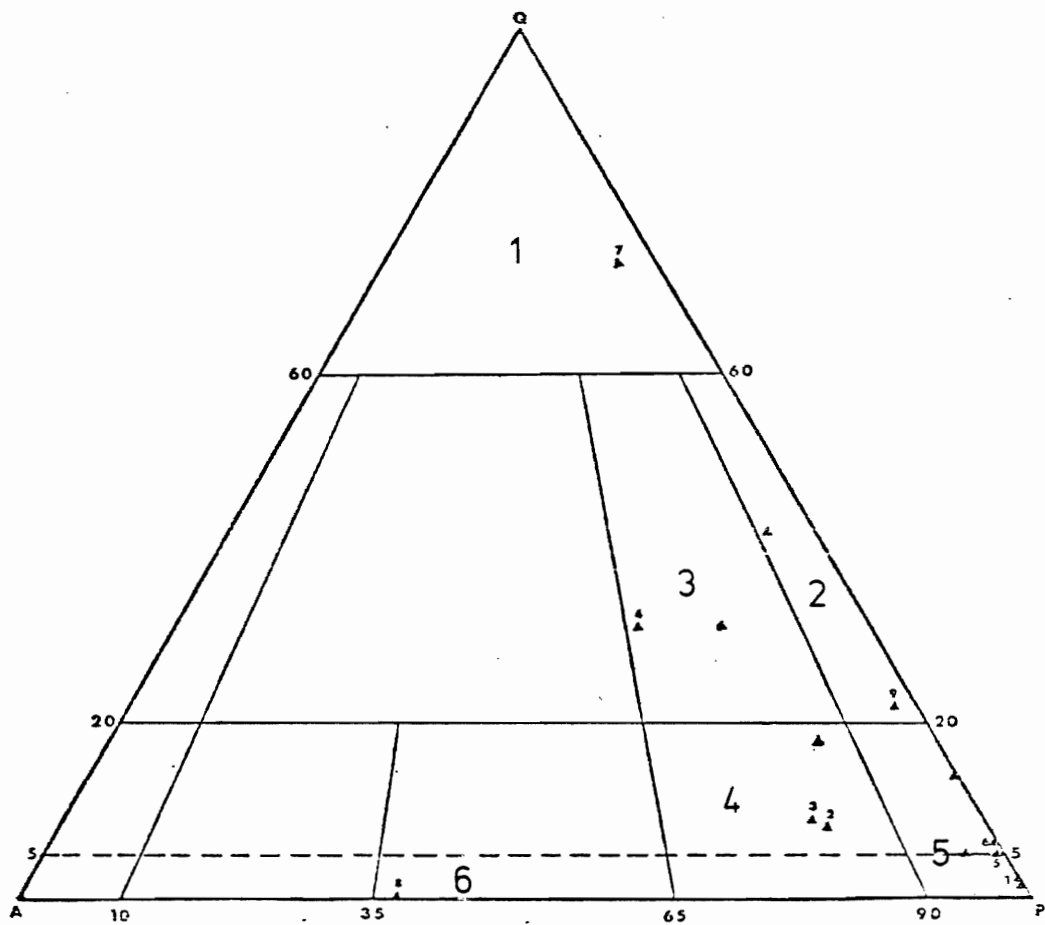


TABLE 2.2

## Chemical analyses of the dated rocks

	1**	2	3	4	5	7	8	12	13	15
SiO <sub>2</sub>	51.01*	59.30	62.21	69.70	51.72	66.54	54.13	58.58	60.77	49.54
Al <sub>2</sub> O <sub>3</sub>	16.81	16.64	15.92	15.05	17.09	14.84	15.69	17.93	17.17	15.19
Fe <sub>2</sub> O <sub>3</sub>	2.59	2.05	2.37	0.29	0.92	1.24	1.01	2.03	2.87	6.59
FeO	4.37	4.12	3.25	2.51	7.14	2.49	6.87	1.02	2.05	5.36
MgO	8.04	2.86	2.43	1.00	5.85	1.09	4.28	2.89	2.18	4.14
CaO	11.23	5.79	4.92	2.45	9.53	2.39	7.30	5.18	2.51	7.84
Na <sub>2</sub> O	2.40	3.02	3.20	4.16	2.59	3.46	3.23	6.71	4.74	3.55
K <sub>2</sub> O	0.27	1.12	2.94	2.32	0.95	4.90	1.75	0.72	4.57	1.61
TiO	0.62	0.80	0.64	0.40	0.83	0.77	1.67	0.46	0.36	2.70
MnO	0.12	0.16	0.11	0.06	0.15	0.06	0.16	0.05	0.13	0.25
P <sub>2</sub> O <sub>5</sub>	0.07	0.15	0.13	0.09	0.11	0.10	0.38	0.10	0.14	0.42
CO <sub>2</sub>	-	0.05	-	-	0.02	-	-	-	0.10	-
H <sub>2</sub> O <sup>+</sup>	1.15	1.13	0.89	0.68	1.80	0.07	0.82	1.40	0.74	0.69
H <sub>2</sub> O <sup>-</sup>	0.21	0.23	0.22	0.20	0.27	0.21	0.18	0.95	0.34	0.20
Total	98.89	97.42	99.23	98.91	98.97	98.16	97.47	98.02	98.67	98.08

\* values in wt. %.

\*\* for numbers refer to Table 3.1 and Figure 3.1.

## Paleozoic Granitic Rocks

Paleozoic granitic rocks crop out on the western margin of the study area (Figure 2.15), parallel to the coastline in a north-south trend and west of Sierra del Carmen (Figure 2.3). They show local textural and compositional variations which could not be mapped at a scale of 1:100,000; as a result, they are mapped as a composite map unit.

Along the coastal border, this granitic batholith, hereafter called the Cifuncho Batholith, intrudes sedimentary rocks of the Las Tortolas Formation. Over this batholith a volcanic rock sequence, probably of Permian age, lies unconformably (RCU). The lithology of the Cifuncho Batholith varies from leucogranite to biotite adamellite to granophyric leucogranite. In the field these rocks are light in colour (pale gray, whitish gray, yellowish gray, pale grayish orange) and coarse grained, displaying a pervasive cleavage and quartzose texture. Modal analysis (Table 2.3) of the biotite adamellites and leucogranites confirm the silicic character of these rocks which contain 25-50% quartz. The leucogranites, in addition, contain 40-65% microperthite, 5-10% oligoclase, and less than 2% biotite; the biotite adamellites, in addition to quartz, contain 20-35% calcic oligoclase to sodic andesine, 15-40% microperthite, and 3-10% biotite (Table 2.3).

The emplacement of this batholith metamorphosed the meta-sedimentary rocks of the Las Tortolas Formation.

FIGURE 2.15 Distribution map of Paleozoic  
granitic intrusions (shaded).

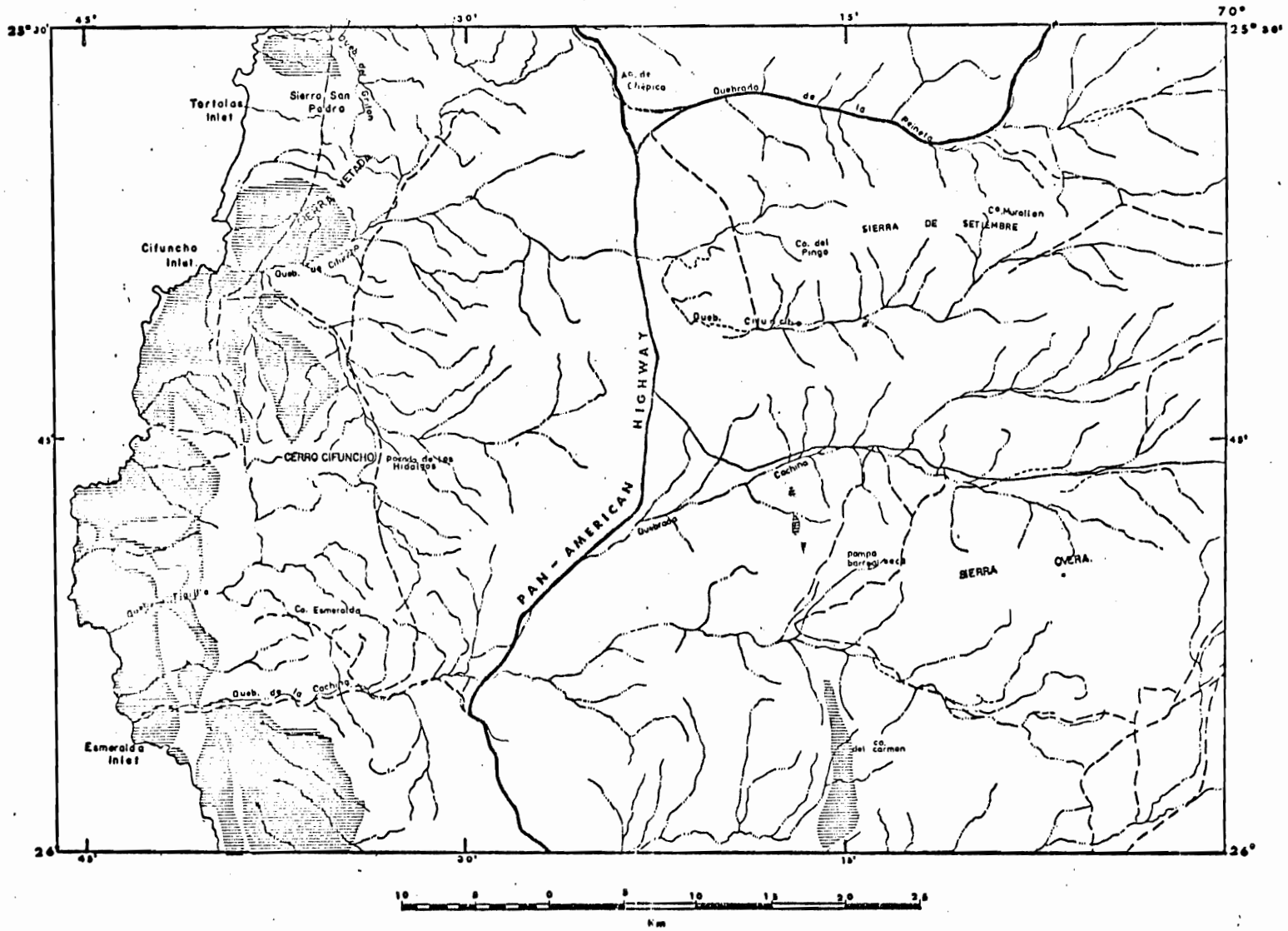


TABLE 2.3

Approximate modes of typical Paleozoic granitic rocks

SAMPLE NO.	<u>Z-713</u>	<u>T-51</u>	<u>T52-A</u>	<u>JN-25</u>	<u>JN-399</u>
Plagioclase (An%)	30-35 An <sub>24-38</sub>	27-33 An <sub>23-39</sub>	20-25 An <sub>29-32</sub>	24	24
K-feldspar	15-17	17-22	30-40	25	28
Quartz	20-25	35-40	35-40	49	39
Biotite	5-7	5-9	3-5	1	7
Hornblende	-	-	Tr	-	-
Opaques	Tr	Tr	Tr	-	-
Non-opaques*	1	1-2	1	1	2

\*Zircon, Apatite, Chlorite, Sericite, Sphene

Z-713 : Biotite Granodiorite 25°39'S-70°38'W  
T-51 : Biotite Adamellite 26°23'S-70°20'W  
T-52A : Biotite Adamellite 26°23'S-70°21'W  
JN-25 : Leucogranite 26°18'S-70°26'W  
JN-399: Leucogranite 26°18'S-70°26'W

## Age

The Cifuncho Batholith has been dated by the Pb/ $\alpha$  and K/Ar methods. A sample collected near the Quebrada Cifuncho yielded a Carboniferous Pb/ $\alpha$  date of  $340 \pm 40$  Ma (Levi et al., 1963). The dated rock was a medium-grained, partially altered adamellite, with plagioclase An<sub>28</sub>, (40%), quartz (30%) with undulose extinction, orthoclase (27%), Biotite (3%). In addition, chlorite, sericite and clay minerals occur as alteration products (Levi et al., 1963). The Biotite from samples collected at Caleta Cifuncho, yielded a Permian K/Ar date of  $267 \pm 8$  Ma (Zentilli, 1974). The rock is a medium-grained, biotite-rich granodiorite.

The same Batholith was sampled at Cerro Vetado (approximately 150 km south from Caleta Cifuncho) and yielded a Pb/ $\alpha$  date of  $280 \pm 50$  Ma (Carboniferous-Permian) (Levi et al., 1963).

In summary, the age of the granitic batholith is probably Permian or even Carboniferous.

## Mesozoic Rocks

The Mesozoic rocks represent the major intrusive episode in the area. South of the study area four intrusive phases were recognized (Haynes, 1975; Zentilli, 1974). Lower and Upper Jurassic and Lower and Middle Cretaceous; however, in the study area only the Lower Jurassic and the Cretaceous phases are present.



The major lithologic types of rocks are of granodioritic composition and subordinate dioritic composition. However, the rocks were mapped as a composite map unit. See Figures 2.16 and 2.17.

#### Jurassic Intrusive Rocks

Jurassic intrusive rocks crop out along the western margin of the study area, north and south of Sierra Esmeralda (Figure 2.3). They are predominantly dioritic rocks, of medium to coarse grain size including diorites and complexes of diorite and meta-andesite.

Closer to the coast, this dioritic pluton, hereafter called Sierra Esmeralda Pluton, intrudes massive sedimentary rocks of the Posada Hidalgos Formation (Lower Jurassic), rocks of the rhyolite conglomerate unit (Permian-Triassic) and rocks of the Cifuncho Formation (Triassic).

The medium-to-coarse grained equigranular diorite is the commonest rock type in the Jurassic plutons. Modal analysis (Table 2.4) shows quartz (2-5%), potassic feldspar (0-3%), plagioclase  $An_{26-42}$  (40-50%), amphibole (hornblende) (2-15%), biotite (5-9%). Depending on whether biotite or hornblende is predominant, biotite diorites or hornblende diorites may be distinguished.

FIGURE 2.16 Distribution map of  
Jurassic intrusions (shaded).

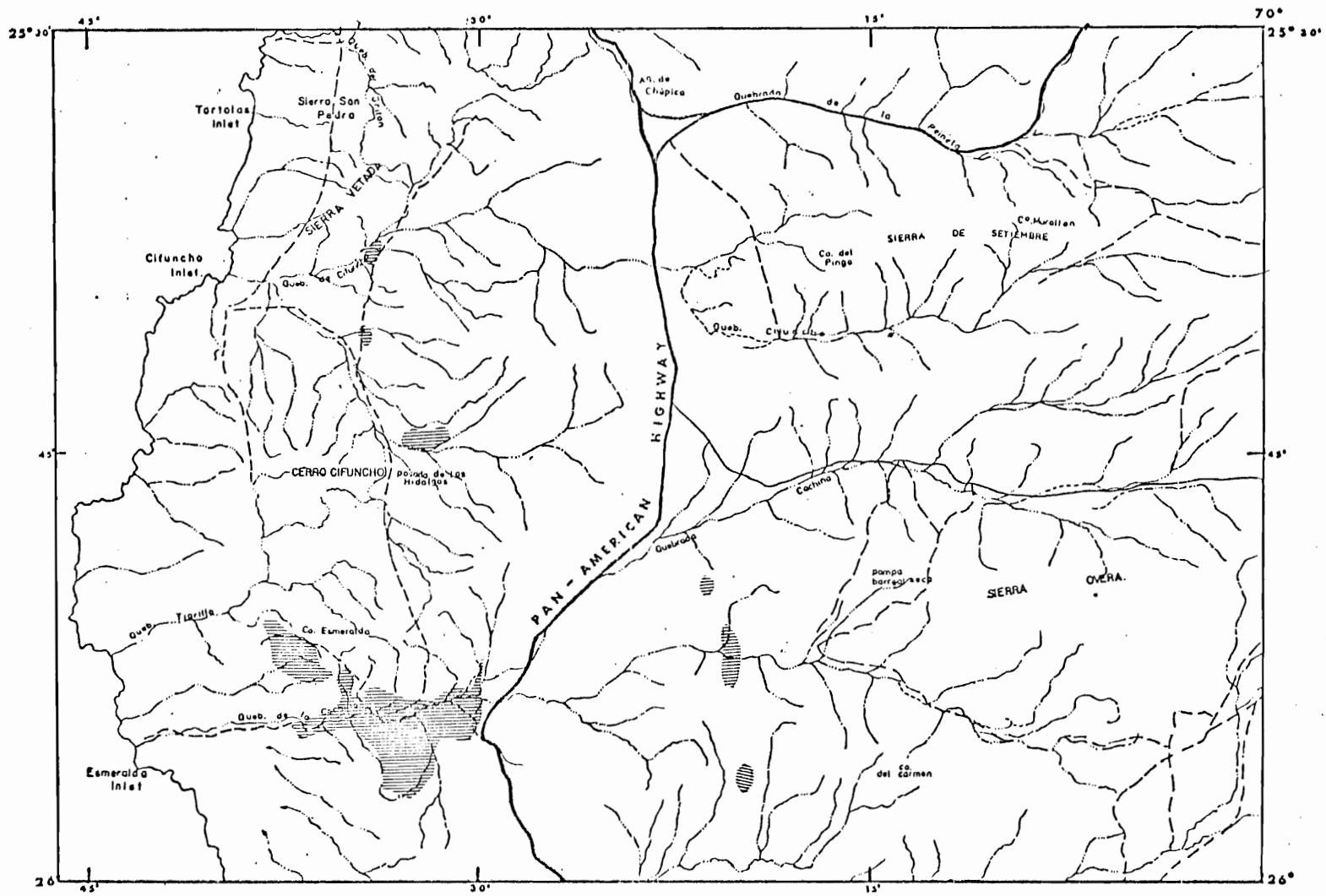


FIGURE 2.17 Distribution map of the  
Cretaceous intrusions (shaded).

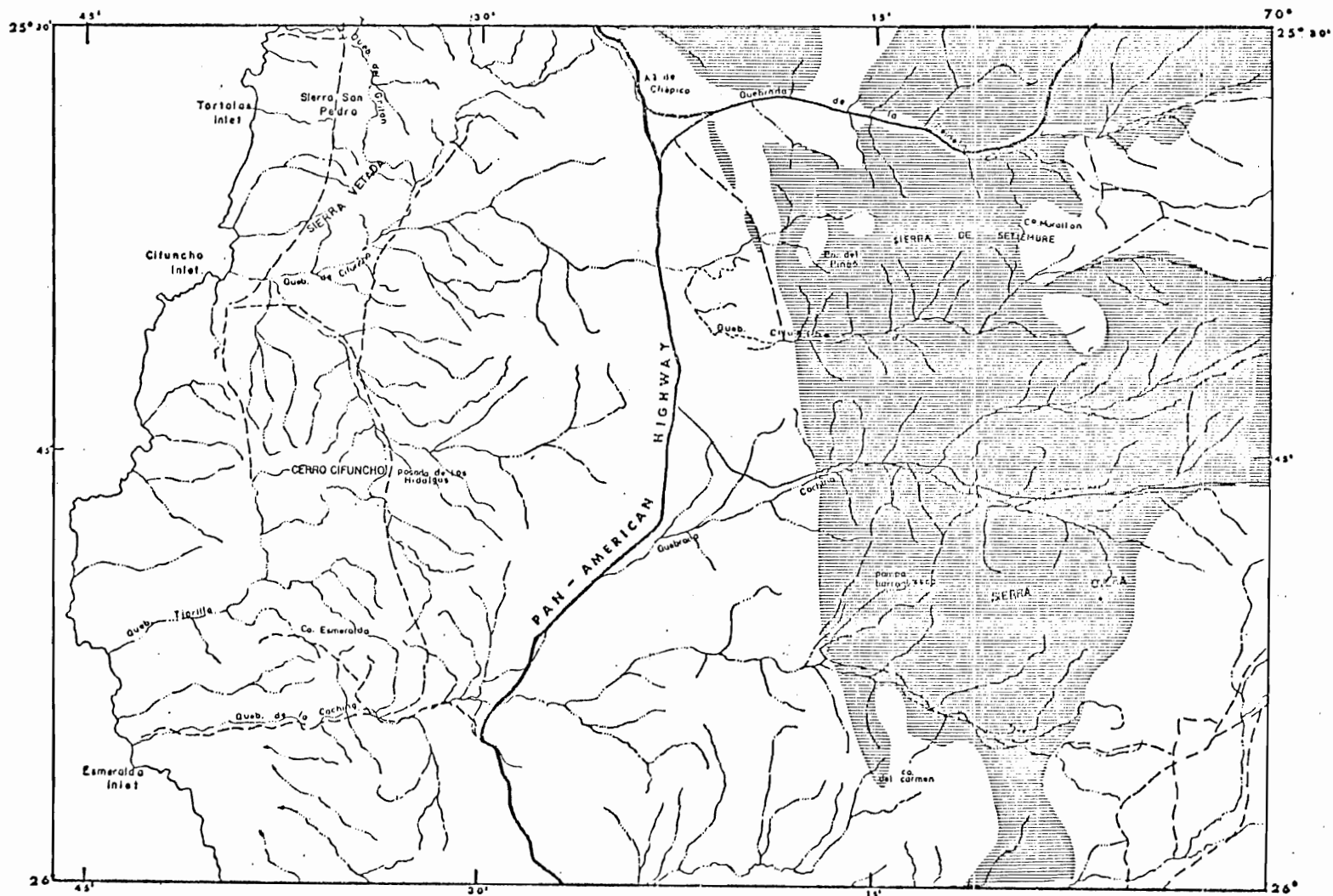


TABLE 2.4

Approximate modes of typical diorites

SAMPLE NO.	<u>Z-715</u>	<u>Z-716</u>	<u>Cu-7</u>	<u>U-174</u>
Plagioclase (An%)	40-45 An <sub>40-42</sub>	40-50 An <sub>26-40</sub>	65-70 An <sub>30-50</sub>	40 An <sub>26-32</sub>
K-Feldspar	1-3	-	-	1
Quartz	2-3	2-5	0.5-1	2
Pyroxene	-	-	-	2-3
Amphibole	2	10-15	5-7	35-40
Biotite	8-9	5-7	0.5	15
Opaques	2-3	1	5	3
Non-opaques*	2-3	2	1-2	1-2

\*Apatite, Sphene, Sericite, Chlorite, Zircon

Z-715 : Biotite diorite 25°51'S-70°28'W  
 Z-716 : Hornblende diorite 25°54'S-70°34'W  
 Cu-7 : Hornblende diorite 25°32'S-70°06'W  
 U-174 : Hornblende diorite 25°55'S-70°12'W

## Age

The Sierra Esmeralda Pluton intrudes marine sediments of Hettangian to Late Sinemurian age. The faunal association indicates Upper Sinemurian and Lotharingian and perhaps the base of the Pliensbachian. Thus, the age of the Pluton is post-Sinemurian and perhaps post-Pliensbachian because before the deposition of the La Negra Formation, erosion of the Pliensbachian beds occurred, exposing the intrusive to the surface.

The isotopic age of the Sierra Esmeralda Pluton (see below) is consistent with a Pliensbachian age for the intrusion.

## Cretaceous Intrusive Rocks

The Cretaceous intrusive rocks represent the more voluminous intrusive phase in the area. The major outcrops of this batholith, hereafter called Cerro del Pingo Batholith, are localized in the central part of the study area, trending north-south. The Cerro del Pingo Batholith extends northward and southward outside of the study area (Figures 2.3 and 2.17).

It includes diorites, granodiorites and adamellites. The contact between the different facies is gradational and field recognition of these varieties is often difficult. The Batholith intrudes Paleozoic metamorphic and granitic rocks and marine-continental sediments of Lower Cretaceous age.

### Dioritic Rocks

Small bodies of fine to medium grained diorite crop out north of Pampa Barreal Seco and La Cachina gully and northeast of Sierra Buena Esperanza (Figure 2.3). Modal analysis (Table 2.4) shows plagioclase  $An_{26-50}$  (40-70%), quartz (0.5-2%), pyroxene (2-3%), hornblende-amphibole (5-40%), biotite (0.5-15%). The rocks are greenish-gray because of alteration of mafic minerals and saussuritization of plagioclase. Gradation to quartz monzo-diorite was locally observed (Table 2.6).

### Granodioritic Rocks

The granodiorite rocks are the most abundant in the study area. They form small intrusive bodies, dikes and may include aplitic dikes. They crop out along the central part of the mapped area and the rocks have been affected by the Atacama Fault Zone and by the Taltal Fault (see below). Modal analysis (Table 2.5) shows plagioclase  $An_{24-33}$  (45-55%), K-feldspar (10-16%), quartz (20-30%), biotite (2-8%), hornblende-amphibole (3-7%).

In hand specimens of these rocks are whitish-gray, gray and pinkish-gray in colour. Dark biotite flakes and prismatic hornblende can be readily distinguished. Fine-grained mafic xenoliths or inclusions within the granodiorites are variable in size and texture; their mineralogy is similar to that of the host rock.



TABLE 2.5

## Approximate modes of granodiorites

SAMPLE NO.	<u>Cul<sup>+</sup></u>	<u>CE-8</u>	<u>CE-31</u>
Plagioclase (An%)	45-50 An <sub>28-32</sub>	45-50 An <sub>24-33</sub>	45-55 An <sub>25-29</sub>
K-feldspar	10-15	10-15	12-16
Quartz	25-30	25-30	20-25
Biotite	2-3	6-8	[10-15]
Hornblende	5-7	3-4	
Pyroxene	-		
Opaques	1	1-2	1
Non-opaques*	1-2	Tr	Tr

\*Apatite, Sphene, Epidote, Sericite, Chlorite, Zircon

Cul<sup>+</sup> : Hornblende granodiorite 25°39'S-70°14'W  
 CE-8 : Hornblende-biotite granodiorite 25°40'S-70°16'W  
 CE-31 : Hornblende-biotite granodiorite 25°43'S-70°14'W

TABLE 2.6

## Approximate modes of miscellaneous rocks

SAMPLE NO.	<u>CE-7</u>	<u>Cu-1</u>	<u>Cu-3</u>	<u>Cu2N</u>
Plagioclase (An%)	35-40 An <sub>23-28</sub>	40-42 An <sub>25-30</sub>	55-60 An <sub>42-44</sub>	45-50 An <sub>34-42</sub>
K-Feldspar	30-35	3.5	10	10
Quartz	25-30	30-35	15	5
Biotite	3-5	1-2	1	7-8
Hornblende	1	15-20	-	2
Opagues	Tr	1	1-2	3-4
Non-opagues*	Tr	1	1	1-2

\*Spheue, Zircon, Chlorite, Sericite, Epidote

CE-7 : Biotite Adamellite 25°38'S-70°13'W  
 Cu-1 : Hornblende Tonalite 25°39'S-70°14'W  
 Cu-3 : Qz Monzo-diorite 25°37'S-70°19'W  
 Cu2N : Qz Monzo-diorite 25°39'S-70°10'W

## Adamellitic Rocks

The adamellitic rocks represent the most common intrusive rocks. They exhibit gradational changes to diorite and granodiorite. A modal analysis (Table 2.6) shows plagioclase  $An_{23-28}$  (35-40%), K-feldspar (30-35%), quartz (25-30%), biotite (3-5%), hornblende (1%).

In hand specimen shows the adamellite gray to pinkish gray in colour. It contains large grains of milky gray or greenish gray plagioclase and fine irregular grains of mafic minerals distributed in a fine-grained quartzo-feldspathic matrix.

Brown biotite and green hornblende are the principal mafic minerals; bleached cores and reaction veins have been observed in hornblendes and pyroxene cores within the hornblendes. Normally zoned plagioclase is common.

All the rocks forming the Cerro del Pingo Batholith show a very high magnetite content, possibly related to hydrothermal alteration associated with the Fe mineralization (see below).

## Age

The Cerro del Pingo Batholith is a multiphase batholith intruding the Aeropuerto Formation of Lower Cretaceous age (Neocomian) and Paleozoic metamorphic rocks of Las Tortolas Formation. Thus the Batholith is post-Neocomian (post-Hauterivian) in age. In addition, on the basis of geochronology dates (see below) a Late Hauterivian-Aptian age can be assigned.

### Minor Intrusive Rocks

Various dykes, predominantly of andesite or basaltic andesite, cross cut the sedimentary, volcanic and intrusive rocks of Paleozoic and Mesozoic ages. Along the coastal cordillera, a set of dykes (N30W) intrudes the Las Tortolas Formation and the Paleozoic granite together with the Cifuncho Formation, the Pan de Azúcar and the Posada Hidalgos Formations. They show a clear pattern easily identifiable on air photos.

This system of dykes has not been found intruding the Cretaceous rocks, so on the basis of the structural relations and geochronology dates, a Lower Jurassic age can be assigned.

### Structural Geology

The coastal cordillera is characterized by deeply weathered rocks, veneered pediments and low-relief surfaces that are interrupted by residual hills of sharp relief. Faults exert a profound topographic control.

The structure of the study area is dominated by the major Atacama Fault Zone, that traverses the area (Figure 2.3), and faults subsidiary to it. The Atacama Fault was recognized and named by St. Amand and Allen (1960). They defined it as an extensive fault zone, which extends from the Copiapo province to Iquique province, over 900 km, approximately. This system is intimately related to the tectonic and the metallogenic history of the area. The Paleozoic basement shows locally

intense folding and foliation, whereas the Mesozoic units are predominantly gently folded or tilted. Unconformities within the sequence reflect important tectonic events during the geologic history. The predominant orientation of dyke swarms, of probable Jurassic age, provides information on the stress fields to which this region was subjected.

#### A. Folding

##### Pre-Mesozoic Basement Rocks

The stratified rocks of the Paleozoic Las Tortolas Formation are strongly folded into tight, locally recumbent and refolded folds. Miller (1970) determined a general axis of folding of 100/30W. The present author measured a number of attitudes of beds (Figure 2.18) from which a general axis can probably be defined at 135/20<sup>o</sup>W. Foliation is generally parallel to the axial planes of folds and has a SW vergence.

##### Mesozoic Rocks

The Mesozoic rocks show different intensities of folding, but generally their deformation is negligible when compared with the Paleozoic rocks. The Triassic Pan de Azucar Formation is folded into upright open, but locally tight, folds. From field measurements by the author, a general fold axis of approximately 60/30 NE can be defined (Figure 2.19). The Jurassic rocks are relatively less deformed, except in areas where more intense folding appears to depend on the lower

competence of impure carbonate sediments. The Lower Jurassic rocks are folded with a general fold axis close to 45/40 NE (Figures 2.20 and 2.21) whereas the La Negra Formation of Middle-Upper Jurassic age is folded after a 135/20 SE (Figure 2.22) axis, hence the angular unconformity between both series is very clear. The attitudes of beds of the Cretaceous Aeropuerto Formation are strongly disturbed by the contact effects of the Cretaceous Batholith.

#### B. Unconformities

The Permo-Triassic Rhyolite Conglomerate Unit (RCU) lies unconformably on Paleozoic rocks and in turn is separated from the overlying Triassic rocks by a slight angular unconformity. An erosional and angular unconformity separates the Triassic Cifuncho Formation from the Jurassic formations. Most of the unconformities are related with more or less important phases of diastrophism.

The relationships between the La Negra Formation and the Aeropuerto Formation are not clear because the bottom of the latter is nowhere visible, being affected by the Atacama Fault and the plutonic rocks of Middle to Upper Cretaceous age.

FIGURE 2.18 Paleozoic rocks, bedding planes.  
Equal area net, lower hemisphere (35 poles).

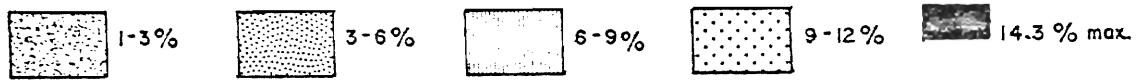
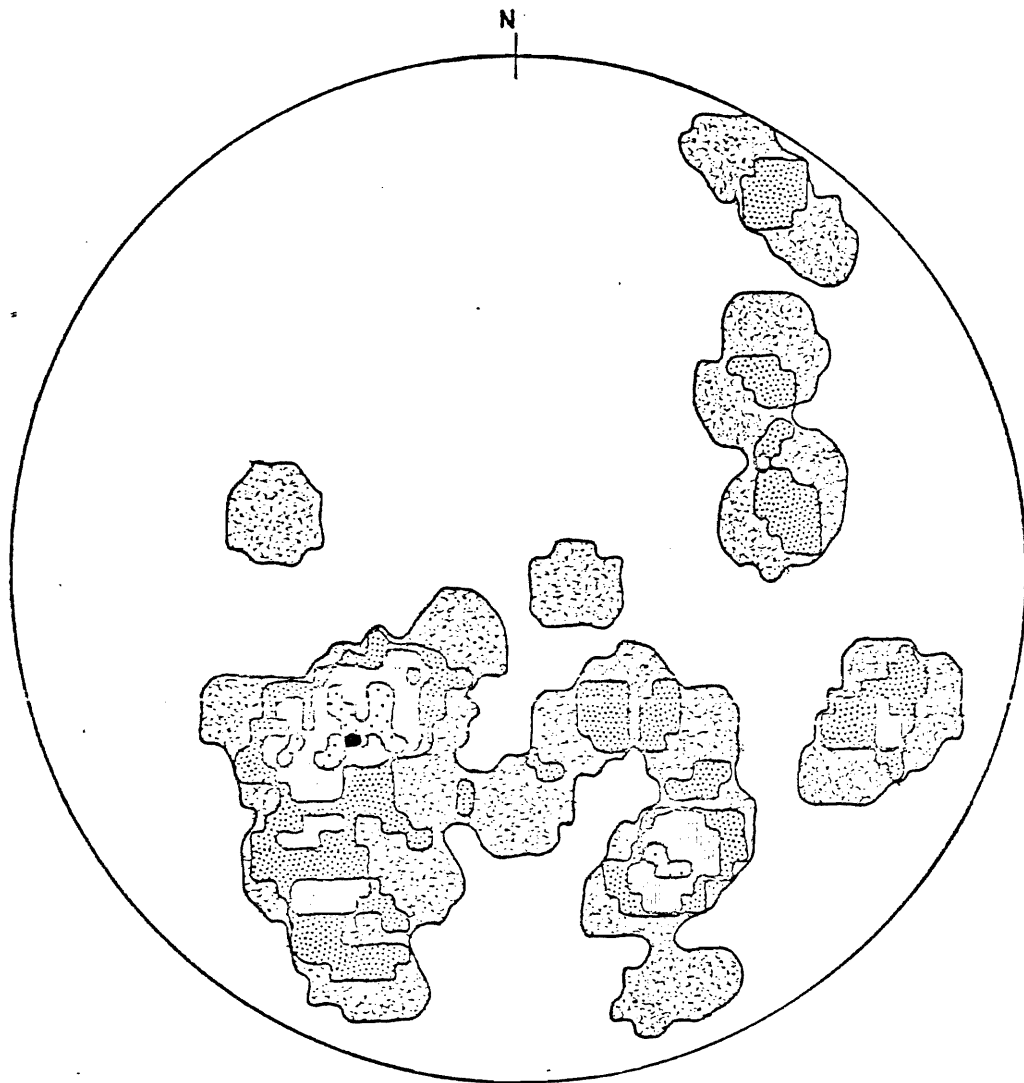




FIGURE 2.19 Triassic rocks, bedding planes.  
Equal area net, lower hemisphere (39 poles).

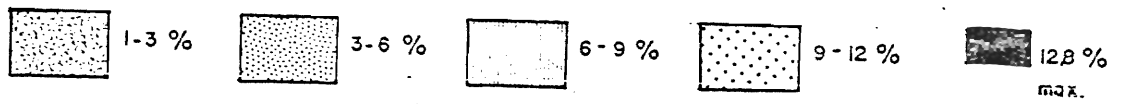
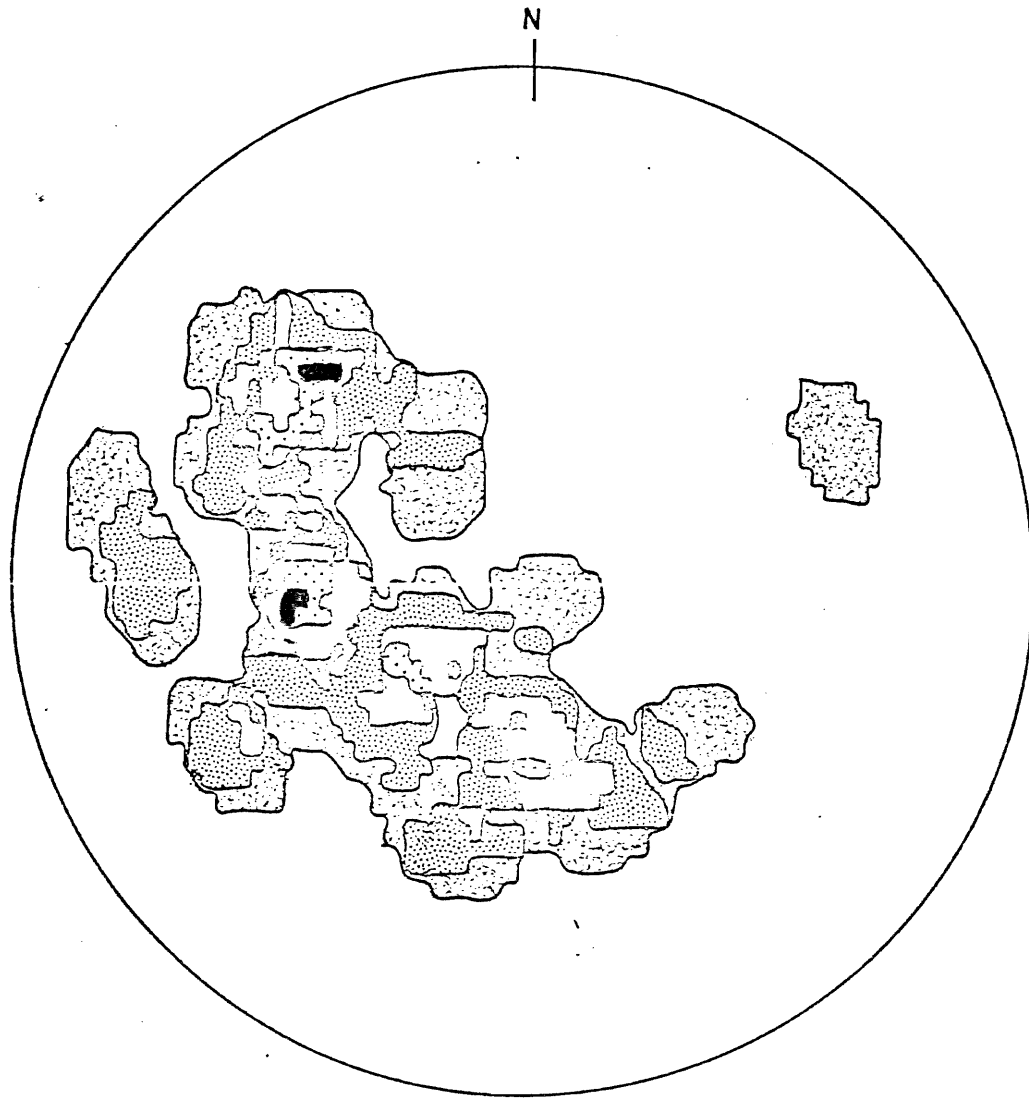
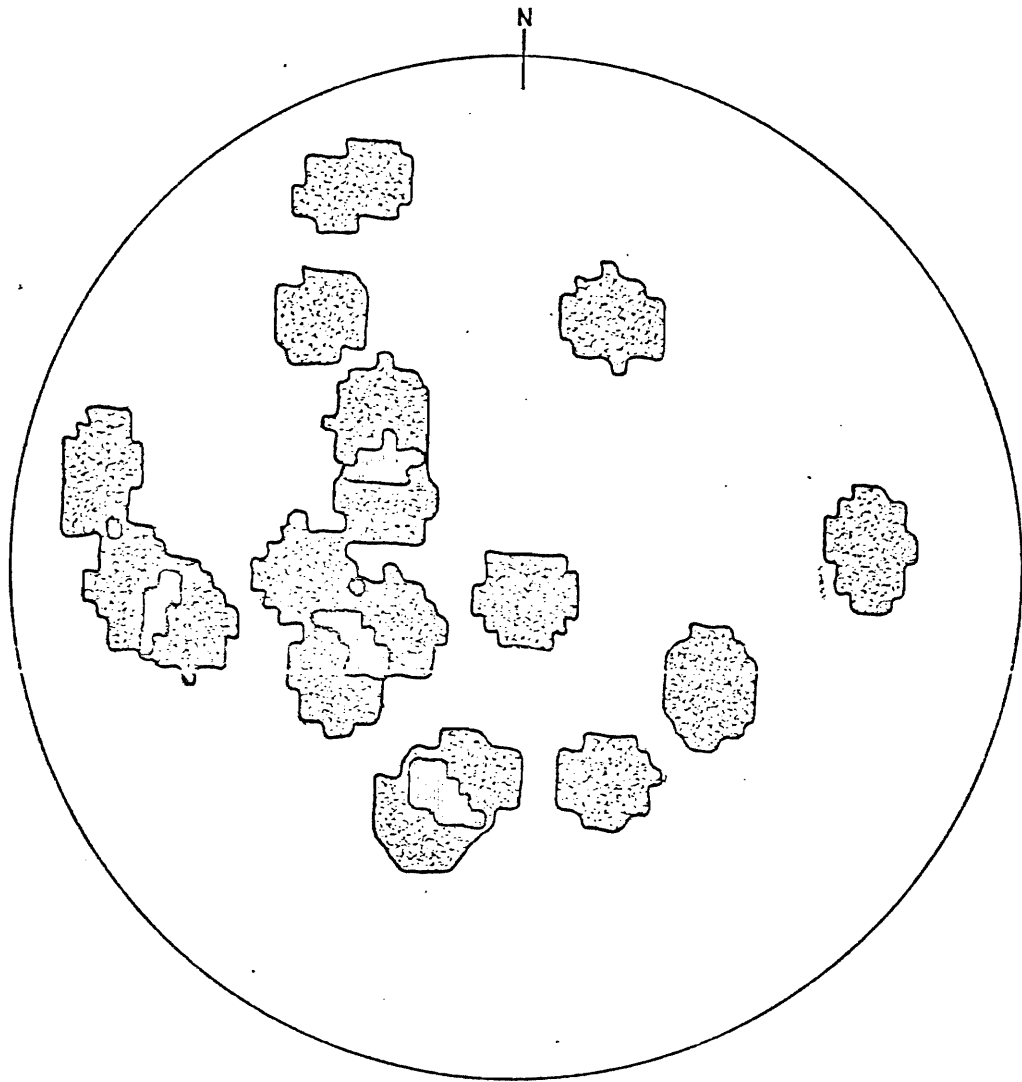


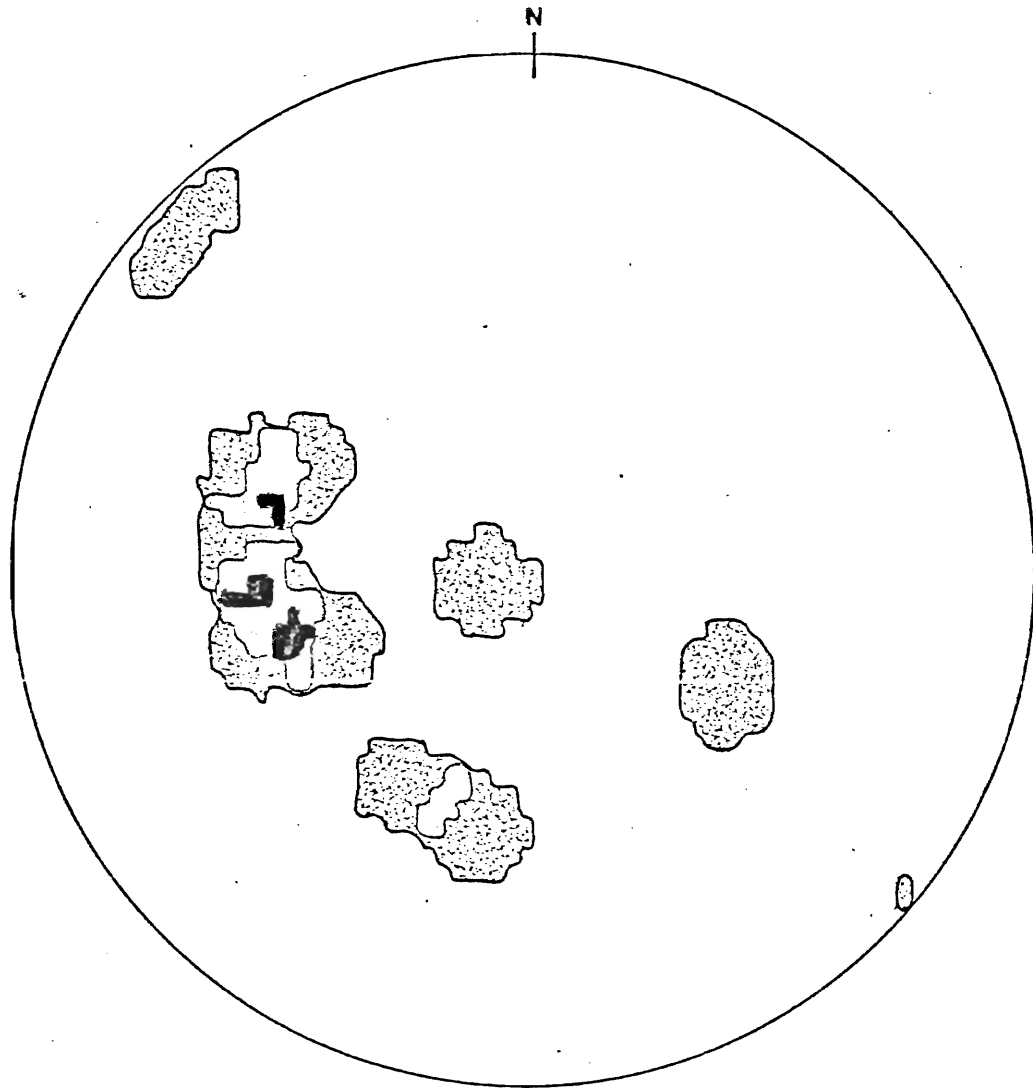
FIGURE 2.20 Lower Jurassic rocks  
(Pan de Azúcar Formation), bedding planes.  
Equal area net, lower hemisphere, (17 poles).




1-3%

9-12%

FIGURE 2.21 Lower Jurassic rocks  
(Posada Hidalgos Formation), bedding planes.  
Equal area net, lower hemisphere (11 poles).



 5-10 %

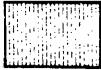

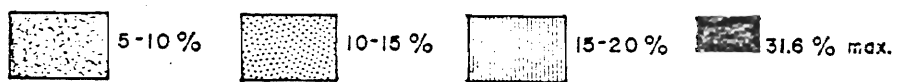
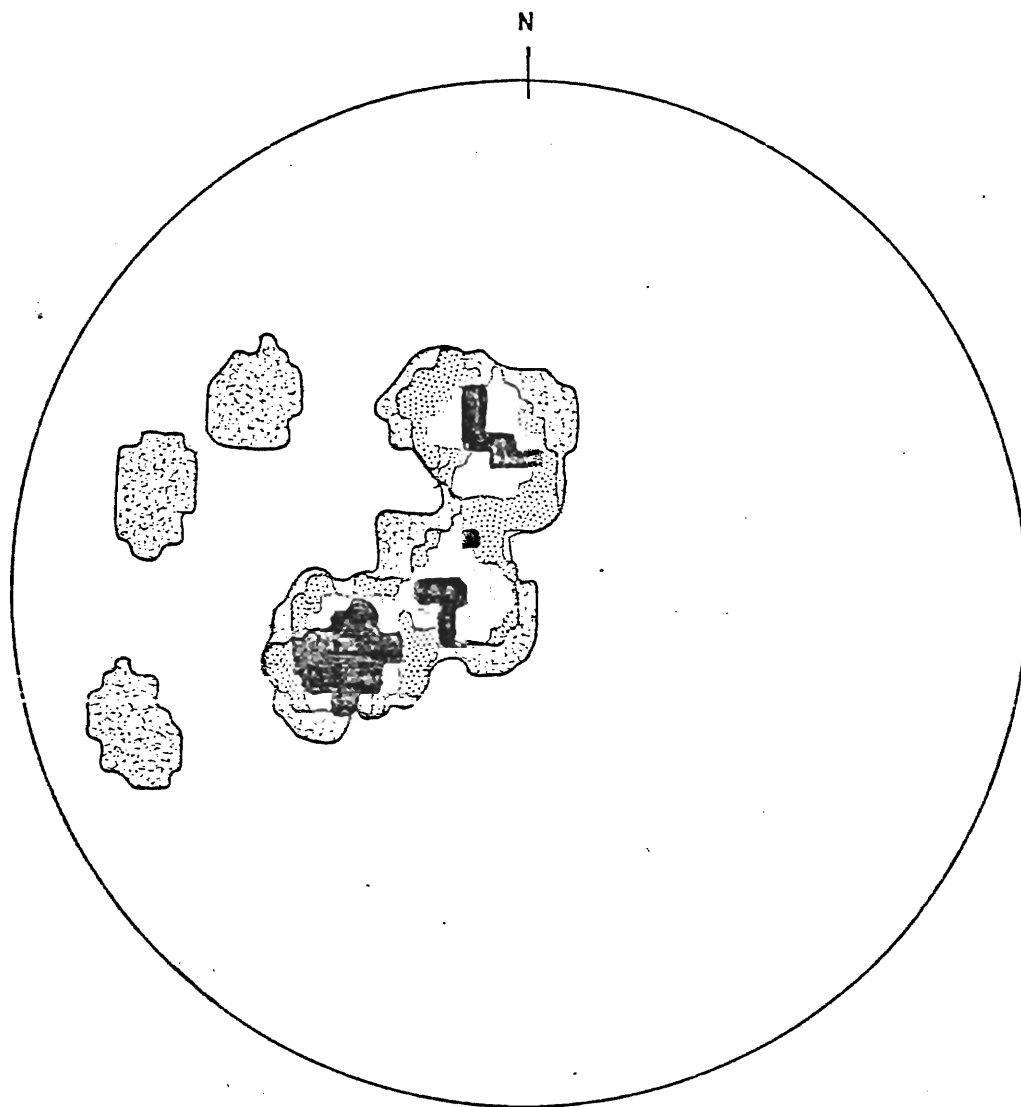
 15-20 %  27.3 max.

FIGURE 2.22 Lower Jurassic rocks (La Negra Formation),  
bedding planes.  
Equal area net, lower hemisphere (19 poles).





### C. Faults

The Atacama Fault Zone (St. Amand and Allen, 1960), has been named differently in different areas. The segment south of Taltal extends over 200 km to the Copiapó region and was named the "El Salado", "Manto Atacama" or "Manto Verde Fault" (Ruiz, 1943; Segerstrom et al., 1960; Bowes et al., 1961; Segerstrom and Ruiz, 1962). North of the study area, the fault was earlier termed the "Salar del Carmen Fault" (Knowles et al., 1959) and locally as "La Negra Fault". Bowes et al. (1961) recognized the continuity of the fault northward and southward. Near the Taltal airport the Atacama Fault is truncated by a northwest trending fault.

The following paragraphs draw freely from the Ph.D. thesis by Arabasz (1970) who focused on the fault problem, and are complemented with personal observations by the author.

A Broad, low-relief trough is occupied by the Atacama Fault Zone and includes numerous branches of it.

South of La Cachina gully, two major fault traces 4-6 km apart have been recognized. North of La Cachina gully a profusion of fault traces can be observed (Figure 2.3) so that a multiplicity of alluvial fault scarps characterize the fault trough.

The Atacama Fault Zone comprises:

1. The eastern Branch: This has been recognized through the

whole area and to the south beyond the study area. Its continuation northward is truncated by the Taltal Fault (Figure 2.3). It appears as a narrow area with crush zones (two parallel bands 100-300 m apart) transecting Paleozoic and Mesozoic sedimentary (Aeropuerto Formation, member 1) and intrusive rocks. A topographic change can be observed along the two parallel bands; the eastern side of the fault stands higher, but its relief decreases southward, and is dissected appearing only as a discontinuous scarp.

In La Cachina gully, both northward and southward, a linear fault trench is developed in alluvium along the trace of the Atacama Fault. Between the Del Pingo gully and the Cifuncho gully, fault benches are developed. Their traces are covered by the colluvium which itself is locally disturbed. South of the La Cachina gully, exposure on the eastern branch is discontinuous. The eastern branch trends  $N10^{\circ}-15^{\circ}W$  throughout most of the study area. Its linearity over irregular topography indicates that the fault is very steeply dipping and near vertical. Dips  $80^{\circ}$  and  $90^{\circ}$ , both east and west, were measured.

2. Central branches: South of the La Cachina gully a single fault trace, describing a gentle arc ( $N5^{\circ}-10^{\circ}W$ ) and extending farther south (27 km) beyond the limit of the study area, can be traced. Its trace is marked by a subdued east-facing fault scarp. The alluvium deposits are uplifted on the west side. Andesite of the La Negra Formation is faulted against rocks of

the Aeropuerto Formation (member 1). North of the La Cachina gully, several faults converge and are truncated by the Taltal Fault (Figure 2.3). Outcrops of the fault are not continuous but the rock exposures show brecciation and shearing. Locally copper-gold and silver mineralization is controlled by the fault. This situation can be observed in the Union mine, a few kilometers south of Taltal airport, and at the Anita mine (Lat.  $25^{\circ}50'S$ ). This mineralized fault affects sedimentary rocks of the Aeropuerto Formation (member 1). In the working mines the fault is N6-10W and dips  $70^{\circ}$ - $84^{\circ}$ E.

3. Aquada de Chépica Fault: This fault corresponds to the northwestward fault branching from the Atacama Fault in the La Cachina gully, and passes through the center of the town of Taltal out into the sea. It appears to be active and has been responsible for several devastating earthquakes. The type locality of the fault is Aquada de Chépica, where fluvial gravels are faulted against andesite of the La Negra Formation (Figure 2.3). The fault can be traced along 42 km onshore and at least 20 km offshore. In the type locality it strikes N15W and dips  $84^{\circ}$ SW. Along its trace, the west side of the fault is the higher-standing block.

The main development of the Aquada de Chépica Fault is along the Taltal gully, outside the study area. There, the Alluvium has been affected by the fault.

Andesites of the La Negra Formation are faulted against sedimentary rocks of the Aeropuerto Formation (member 1).

4. The Taltal Fault: East and north of the Taltal airport the Atacama Fault Zone is truncated by a fault named the Taltal Fault which can be traced for 35 km from the Sierra del Pingo to the town of Taltal (Figure 2.3). The fault trace is clearly defined north of the Taltal airport, trending N50W and dipping  $75^{\circ}$ - $80^{\circ}$ NE. Paleozoic metamorphic rocks and Mesozoic plutonic rocks are faulted against Neocomian sedimentary rocks, Paleozoic metamorphic rocks and Mesozoic intrusive rocks.

#### Age of the Faults

Evidence of a horizontal movement during some period of the fault's history is provided by slickensides and mullions. In several sectors of the faults (e.g. Copiapó), horizontal slickensides have been reported (e.g. Segerstrom, 1960; Segerstrom and Ruiz, 1962). AraBasz (1971) observed near-horizontal slickensides plunging between  $23^{\circ}$ - $17^{\circ}$ ; he noted superposed slickensides along the eastern branch plunging  $60^{\circ}$ - $70^{\circ}$  which appeared to be younger than the other set.

At the Unión mine, two sets of slickensides were measured, one (older) plunging  $12^{\circ}$  and another (younger) plunging  $68^{\circ}$ . In the Anita mine one set plunges  $18^{\circ}$  and the other  $83^{\circ}$ .

In east-west fractures (parallel to the Taltal Fault) near-horizontal slickensides were observed. In an open trench

(16 km SSE Union mine) on the smooth fault surface separating the rock units, slickensides plunging  $79-81^{\circ}$  were observed; in the Bandurrias mine the slickensides plunge  $12^{\circ}$ N. On the basis of these data Arabazs (1971) concluded that the faults had both strike-slip motion and dip-slip motion, but little could be said about its magnitude and absolute age.

To determine the sense of the displacement it is necessary to understand the stratigraphic relationships on both sides of the fault. The Atacama Fault separates Paleozoic rocks of the Las Tórtolas Formation and Paleozoic and Mesozoic intrusive rocks, sedimentary and volcanic rocks of the Aeropuerto Formation (member 1) from volcanic rocks of the La Negra Formation. One can speculate that the eastern block moved upward and the western one downward; because the Aeropuerto Formation deposited marine sediments directly onto Paleozoic metamorphic basement. The Triassic and Lower Jurassic formations were eroded before the Cretaceous transgression. This would imply a net displacement of up to 5000 m, the total aggregate thickness of the Mesozoic formations west of the fault.

Alternative hypotheses could suggest a large strike-slip movement or the existence of a topographic high to coincide with the easternmost boundary of the La Negra Formation, which would therefore never have been deposited east of the Atacama Fault. These alternatives can be easily eliminated with evidence from outside the Cifuncho-Cerro del Pingo area. The fate of the huge

amount of debris that the proposed fault movement would have generated is problematic. They may be represented by the thick conglomerate unit known as Caleta Coloso Formation near Antofagasta (Lat.  $24^{\circ}$ S), but undoubtedly a large proportion of the debris could have gone into the Chile Trench (which is another problem, because the Chile Trench at this latitude is free of sediment).

The presence in branches of the Atacama Fault of iron and copper mineralization now interpreted to be of Early Cretaceous age (see below) is supporting evidence for a (pre?) Early Cretaceous movement of the Atacama Fault Zone.

The Aguada de Chépica Fault shows outside of the study area, evidence of vertical motions during its recent history. Faulting of fluvial gravels are in direct contact with brecciated andesites of the La Negra Formation. Difference in the relative elevations of blocks on both sides of the fault imply vertical movement.

North of the area, the fault shows similar structural relationships as the Atacama Fault, thus a Late Jurassic age is assigned to the Aguada de Chépica Fault.

There is not enough evidence in the study area to assign an age to the Taltal Fault. The maximum extension of the fault is outside of the mapped area; however, east of the Taltal Airport, the fault affects Paleozoic metamorphic basement and the Lower Cretaceous Cerro Del Pingo Batholith. Thus a post-early Late Cretaceous age can be assumed.

## CHAPTER III

### GEOCHRONOLOGY

The Pacific margin of South America has become the type example for subduction at a continental margin (e.g. Dewey and Bird, 1970); Kulm et al., 1977). In recent years, geological and geophysical studies focussed on the Central Andes of Peru, Bolivia and northern Chile. The majority of these investigations have been concerned with the post-Paleozoic development of the Central Andes and have attempted to explain different models related to interactions of the consuming plate boundary. In contrast to elsewhere in northern Chile, geological data on the study area proper are scarce. The purpose of this chapter is to present new geochronological data on 15 samples and discuss these data in the context of previous knowledge.

#### Previous Dates

A brief review of the available isotopic age data of the surrounding area is here presented as a background of the geochronological study of the Cifuncho-Cerro del Pingo area (study area). A compilation of the previous isotopic age data is presented in Table 3.1 and their locations shown in Figure 3.1.

Approximately 40 Pb/ $\alpha$  dates have been reported for zircon samples from the surrounding area (Levi et al., 1972). These dates were used to help define several periods of igneous

activity (Ruiz et al., 1965). The Pb/ $\alpha$  method is reviewed by Hamilton (1965). This method has the advantage of relative simplicity compared to other dating techniques; however, it often gives ages that have no geologic significance, or are difficult to interpret due to the presence of non-radiogenic lead, and leaching or addition of U, Th and Pb (Fullagar, 1971). The method is at best a reconnaissance tool. All the isotopic methods (Pb/ $\alpha$  , K/Ar, Rb/Sr) indicate that Paleozoic rocks are exposed at several localities. Age discordance is apparent in some instances, but satisfactory agreement between Pb/ $\alpha$  and Rb/Sr dates is found for specimens taken from the Imilac region ( $24^{\circ}15'S-68^{\circ}30'W$ ) of the Alta Cordillera. These samples yielded a Pb/ $\alpha$  age of  $487 \pm 50$  Ma (IIG, 1972); however, the potassium-argon method yielded an age of 318 Ma. The imprecision of the Pb/ $\alpha$  technique becomes conspicuous when applied to young specimens as in the case of the El Salvador area (Table 3.1). In general Pb/ $\alpha$  ages tend to be older than the potassium-argon ages. Levi et al. (1962) and Ruiz et al. (1965) defined four periods of magmatic activity - Paleozoic ( $260 \pm 30$  to  $340 \pm 40$  Ma), Jurassic ( $120 \pm 15$  to  $170 \pm 20$  Ma), Cretaceous ( $90 \pm 10$  to  $105 \pm 10$  Ma) and Tertiary ( $30 \pm 20$  to  $60 \pm 10$  Ma). The Paleozoic intrusive rocks are described predominantly as granites; the Jurassic rocks range from diorite to granodiorite and the Tertiary from adamellite and granodiorite to tonalitic, granodioritic and monzonitic porphyries (Ruiz et al., 1965). The most important periods of mineralization would correspond to Mesozoic and Cenozoic eras (op. cit.).



TABLE 3.1

## Compilation of Previous Isotopic Age Data of Northern Chile

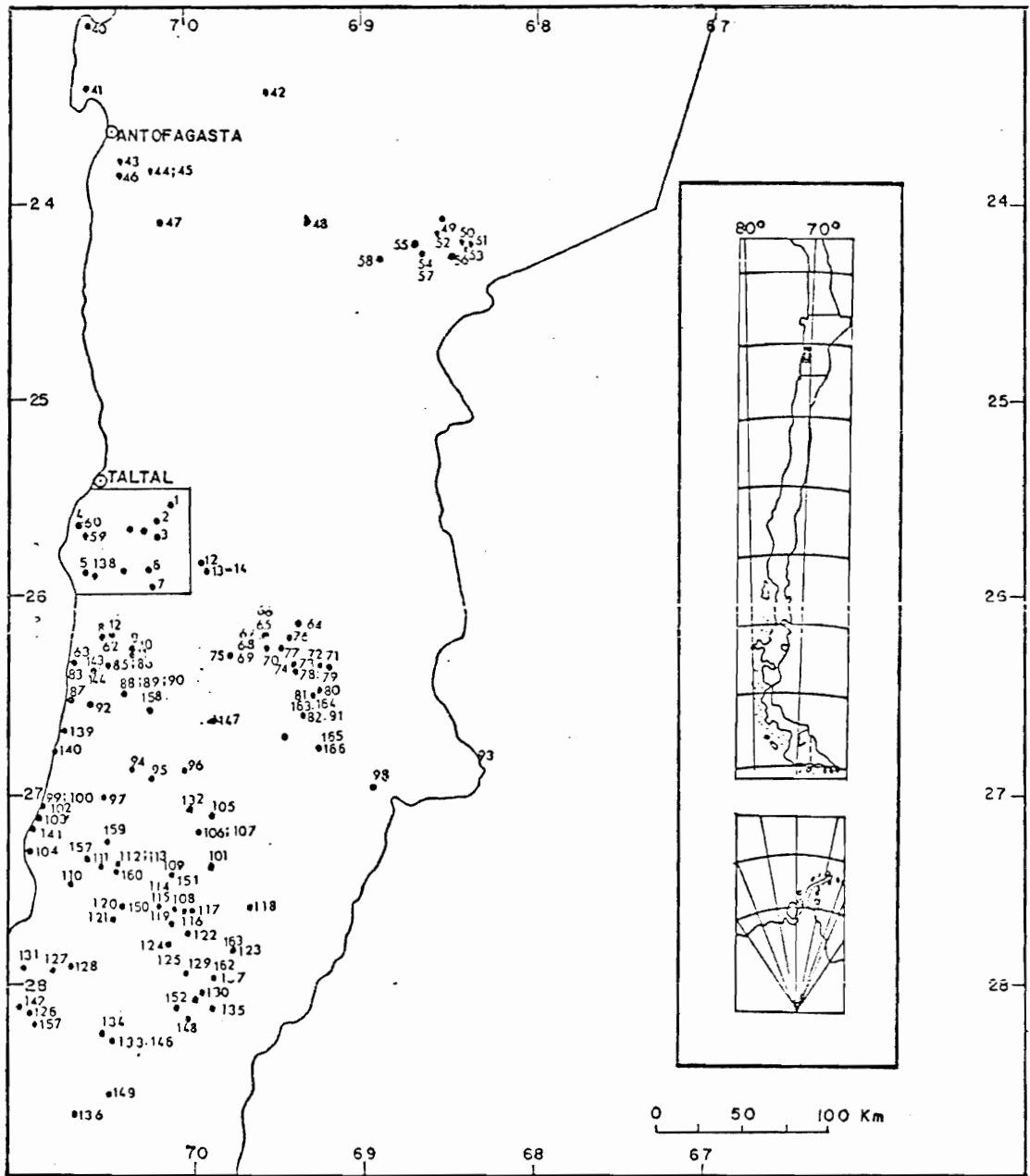
<u>No.</u>	<u>Location</u>	<u>Pb/<math>\alpha</math></u>	<u>Rb/Sr</u>	<u>K/Ar</u>	<u>Source</u>
40	70°30'-23°05'	200±20	160		Halpern (1978); Ruiz <u>et al.</u> (1965)
41	70°32.5'-23°25'		118		Halpern (1978)
42	69°34.3'-23°27'	69±10			IIG (1972)
43	70°12.6'-22°58.3'	158±20			IIG (1972)
44	70°16.8'-23°50'	137±15			IIG (1972)
45	70°17'-23°49.6'	150±20			IIG (1972)
46	70°24.1'-23°51.8'	134±15			IIG (1972)
47	70°7.5'-24°05'		120		Halpern (1978)
48	69°20'-24°05'		43		Halpern (1978)
49	68°35'-24°05'	168±20	250		Halpern (1978); IIG (1972)
50	68°29.4'-24°17.7'	487±50		318.7	IIG (1972)
51	68°25'-24°15'		255		Halpern (1978)
52	68°36.3'-24°09'	168±20			IIG (1972)
53	68°27.6'-24°16.7'	467±50			IIG (1972)
54	68°40'-24°15'		246		Halpern (1978)
55	68°45'-24°10.2'		276		Halpern (1978)
56	68°30'-24°15.2'		468		Halpern (1978)
57	68°25'-24°15'		246		Halpern (1978)
58	68°55'-24°15.2'		250 to 280		Halpern (1978)
59	70°35.5'-25°43'	350±40			IIG (1972)
60	70°38'-25°39'			267±8	Quirt (1972); Zentilli (1974)
61	70°25'-26°20'		218 to 186		Halpern (1978)
62	70°27.8'-26°20.7'	280±50			IIG (1972)
63	70°40'-26°22'			188±5.8	Quirt (1972); Zentilli (1974)
64	69°20'-26°10'		269		Halpern (1978)
65	69°34.5'-26°14'	243±25			IIG (1972)
66	69°34.5'-26°14'	67±10			IIG (1972)
67	69°34'-26°17'			39.8±1.2	Quirt (1972); Zentilli (1974)
68	69°34'-26°17'			39.1±1.2	Quirt (1972); Zentilli (1974)
69	69°34.1'-26°16'	45±10			IIG (1972)
70	69°27.7'-26°17'	276±30			IIG (1972)

<u>No.</u>	<u>Location</u>	<u>Pb/<math>\alpha</math></u>	<u>Rb/Sr</u>	<u>K/Ar</u>	<u>Source</u>
71	69°10' - 26°25'		268		Halpern (1978)
72	69°16.4' - 26°18.8'	250±30			IIG (1972)
73	69°26' - 26°23.1'	293±30			IIG (1972)
74	69°25.6' - 26°23.4'	287±30			IIG (1972)
75	69°34' - 26°17'		50	40	Halpern (1978)
76	69°31.9' - 26°13'	61±10			IIG (1972)
77	69°29.4' - 26°22.8'	276±30			IIG (1972)
78	69°17.6' - 26°30.6'	293±30			IIG (1972)
79	69°25.6' - 26°23.4'	287±30			IIG (1972)
80	69°18.4' - 26°29.5'	223±25			IIG (1972)
81	69°25' - 26°25'		244		Halpern (1978)
82	70°15' - 26°37'			117±3.8	Quirt (1972); Zentilli (1974)
83	70°40' - 26°22'			188±5.8	Quirt (1972); Zentilli (1974)
84	70°49' - 26°48'			188±5.6	Quirt (1972); Zentilli (1974)
85	70°29' - 26°72'			144±4.4	Quirt (1972); Zentilli (1974)
86	70°27.8' - 26°20.7'	280±50			IIG (1972)
87	70°41' - 26°34'			191±5.8	Quirt (1972); Zentilli (1974)
88	70°24' - 26°33'			137±4.4	Quirt (1972); Zentilli (1974)
89	70°28' - 26°33'			147±5.0	Quirt (1972); Zentilli (1974)
90	70°21' - 26°33'			125±4.0	Quirt (1972); Zentilli (1974)
91	69°22' - 26°49'			117±4.0	Quirt (1972); Zentilli (1974)
92	70°34' - 26°35'			177±5.4	Quirt (1972); Zentilli (1974)
93	68°19' - 26°53'			0.88	Quirt (1972); Zentilli (1974)
94	70°21.8' - 26°49.6'	158±20			IIG (1972)
95	70°14.5' - 26°52.4'	121±10			IIG (1972)
96	70°01' - 26°52.3'	190±20			IIG (1972)
97	70°32.4' - 27°0.5'	345±10			IIG (1972)
98	68°58' - 27°01'			253±7.8	Quirt (1972); Zentilli (1974)
99	70°51.3' - 27°03.7'	226±25			IIG (1972)
100	70°48' - 27°02.2'	230±30			IIG (1972)
101	70°01' - 27°01'			60.6±2.0	Quirt (1972); Zentilli (1974)
102	70°47' - 27°00'			187±5.8	Quirt (1972); Zentilli (1974)
103	70°56' - 27°21'			182±5.6	Quirt (1972); Zentilli (1974)
104	70°59' - 27°11'			182±5.6	Quirt (1972); Zentilli (1974)
105	69°53' - 27°09'			110	McNutt <u>et al.</u> (1975)

<u>No.</u>	<u>Location</u>	<u>Pb/<math>\alpha</math></u>	<u>Rb/Sr</u>	<u>K/Ar</u>	<u>Source</u>
106	69°59'-27°16'			65-75	McNutt <u>et al.</u> (1975)
107	70°05'-27°48'			65-75	McNutt <u>et al.</u> (1975)
108	69°53'-27°24'			60.4 $\pm$ 2.0	Quirt (1972); Zentilli (1974)
109	70°08'-27°49'			61.8 $\pm$ 2.0	Quirt (1972); Zentilli (1974)
110	70°41.8'-27°25'	318 $\pm$ 30			IIG (1972)
111	70°36.3'-27°22.3'	120 $\pm$ 20			IIG (1972)
112	70°29'-27°22'	128 $\pm$ 20			IIG (1972)
113	70°29'-27°22'	92 $\pm$ 10			IIG (1972)
114	70°05'-27°35.8'	58 $\pm$ 10			IIG (1972)
115	70°04'-27°36.2'	42 $\pm$ 10		59	IIG (1972)
116	70°04'-27°35.7'	64 $\pm$ 10			IIG (1972)
117	70°01'-27°35.2'	51 $\pm$ 10			IIG (1972)
118	69°40'-27°39'			42 $\pm$ 1.4	Quirt (1972); Zentilli (1974)
119	70°05'-27°36'			59 $\pm$ 1.8	Quirt (1972); Zentilli (1974)
120	70°24'-27°36'			107 $\pm$ 3.4	Quirt (1972); Zentilli (1974)
121	70°28'-27°40'			95.5 $\pm$ 3.0	Quirt (1972); Zentilli (1974)
122	70°01'-27°46'			53	McNutt <u>et al.</u> (1975)
123	69°45.2'-27°45'	44 $\pm$ 10			IIG (1972)
124	70°28'-28°20'			62.5 $\pm$ 2.0	Quirt (1972); Zentilli (1974)
125	70°05'-27°48'			75-65	McNutt <u>et al.</u> (1975)
126	70°54.7'-28°07'	130 $\pm$ 20			IIG (1972)
127	70°48.1'-27°52.2'	75 $\pm$ 10			IIG (1972)
128	70°41.2'-27°49.5'	102 $\pm$ 10			IIG (1972)
129	70°07'-27°49.7'	105 $\pm$ 10		62	IIG (1972)
130	69°59.5'-28°03.3'	265 $\pm$ 30			IIG (1972)
131	70°54.7'-28°07'	130 $\pm$ 20			IIG (1972)
132	69°59'-28°07'			60.7	McNutt <u>et al.</u> (1975)
133	70°31'-28°20'			66.6	McNutt <u>et al.</u> (1975)
134	70°30'-28°18'			59.8 $\pm$ 1.8	Quirt (1972); Zentilli (1974)
135	69°53'-28°10'			236 $\pm$ 7.0	Quirt (1972); Zentilli (1974)
136	70°10'-28°42'			87.1 $\pm$ 2.8	Quirt (1972); Zentilli (1974)
137	69°52'-27°59'			262 $\pm$ 10	Quirt (1972); Zentilli (1974)
138	70°34'-25°54'			189 $\pm$ 8.8	Quirt (1972); Zentilli (1974)
139	70°44'-26°43'			185 $\pm$ 5.6	Quirt (1972); Zentilli (1974)
140	70°47'-26°49'			176 $\pm$ 5.4	Quirt (1972); Zentilli (1974)

<u>No.</u>	<u>Location</u>	<u>Pb/<math>\alpha</math></u>	<u>Rb/Sr</u>	<u>K/Ar</u>	<u>Source</u>
141	70°55' - 27°22'			156±4.8	Quirt (1972); Zentilli (1974)
142	70°56' - 28°06'			151±4.6	Quirt (1972); Zentilli (1974)
143	70°54' - 28°05'			148±4.6	Quirt (1972); Zentilli (1974)
144	70°56' - 28°08'			148±8.8	Quirt (1972); Zentilli (1974)
145	70°36' - 26°23'			148±7.0	Quirt (1972); Zentilli (1974)
146	70°21' - 28°20'			66.6±2.4	Quirt (1972); Zentilli (1974)
147	69°50' - 26°45'			64.7±2.0	Quirt (1972); Zentilli (1974)
148	70°02' - 28°09'			64.4±2.0	Quirt (1972); Zentilli (1974)
				62.3±2.0	
149	70°29' - 28°32'			63.3±2.0	Quirt (1972); Zentilli (1974)
150	70°10' - 27°35'			63.1±2.0	Quirt (1972); Zentilli (1974)
151	70°03' - 27°29'			60.8±2.0	Quirt (1972); Zentilli (1974)
152	70°02' - 28°09'			52.3±2.6	Quirt (1972); Zentilli (1974)
				48.0±5.3	
153	70°56' - 28°04'			138±4.0	Quirt (1972); Zentilli (1974)
154	70°20' - 26°25'			123±3.8	Quirt (1972); Zentilli (1974)
155	70°31' - 27°20'			123±3.8	Quirt (1972); Zentilli (1974)
156	70°35' - 27°27'			121±3.8	Quirt (1972); Zentilli (1974)
157	70°50' - 28°13'			120±3.8	Quirt (1972); Zentilli (1974)
158	70°15' - 26°37'			112±3.4	Quirt (1972); Zentilli (1972)
159	70°26' - 27°16'			102±3.2	Quirt (1972); Zentilli (1974)
160	70°23' - 27°22'			90.1±2.8	Quirt (1972); Zentilli (1974)
161	69°18' - 26°47'			41.5±1.4	Quirt (1972); Zentilli (1974)
162	69°56' - 27°48'			43.5±1.4	Quirt (1972); Zentilli (1974)
163	69°25' - 26°30'			37.7±1.2	Quirt (1972); Zentilli (1974)
164	69°25' - 26°30'			34.1±1.0	Quirt (1972); Zentilli (1974)
165	69°15' - 26°49'			23.1±0.8	Quirt (1972); Zentilli (1974)
166	69°15' - 26°49'			22.3±0.8	Quirt (1972); Zentilli (1974)

FIGURE 3.1 Geographic distribution of previous geochronological  
dates of northern Chile.  
Numbers refer to Table 3.1;  
references indexed in Table 3.1.



A chronologic and isotopic study of the plutonism and volcanism of the Copiapó area, reported by Farrar et al., (1970), McNutt et al. (1975) and McBride et al. (1976), suggested that five periods of intrusion occurred during Permian, Lower Jurassic, Middle Cretaceous, Lower Paleocene and Upper Eocene times. Also, the locus of granitic intrusion has apparently migrated eastwards from the present coastal region during Lower Jurassic to Upper Eocene times (Farrar et al., 1970).

Continuous magmatic activity in the Central Andean orogen of northern Chile from "at least Permian to the present" has been suggested by Halpern (1978) on the basis of Rb/Sr total rock and mineral data.

The geologic history of the area had been based on scattered reports dealing with specific aspects of the geology and mineral occurrences and on a few radiometric dates. There was considerable doubt as to the applicability of the geochronological data outside of the area immediately surrounding the sampled plutons.

The majority of the ore deposits of the study area appear to be related to magmatic processes (intrusive or volcanic) but there was no reliable information about the age of the magmatic activity and the associated mineralization.

A geochronological investigation directed toward the establishment of a chronology of plutonism and ore formation was therefore decided upon. With this aim, samples were collected in the study area and in the surrounding area, from which 15 were

dated by the K/Ar or the  $^{40}\text{Ar}/^{39}\text{Ar}$  methods.

#### Method

The samples selected for this study were dated by the K/Ar and/or  $^{40}\text{Ar}/^{39}\text{Ar}$  method. The principles, constants used, sample preparation techniques, etc. are discussed in Appendix I.

#### Results and Discussion

The location of each sample is given in Figure 3.2 and the dated specimens have been assigned numbers from 1 to 15, in approximate order from north to south. The analytical data for each determination, the grid reference, and the petrographic classification of each specimen can be found in Tables 3.2 and 3.3. Age data for rocks located outside of the study area have been included (Figure 3.1).

Most of the samples show a low potassium content. This is due to partial alteration (e.g. chloritization), or the presence of impurities of either hornblende or other potassium-poor accessory minerals. The chlorite might be due to a significantly later episode of alteration or weathering, which could have led to partial argon outgassing. The apparent ages should therefore be considered minimum values.

Some separates were dated despite their low K content because of the need for age data for certain critical areas where no fresher material could be found.



TABLE 3.2

## Radiometric Data for the Plutonic Rocks, Cifuncho-Cerro del Pingo Area

SAMPLE	Field Number	Location Lat.S. Long.W.		Rock Type	Material Analyzed	%K (Weight)	$^{40}\text{Ar}/^{39}\text{Ar}$ Rad/ $^{40}\text{Ar}$ Total	$^{40}\text{Ar}/^{39}\text{Ar}$ Age Plateau	Age Total Gas	K/Ar Age
1	UP-7	25°32'	70°06'	Diorite	Horn- blende			127	121±66*1	
2	UP-2N	25°39'	70°10'	Monzo- diorite	Biotite	2.324	0.483			111±3*2
3	UP-2S	25°42'	70°11'	Monzo- diorite	Biotite	2.748	0.783			117±3
4	Z-713	25°39'	70°38'	Grano- diorite	Biotite			261	259±8	
5	Z-716	25°54'	70°34'	Diorite	Biotite	2.419	0.896			186±6
6	U-174	25°55'	70°12'	Diorite	Biotite	6.558	0.964	127	124±4	120±3
7	UP-4	25°56'	70°08'	Grano- diorite	Biotite	4.516	0.278			112±4
8	3B-243	26°19'	70°26'	Andesite	Whole rock	1.62	0.600			142±12
9	JN-111-322	26°18'	70°23'	Monzo- diorite	Biotite	7.050	0.979			130±4
10	JN-111-348	26°18'	70°20'	Monzo- diorite	Biotite	6.538	0.582			129±4
11	UP-12	26°19'	70°26'	Pegmatite	Biotite	7.681	0.937			150±5
12	Z-1-75	25°57'	69°58'	Porphyry	Horn- blende			105	115±28	
13	Z-2-75	25°54'	69°55'	Tonalite	Horn- blende	0.464	0.665			96±2
14	Z-3-75	25°54'	69°55'	Andesite	Whole rock	3.67	0.639			106±3
15	UP-6	25°36'	70°12'	Andesite	Biotite	1.596	0.660			111±3
16	UP-6	25°36'	70°12'	Andesite	Whole rock	1.31	0.561			115±11

\*1 = 2σ absolute error

\*2 = 1σ absolute error

TABLE 3.3

Analytical Data for  $^{40}\text{Ar}/^{39}\text{Ar}$  Incremental Heating

Sample Mineral (J-value)	Steps Temp. C <sup>o</sup>	Ar Released%	$^{40}\text{Ar}/^{36}\text{Ar}$	$^{39}\text{Ar}/^{36}\text{Ar}$	Atmos. Ar Correction %	Rock Type	App. Age (Ma $\pm$ 1 $\sigma$ )	Field No.
1 Horn- blende (0.04234)	200-600	18.1	302.328	1.160520	97.70	Diorite	44 $\pm$ 10	UP-7
	600-700	7.2	298.319	0.222796	99.05		94 $\pm$ 103	
	700-800	10.1	309.461	0.529445	95.49		191 $\pm$ 20	
	800-900	14.4	317.107	1.178120	93.18		135 $\pm$ 9	
	900-960	17.3	316.466	1.267090	93.37		122 $\pm$ 8	
	960-1020	19.9	307.256	0.771221	96.17		113 $\pm$ 15	
	1020-1080	9.3	300.530	0.217042	98.33		169 $\pm$ 144	
	1080-1140	3.7	302.505	0.285830	97.68		178 $\pm$ 74	
Total Gas Age							121 $\pm$ 66 <sup>*2</sup>	
4 Biotite (0.001784)	200-600	6.9	429.218	6.20008	68.85	Grano- diorite	68.1 $\pm$ 2.3 <sup>*1</sup>	Z-713
	600-675	2.4	1244.68	10.9192	23.74		260.1 $\pm$ 2.0	
	675-750	10.4	1768.89	16.8873	16.70		261 $\pm$ 1.9	
	750-825	17.2	5904.32	62.6856	5.00		267.2 $\pm$ 1.3	
	825-900	13.2	1451.96	12.3957	20.35		277.7 $\pm$ 2.1	
	900-975	27.3	1743.93	16.5769	16.94		261.3 $\pm$ 0.9	
	975-1050	15.4	2066.31	17.9661	14.30		292.2 $\pm$ 1.1	
	1050-1200	7.2	453.626	1.91955	65.14		247.4 $\pm$ 4.1	
Total Gas Age							259 $\pm$ 8.22 <sup>*2</sup>	

Sample Mineral (J-value)	Steps Temp. C°	Ar Released%	$^{40}\text{Ar}/^{36}\text{Ar}$	$^{39}\text{Ar}/^{36}\text{Ar}$	Atmos. Ar Correction %	Rock Type	App. Age (Ma $\pm$ 1 $\sigma$ )	Field No.
6 Biotite (0.001784)	200-600	2.3	328.303	2.02684	90.0	Diorite	51.4 $\pm$ 2.6	U-174
	600-700	5.0	543.074	6.04903	54.41		127.1 $\pm$ 1.4	
	700-775	7.2	827.177	13.1682	35.72		125.5 $\pm$ 0.6	
	775-850	7.4	474.293	4.34738	62.30		127.7 $\pm$ 1.8	
	850-925	5.0	423.873	3.03738	69.71		131.1 $\pm$ 2.5	
	925-1000	27.0	1079.78	19.2245	27.37		126.7 $\pm$ 0.3	
	1000-1075	43.8	878.389	14.6701	33.64		123.6 $\pm$ 0.4	
	1075-1150	2.3	326.169	0.732247	90.60		130.0 $\pm$ 11.9	
Total Gas Age							124 $\pm$ 4.58 <sup>*2</sup>	
12 Horn- blende (0.004124)	200-600	5.0	299.403	0.388815	98.69		73 $\pm$ 71	Z-1-75
	600-750	8.8	343.616	1.66422	85.99		203 $\pm$ 6	
	750-850	13.0	322.049	1.82477	91.75		105 $\pm$ 6	
	850-950	13.4	329.632	2.3874	89.64		103 $\pm$ 5	
	950-1050	30.7	364.215	4.82273	81.13		103 $\pm$ 3	
	1050-1150	17.2	325.703	2.10965	90.72		104 $\pm$ 5	
	1150-1250	11.9	301.412	0.365004	98.04		117 $\pm$ 5.3	
	Total Gas Age							

\*1 interstep uncertainty

\*2 2 $\sigma$  absolute error

FIGURE 3.2 Localities of the dated samples of  
Table 3.2 and 3.3.  
Outlined are areas with granitic outcrops.

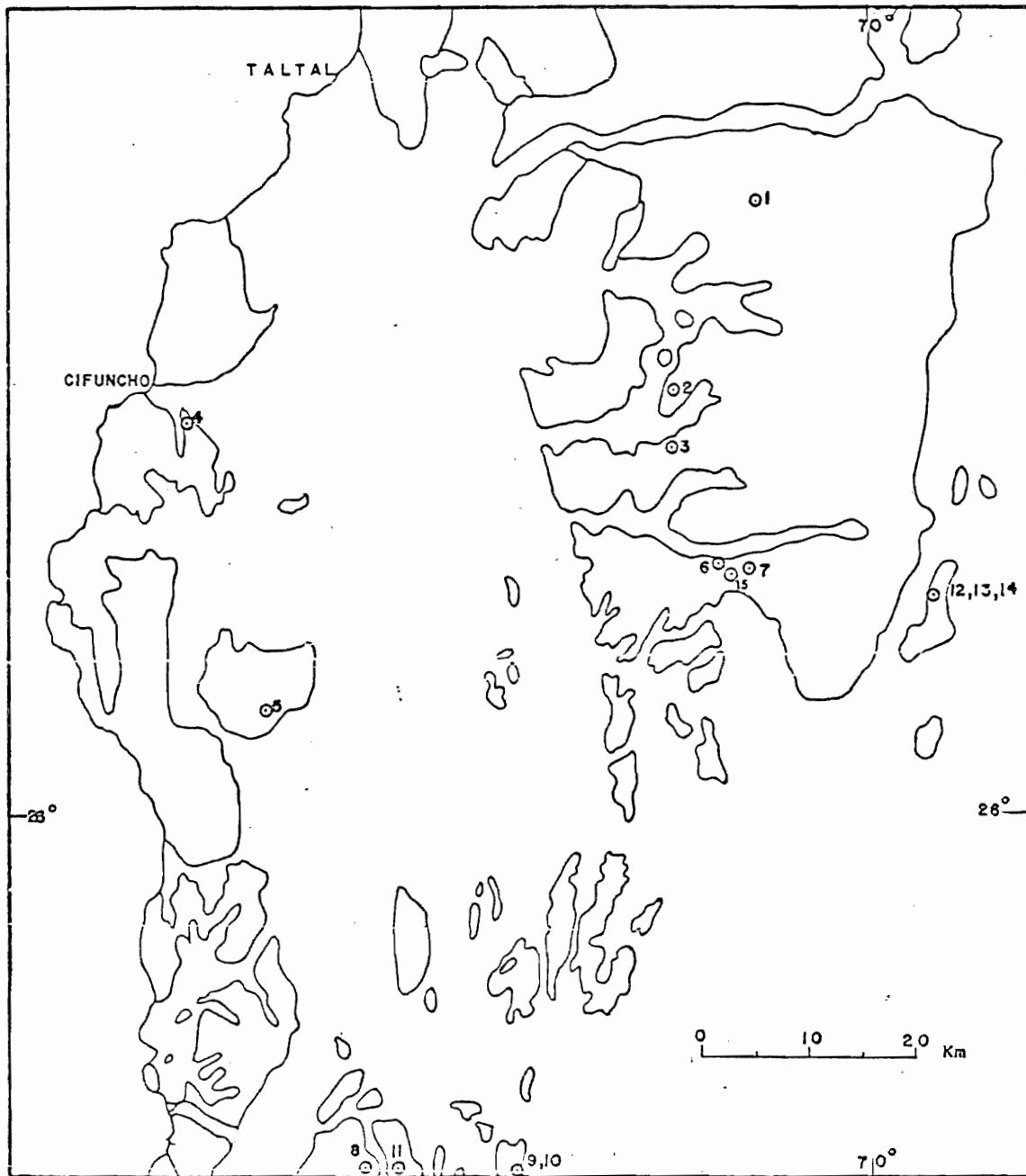


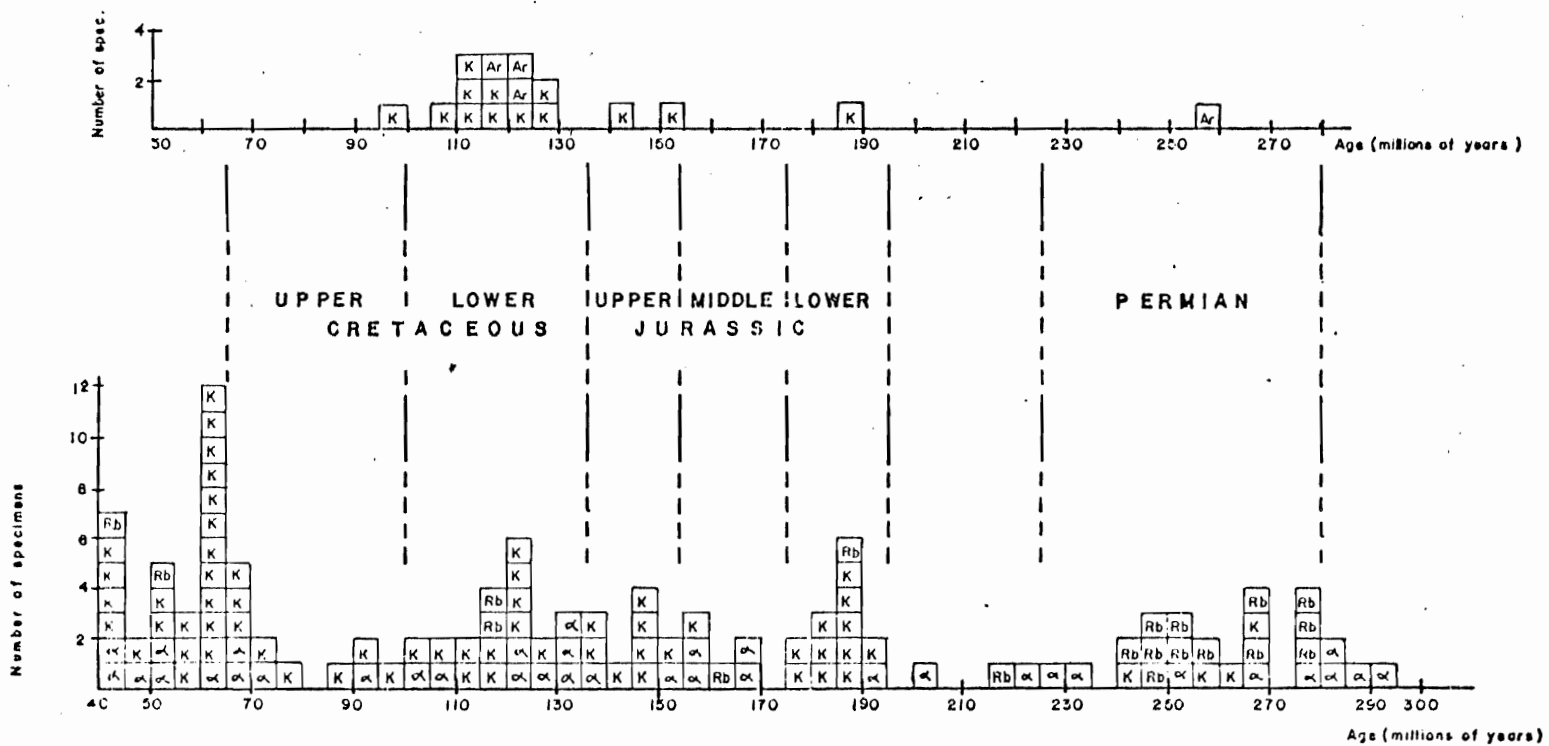
FIGURE 3.3 A histogram of the new dated samples (above)  
and previous dates (below)  
in northern Chile

$$K = K/Ar$$

$$Ar = {}^{40}_{Ar}/{}^{39}_{Ar}$$

$$\alpha = Pb/\alpha$$

$$Rb = Rb/Sr$$



The K/Ar and  $^{40}\text{Ar}/^{39}\text{Ar}$  age dates can be classified into the following time intervals (see Appendix 2) (Figure 3.3):

284 - 242 Ma	Sample 4	Permian
208 - 176 Ma	Sample 5	Lower Jurassic
176 - 140 Ma	Samples 8, 11	Upper Jurassic
140 - 102 Ma	Samples 1, 2, 3, 6, 7, 9, 12, 14, 15, 10	Lower Cretaceous
102 - 64 Ma	Sample 13	Upper Cretaceous

From Figures 3.4 and 3.5 it is evident that Paleozoic granitic rocks are distributed along the present coast. There follows (inland) a narrow belt of Jurassic rocks, and to the east occur younger (Upper and Lower Cretaceous) rocks. If it is assumed that the K/Ar and  $^{40}\text{Ar}/^{39}\text{Ar}$  ages represent the approximate ages of pluton emplacement and initial cooling, then Figures 2.3 and 3.5 suggest an overprinting of Mesozoic magmatic activity onto a Paleozoic basement and a migration of the locus of intrusion eastwards from the present coast.



FIGURE 3.4 A map of the Taltal-Copiapó area showing  
the belts of granitic rocks.  
(Modified after Zentilli, 1974).

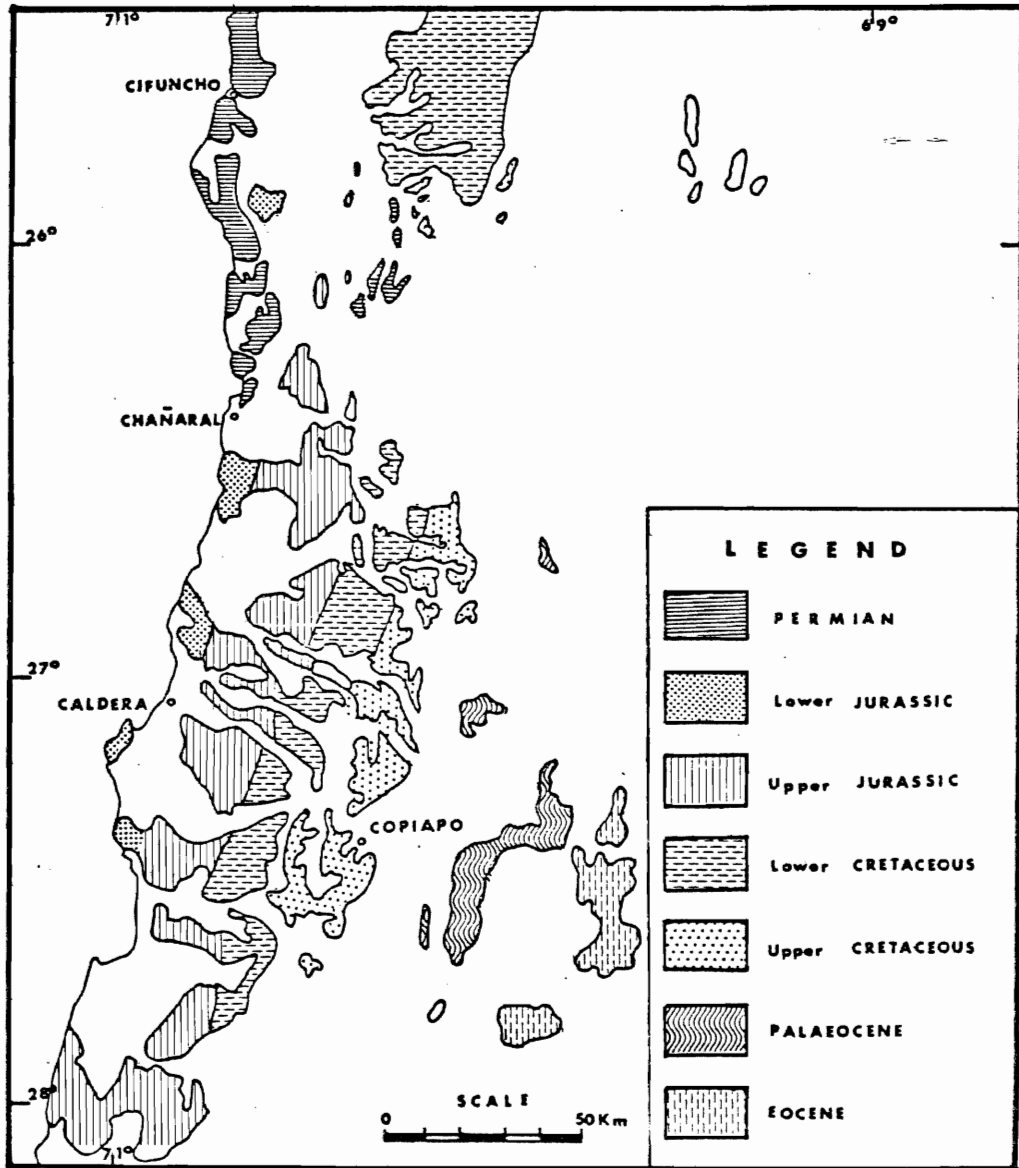
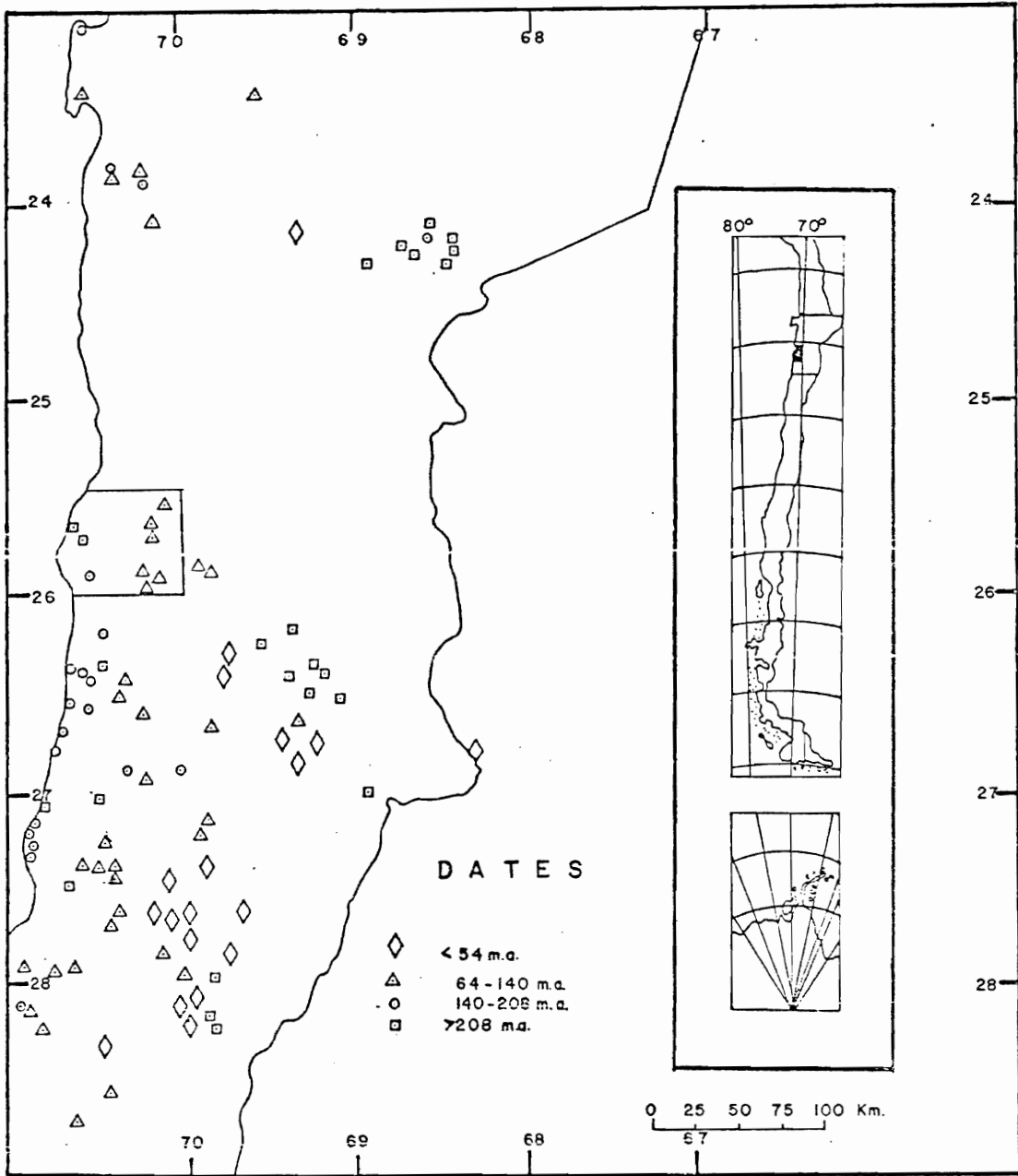


FIGURE 3.5 Partial compilation of radiometric dates  
from the study area and northern Chile.

See Table 3.1.



## Paleozoic Dates

Along the coast in the central part of the study area and farther south outside the area, a series of outcrops of granitic rocks occur. Sample 4 was collected in Caleta Cifuncho; biotite from this rock yielded a (total gas)  $^{40}\text{Ar}/^{39}\text{Ar}$  date of  $259 \pm 8$  Ma, which is in excellent agreement with a previous K/Ar date for the same pluton of  $267 \pm 8$  Ma (Zentilli, 1974). The age spectrum of this sample (Figure 3.7) is, however, quite discordant and does not have an age plateau; obviously the system has been disturbed by later magmatic activity, and so the total gas ages must be considered minimum values.

A Pb/ $\alpha$  age of  $340 \pm 40$  Ma was obtained for zircon from an adamellite from the Cifuncho area, 1.5 km east of the above sample locality. The adamellite described in Levi et al. (1963) is altered and has a granular texture. Stratigraphically, it is intruding a meta-sedimentary sequence (slates, quartzites) and it is overlain unconformably by conglomerates of the Rhyolite Conglomerate Unit (RCU) and by conglomerates of the Cifuncho Formation which clearly contain clasts of the same adamellite. The Cifuncho Formation is considered to be of Triassic age and is overlain by marine limestone of Early Jurassic age. The Rhyolite Conglomerate Unit is overlain by sandstones and limestones of the Cifuncho Formation. Thus, a stratigraphically well-documented pre-Mesozoic pluton yields Paleozoic dates, as is generally the case in the Andes at these latitudes (Zentilli, 1974). This has important implications concerning the

Axis of Pleistocene Volcanism

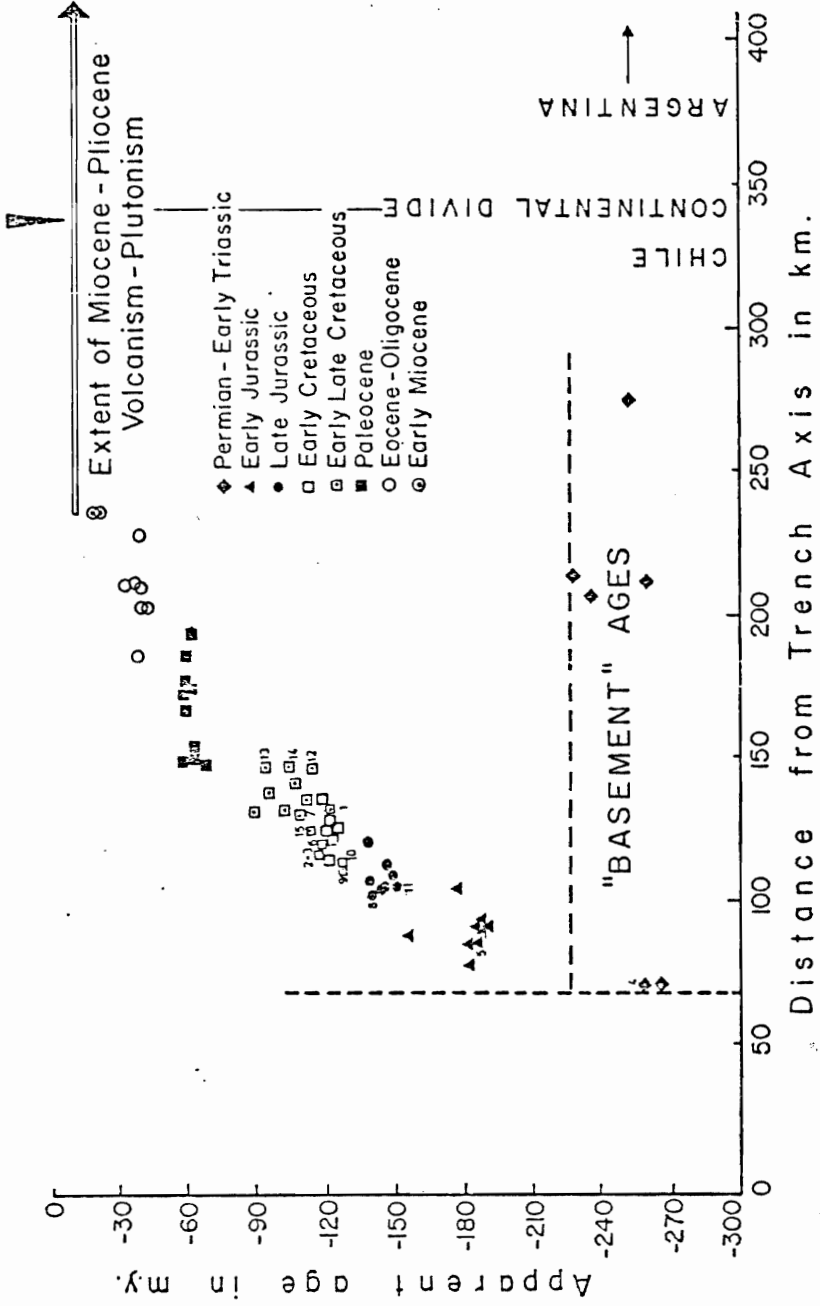
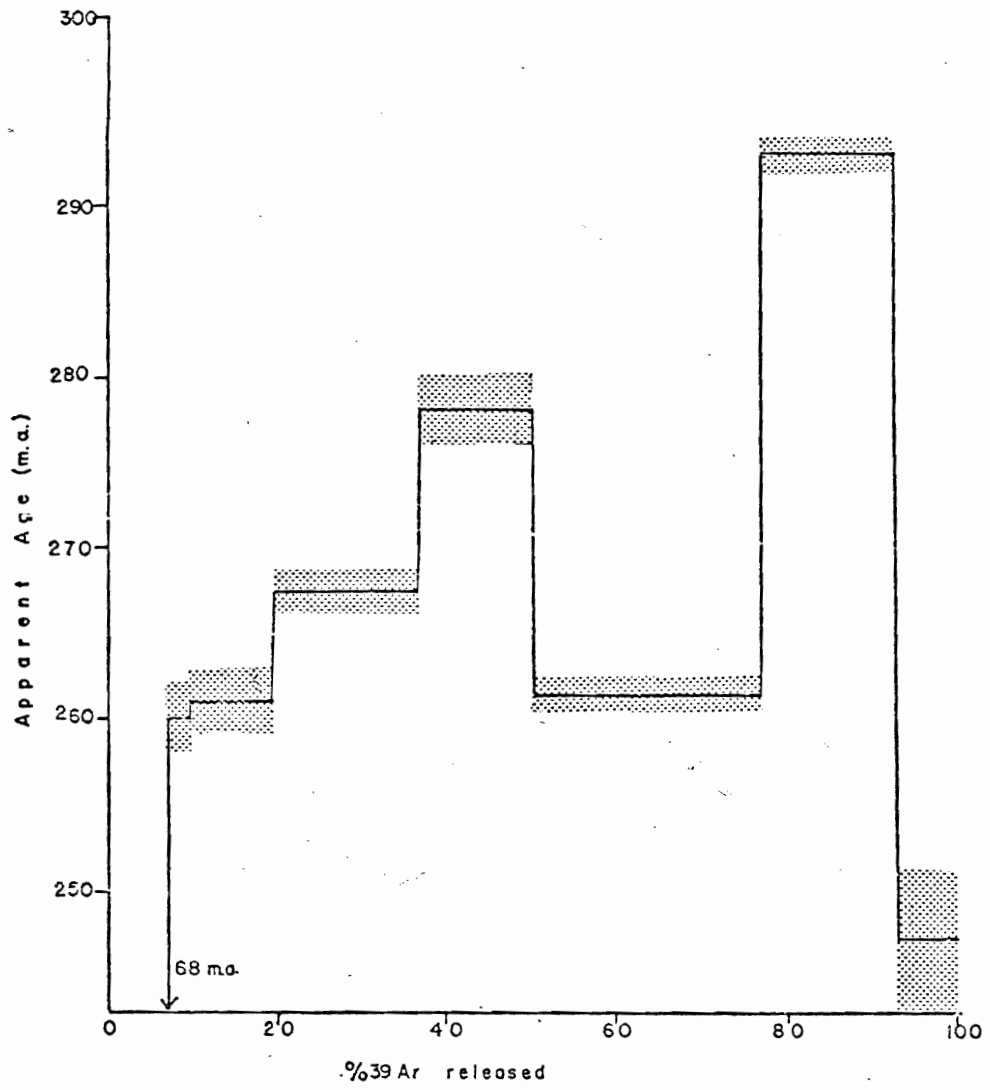


FIGURE 3.7 Stepwise degassing release curves  
for sample 4 (Paleozoic granodiorite).





interpretation of younger dates.

#### Mesozoic Dates

Interpretation of the radiometric dating of the Mesozoic granitic rocks is more problematic. Although in many cases the stratigraphic relationships between intrusive and sedimentary rocks are clear, later hydrothermal alteration associated with mineralization has reset the argon clock.

Sample 5, a diorite collected in the La Cachina gully, yielded a K/Ar (biotite) age of  $186 \pm 6$  Ma. The diorite intrudes volcanics of Permian-Triassic age (RCU) and marine fossiliferous sediments of Hettangian to Early Pliensbachian age and is therefore clearly post-Paleozoic and at least (post) Pliensbachian in age. A sample from the same locality analyzed by Zentilli (1974) yielded a K/Ar (biotite) age of  $189 \pm 9$  Ma. The biotite in both of these samples is altered. However, the diorite belonging to the Sierra Esmeralda Pluton is clearly intruding the Lower Triassic marine sediments whose age is controlled by fossils with a specific range of age.

South of the present study area, Farrar et al. (1970) have documented a  $186 \pm 6$  Ma (Early Jurassic) thermal episode. There, however, stratigraphic relationships are not clear, and the dated rocks could possibly be much older. Zentilli (1974) and later Haymes (1975) discuss three possible interpretations for the Jurassic K/Ar dates in the southern area: a) rapid uplift

and unroofing of the coastal Paleozoic basement during the Lower Jurassic, the event which initiated argon retention; b) a re-setting of argon clocks due to metamorphism of the Paleozoic basement associated with a Jurassic intrusive episode; and c) actual intrusion in Jurassic times. None of the explanations seems totally satisfactory.

The concept of the metamorphic outgassing of the Paleozoic basement by Late Jurassic plutonic episode, at first glance appears attractive. The plutonic body has been affected by hydrothermal activity, as evidenced by silver, gold and copper mineralization along the contact with the sedimentary rocks. This hydrothermal activity could well have outgassed the biotites within Paleozoic plutons.

Alternatively, one might propose that the Cifuncho Batholith was intruded along its eastern border by Jurassic plutons (Upper Jurassic?) and the dated rocks were derived from the assimilation of older granitic rocks by the new intrusive body. All these arguments are unnecessary for the present study area. The diorite (sample 5) is compositionally different from the Paleozoic rocks and the stratigraphic relationships are well documented, therefore, the diorite represents an Early Jurassic intrusive episode.

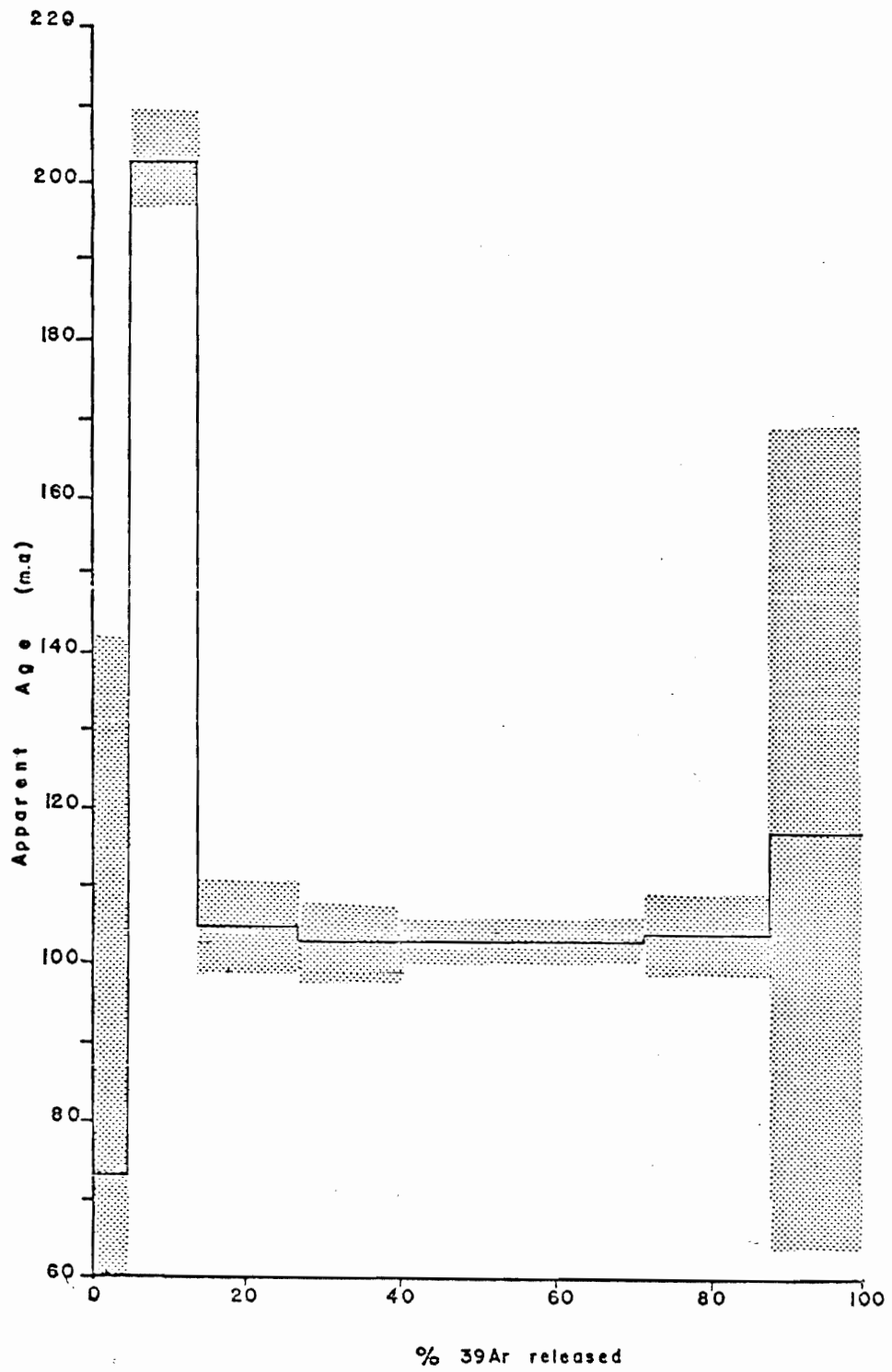
Sample 8 was collected from an andesitic dyke in Cerro Vetado (Copiapo) outside the boundary of the study area where the exposure is better. The author considers it representative

of the dykes of Cifuncho-Cerro del Pingo area described within the area (Chapter II). The sample yielded a K/Ar whole rock age of  $142 \pm 14$  Ma. The dykes cross-cut the Permian granite, forming a lattice-like pattern conspicuous on the air photos. These dykes intrude, as well, Triassic and Early Jurassic rocks. The reliability of the age is questionable because of both the inhomogeneity of the sample and the strong chloritic alteration. However, these effects generally lead to an age that is too young, not too old, and thus the data are consistent with a Late Jurassic episode of dyke intrusion.

Sample 12 (diorite) was collected close to Altamira, outside the boundary of the study area. The  $^{40}\text{Ar}/^{39}\text{Ar}$  stepwise outgassing data define an age plateau over 80% of the total gas released (Figure 3.8). Small differences in apparent age may result from a very limited amount of irradiation-induced lattice disorder and consequent effective redistribution of argon isotopes within each sample (Turner and Codogan, 1974; Brereton, 1972). The plateau age is 105 Ma: the total gas age is 115 Ma, compatible with the expected Cretaceous age of the rocks.

Sample 14, an andesite, was collected close to Altamira, again outside the eastern boundary of the study area. It yielded a K/Ar whole rock age of  $106 \pm 3$  Ma. The sample has been affected by a post-crystallization thermal event probably related to hydrothermal alteration and copper mineralization.

FIGURE 3.8 Stepwise degassing release curves for  
Sample 12 (Lower Cretaceous porphyry).



Sample 11 was collected from a pegmatite from Cerro Vetado, south of the border of the study area. It yielded a K/Ar (biotite) age of  $150 \pm 5$  Ma. The pegmatite occurs within the large Cerro Vetado batholith (Naranjo, 1978) of Paleozoic age. The pegmatite event could belong to the same Late Jurassic episode of dyke intrusion as discussed above for sample 8, but could be interpreted as an older date disturbed by the above episode of dyke intrusion. Samples 1, 2, 3, 6 and 7 (Figures 3.9 and 3.10) were collected from different localities of the study area, but all belong to the same dioritic-granodioritic batholith which intrudes sedimentary and volcanic rocks of the Lower Cretaceous Aeropuerto Formation (Chapter II). The poly-phase nature of this batholith was described in Chapter II. Most of the samples yield a rather similar Early Cretaceous date (see Tables 3.2 and 3.3). Sample 1, a hornblende diorite, was collected north of La Peineta gully and yielded a  $^{40}\text{Ar}/^{39}\text{Ar}$  total gas hornblende gas of  $121 \pm 66$  Ma. The age spectrum (Figure 3.9) exhibits a rather poorly-defined age plateau over 60% of the gas released at approximately 125 Ma.

Sample 15, an andesite from the Aeropuerto Formation was collected in Sierra del Carmen and yielded a K/Ar (biotite) age of  $111 \pm 3$  Ma and a K/Ar whole rock age of  $115 \pm 11$  Ma.

FIGURE 3.9 Stepwise degassing release curves  
for Sample 1 (Lower Cretaceous Diorite).

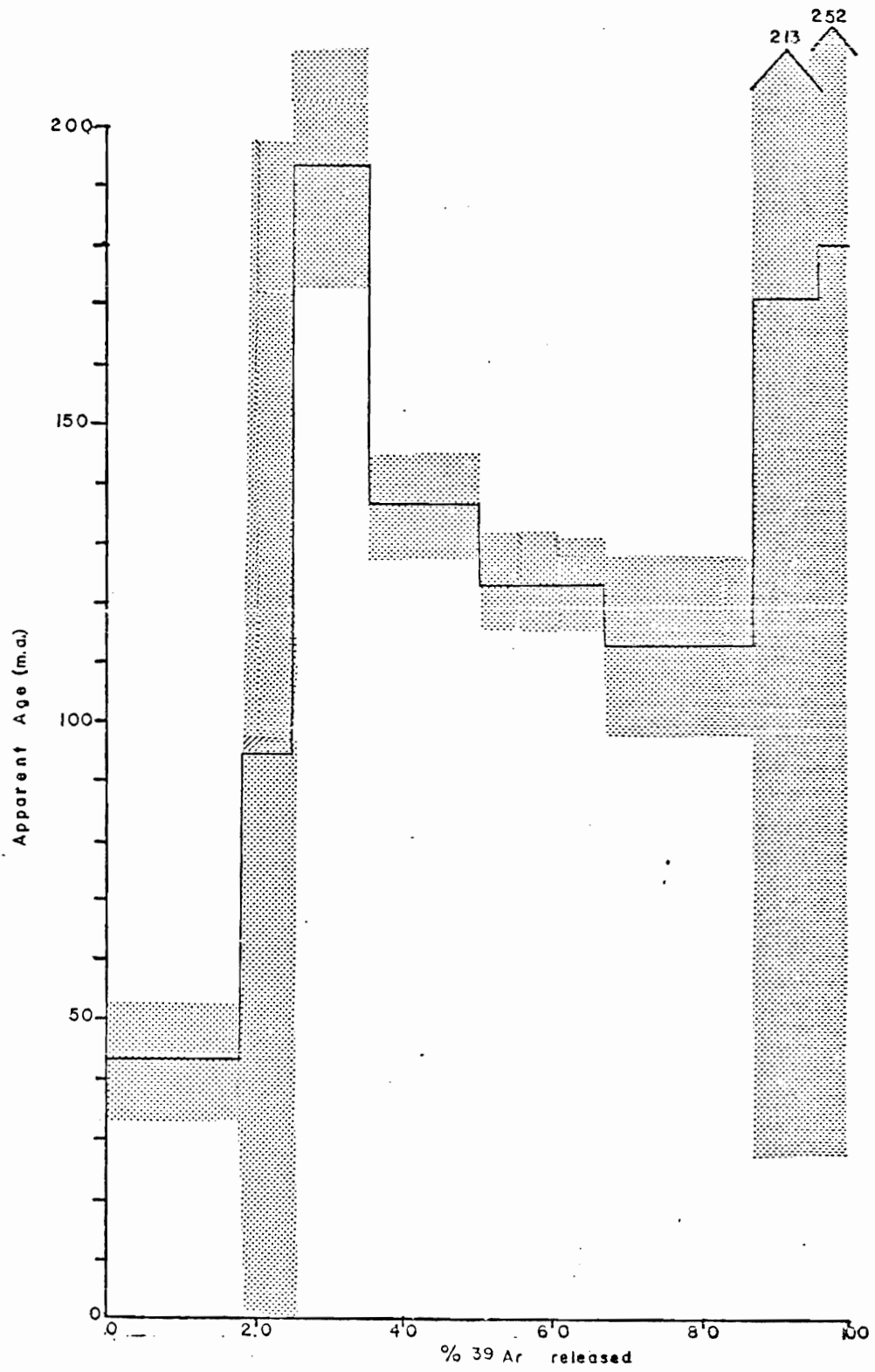
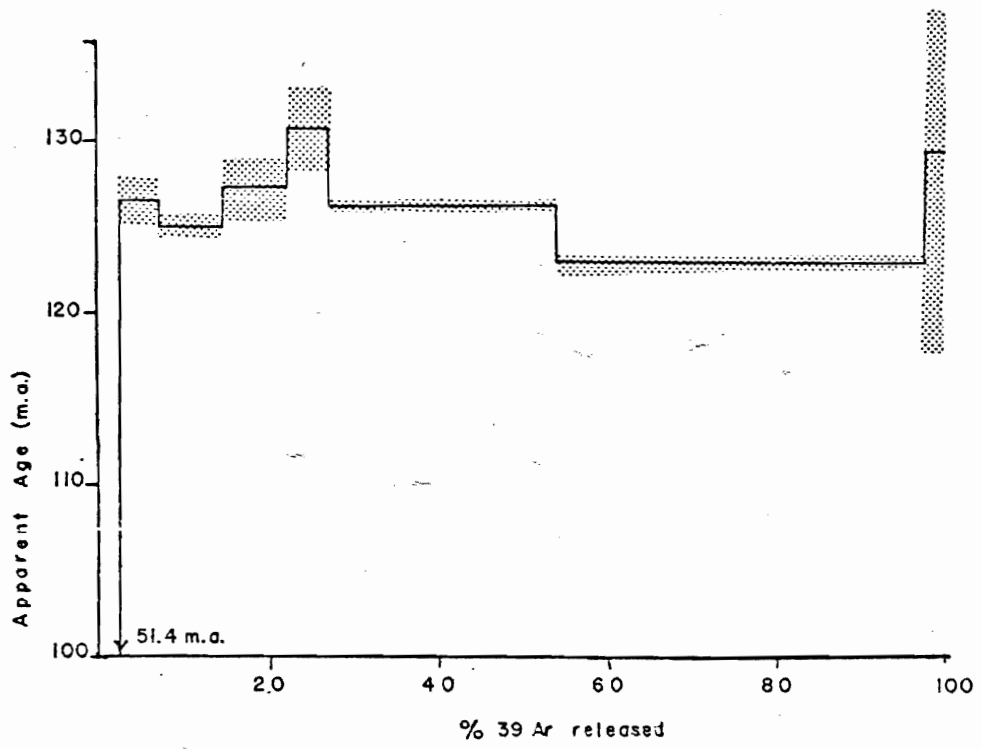




FIGURE 3.10 Stepwise degassing release curves  
for Sample 6 (Lower Cretaceous Diorite).



Samples 9 and 10, monzodiorites, were collected south of the study area and yielded K/Ar (biotite) ages of  $130 \pm 4$  Ma and  $129 \pm 4$  Ma, respectively. These samples are from the Sierra Minillas Batholith which intrudes Jurassic volcanic rocks of the La Negra Formation and Paleozoic intrusive and metamorphic rocks (Naranjo, 1978). The above dates are therefore consistent with the stratigraphic relationships.

Sample 13, a tonalitic dyke intruding above diorite and andesite (samples 12 and 14), yielded a K/Ar hornblende age of  $96 \pm 2$  Ma.

This work has confirmed the existence of Late Paleozoic, Early Jurassic, Late Jurassic and Early Cretaceous to early Late Cretaceous magmatic episodes and an eastward migration of granitic intrusions with time (Farrar et al., 1971; Quirt, 1972; Zentilli, 1974; McNutt et al., 1975).

Thus, migration of igneous activity seems to be a dynamic characteristic of this continental border region, at least since Early Mesozoic times.

## CHAPTER IV

### MINERALIZATION AND ITS RELATIONSHIP TO THE GEOLOGICAL EVOLUTION: METALLOGENY

Paleozoic rocks in the study area are devoid of known economic mineralization, in contrast with the Mesozoic rocks which are rich in metallic ore deposits. Most of the ore deposits are related to intrusive bodies of different ages discussed in previous chapters. The mineralization becomes younger from west to east, forming a series of longitudinal subprovinces or belts with contrasting mineral types. In this chapter a summary of the distribution of the mineralization, typical for each subprovince, is explained.

The geographic distribution of the mineral deposits in the study area is shown in Figure 4.1; the numbered mines or districts are listed in Table 4.1.

#### Mineralization in Paleozoic Rocks

Along the coastal area of the Cifuncho-Cerro del Pingo map sheet, Pb, Zn and Au mineralization has been recognized, although it does not attain the magnitude of the Mesozoic mineralization.

TABLE 4.1

## List of Mineral Deposits, Cifuncho del Pingo Area

Abbreviations

Ag	=	silver
ak	=	amphibole, predominantly actinolite
ap	=	apatite
asp	=	arsenopyrite
Au	=	gold
ba	=	barite
bo	=	bornite
brthp-skut	=	breithauptite-skutterudite
brau	=	braunite
ca	=	calcite
cc	=	chalcocite; in part djurleite
cp	=	chalcopyrite
ga	=	galena
gersd	=	gersdorffite
hem	=	hematite; includes specularite
mag	=	magnetite
nicc	=	niccolite
ox	=	copper, supergene minerals
(psil	=	psilomelane)
py	=	pyrite
ramm	=	rammelsbergite
saff	=	safflorite
sp	=	sphalerite
tl	=	tourmaline
sc	=	scapolite

(\*) = Number corresponds to symbols in Figure 4.1.

(\*\*) = Main element recovered.

(\*\*\*) = Partial mineralogy, mainly from macroscopic observations.

(\*\*\*\*) = Partial gangue, mainly from macroscopic observations.

TABLE 4.1

Number*	Element**	Mine	Location		Form	Mineralogy***	Gangue****
			Lat. S	Long. W			
1	Cu		25°30'50"	70°28'00"	Vein	cp, cc	py, hem., ca, q
2	Cu		25°32'25"	70°24'40"	Vein	ox	hm, ch, ep, q
3	Cu		25°32'30"	70°16'30"	Vein	cp, ox	py, ca, q, sc, hem, lim
4	Cu		25°33'30"	70°24'20"	Manto	cc, ox	py, lim, ep, ca
5	Cu		25°33'30"	70°25'00"	Vein	ox, cc	lim, q, ch, hem, ca
6	Cu		25°33'00"	70°16'35"	Vein	cp, ox	lim, q, ca, hem
7	Cu		25°33'45"	70°13'30"	Vein	ox	hem, q, ca
8	Cu		25°33'20"	70°14'00"	Vein	ox	q, hem, lim, sc, ca
9	Cu		25°34'00"	70°25'00"	Vein	cp, ox	hem, ch, ca
10	Cu		25°34'15"	70°18'10"	Vein	cp, ox	lim, q, ca, hem, sc
11	Cu		25°34'20"	70°10'15"	Vein	cp, ox	py, hem, ca, q, sa, lim
12	Cu		25°34'30"	70°06'50"	Vein	cp, ox	hem, q, sc, ca, py
13	Cu		25°34'30"	70°10'30"	Vein	ox	py, lim, q, ca, sc, hem
14	Cu		25°34'30"	70°24'50"	Vein	ox	ca
15	Cu		25°34'45"	70°06'50"	Vein	ox	hem, q, sc, py, ca
16	Cu	Arenillas	25°34'40"	70°13'15"	Vein	ox	lim, hem
17	Cu		25°34'50"	70°10'30"	Vein	cp, ox	q, sc, ca, lim, hem
18	Cu		25°34'50"	70°10'15"	Vein	ox	lim, q, ca, sc
19	Cu		25°35'00"	70°20'00"	Veins	ox	py, sc, hem
20	Cu		25°35'00"	70°15'45"	Vein	ox	py, sc

Number**	Element**	Mine	Location		Form	Mineralogy***	Gangue****
			Lat. S	Long. W			
21	Cu		25°35'00"	70°20'00"	Vein	ox	py, hem
22	Cu		25°35'15"	70°25'00"	Manto	cp, bo, ox	ch, ep, ca, hem, lim, q
23	Cu		25°35'15"	70°12'15"	Vein	cp, bo, ox	hem, q, ch, cc, lim
24	Cu		25°35'10"	70°12'15"	Vein	ox	hem, q, ca, sc, lim
25	Cu		25°35'17"	70°12'15"	Vein	ox	hem, ca
26	Cu		25°35'20"	70°12'15"	Vein	ox	hem, sc, ca, q
27	Cu		25°35'30"	70°28'30"	Veins	cp, ox	ca, hem, lim
28	Cu		25°35'45"	70°08'15"	Vein	cp, ox	py, sc, hem
29	Cu	Sta. Rita Islena	25°35'45"	70°20'30"	Veins	ox	hem, ca, q
30	Ag Cu		25°35'50"	70°20'30"	Veins	bo, ox, Au, Cu	ca, q, hem
31	Cu		25°35'50"	70°05'53"	Vein	cp, ox	hem, sc, q, py, ca
32	Cu		25°36'00"	70°21'00"	Vein	ox	hem
33	Cu		25°36'10"	70°18'20"	Veins	ox	q, py, lim
34	Cu		25°36'15"	70°27'30"	Manto	cp, ox	ca, hem
35	Cu		25°36'20"	70°24'00"	Manto	cp, ox	lim, hem, q
36	Cu		25°36'20"	70°25'50"	Vein	cc, ox	ca, ch
37	Cu		25°37'15"	70°24'00"	Vein	ox	hem, ca, lim
38	Cu		25°37'20"	70°20'45"	Manto	ox	py, q, ca
39	Cu		25°37'30"	70°35'15"	Vein	cp, ox	ca, lim
40	Cu		25°38'30"	70°28'00"	Manto	bo, ox	ca, hem
41	Cu		25°38'35"	70°28'45"	Manto	ox	ep, ca
42	Cu		25°38'50"	70°28'00"	Veins	ox, cc	hem, ca, lim
43			25°39'00"	70°23'45"	Vein	ox, cc	ca
44	Cu		25°39'15"	70°25'50"	Manto	cp, ox	ch, lim
45	Cu		25°39'20"	70°26'00"	Manto	cc, ox	ca, ch
46	Cu		25°39'30"	70°22'50"	Vein	cp, bo, ox	ca, lim
47	Cu		25°41'15"	70°25'45"	Manto	ox	ca

Number*	Element**	Mine	Location		Form	Mineralogy***	Gangue****
			Lat. S.	Long. W			
48	Cu	Feiru	25°41'00"	70°26'40"	Manto	ox, cc	ch
49	Cu		25°39'00"	70°23'00"	Manto	ox	lim, ch
50	Cu	Por- venir	25°40'20"	70°28'30"	Manto	ox	q, hem
51	Cu		25°41'00"	70°28'30"	Veins	ox	ch, ca, hem
52	Cu		25°41'07"	70°28'30"	Veins	cc, cp, bo	ca, hem
53	Cu		25°42'50"	70°16'00"	Vein	cp, ox	py, q, ca, sc, lim
54	Cu	San Pedro	25°43'00"	70°13'00"	Vein	cp, cc, ox	ca, q, py
55	Cu		25°43'25"	70°16'15"	Vein	cp, ox	ca, q, lim, ch, sc
56	Cu		25°43'40"	70°17'20"	Vein	ox	hem, mag, ch, sa, ca
57	Cu		25°43'45"	70°20'15"	Vein	ox, cp	ca
58	Cu		25°44'00"	70°17'30"	Vein	ox	hem, ch, ca
59	Cu		25°45'10"	70°03'30"	Vein	ox	hem
60	Cu		25°41'08"	70°28'50"	Vein	cp, bo, ox	ca
61	Cu		25°42'20"	70°24'50"	Veins	ox	ca, hem, ch
62	Ag	San Jose del Pingo	25°42'20"	70°25'30"	Vein	Ag	ca, ak, q, ch, lim
63	Fe		25°42'50"	70°17'80"	Vein	mag, ox	lim, sc, q
64	Fe	Monte- cristo	25°42'35"	70°16'30"	Vein	mag, ox	sc, q
65	Cu		25°42'30"	70°14'00"	Vein	cc, ox	hem, py
66	Cu		25°41'30"	70°18'35"	Vein	ox, cp, bo	ch, ep, ca, lim, hem
67	Cu		25°45'00"	70°09'30"	Vein	cp, ox	lim, q, ca, hem, py
68			25°45'30"	70°25'30"	Manto	ox, cp	ca, ch
69	Cu		25°45'30"	70°22'30"	Manto	cc, ox	ca, ch, ep
70	Fe		25°46'10"	70°16'45"	Veins	mag	lim, hem
71	Cu		25°46'00"	70°08'30"	Vein	ox	hem, lim, ca, sc
72	Cu		25°49'00"	70°00'45"	Irreg. body	ox	ca



Number*	Element**	Mine	Location		Form	Mineralogy***	Gangue****
			Lat. S	Long. W			
73	Fe		25°50'45"	70°04'25"	Tabular body mag		ep, q
74	Cu		25°50'25"	70°22'50"	Manto ox		hem, ch, ca, PY
75	Cu		25°50'48"	70°29'00"	Vein ox, cc		ca, lim
76	Cu		25°50'10"	70°30'45"	Vein ox		ca, hem, lim
77	Cu		25°50'28"	70°30'30"	Vein ox		lim, ca, hem
78	Cu	Olga	25°52'08"	70°26'30"	Veins ox		ca, hem
79	Cu	Cuatro Amigos	25°52'30"	70°24'30"	Manto ox		ch, ca, hem, q, ze
80	Cu		25°52'00"	70°24'00"	Vein ox		ch, q, ca
81	Cu		25°53'20"	70°28'00"	Vein cp, ox		py, ca, lim, hem, q, ch
82	Cu		25°52'30"	70°12'50"	Vein cp, ox		py, ca, ch, lim
83	Cu		25°52'30"	70°03'30"	Vein ox		hem, ch, ep
84			25°54'15"	70°03'00"	Vein ox		mag
85	Fe		25°54'45"	70°32'34"	Vein Fe		op, q
86	Cu		25°55'15"	70°22'35"	Vein cc, ox		ca, hem
87	Cu		25°55'45"	70°22'00"	Vein cc, ox		ep, ch, ca, hem
88	Cu		25°55'46"	70°20'50"	Vein cc, ox		ca, ch, hem
89	Cu		25°56'30"	70°27'00"	Vein ox		lim, hem, ca
90	Cu		25°57'00"	70°25'28"	Vein ox		q, hem, ca
91	Cu		25°57'40"	70°13'40"	Vein ox		ca, py, hem, lim
92	Cu	Casqui- bana	25°57'55"	70°17'10"	Vein ox, cc		ca, ep
93	Fe		25°57'10"	70°07'30"	Vein mag		q, ap
94	Cu		25°52'45"	70°13'00"	Vein cp, ox		hem, lim
95	Cu		25°52'50"	70°13'00"	Vein ox		hem, lim
96	Cu		25°52'35"	70°13'00"	Vein cp, ox		hem, lim
97			25°53'00"	70°13'00"	Vein cp, ox		ca, ep
98	Cu		25°53'15"	70°13'00"	Vein cp, ox		hem, lim

Number*	Element**	Mine	Location		Form	Mineralogy***	Gangue****
			Lat. S	Long. W			
99	Cu		25°53'30"	70°13'00"	Veins	cp, ox	q, hem, lim
100	Cu		25°53'50"	70°13'00"	Vein	ox, cp	q, hem, lim
101	Cu		25°54'20"	70°13'00"	Vein	cp, ox	py, hem, lim
102	Fe		25°56'30"	70°07'45"	Vein	Fe, ox	sk, ap, q
103	Cu	Silvita	25°30'40"	70°18'20"	Irreg. body	ox, cp, bo	py, q, tl, lim
104	Cu	Maruja	25°32'00"	70°11'00"	Breccia miner. oc, cp		q, hem, ca
105	Cu Au	Union	25°36'00"	70°22'00"	Veins	ox, cc, bo, Au, Ag	hem, lim, ca
106	Cu	Humberto	25°36'45"	70°23'45"	Veins	ox	ca, hem
107	Cu	Vallenar- ina	25°36'30"	70°23'	Vein	ox	ca
108	Cu	Avion Norte	25°37'00"	70°23'30"	Vein	ox, cc	hem, ca
109	Cu	Avion Sur	25°37'15"	70°24'20"	Vein	ox	ca, q, hem
110	Cu		25°37'15"	70°24'20"	Vein	ox	ca, q, hem
111	Cu	Las Luces	25°41'45"	70°09'30"	Mantos Veins	CS, ox	ca, q, ch, ep, lim
112	Cu	Bandurrias	25°42'30"	70°20'30"	Shean zone Veins	ox	ca, q, hem, lim
113		Ronald	25°43'	70°20'	Vein	ox	ca, hem
114	Cu	Los Alfonsos Sta.	25°47'	70°25'	Veins	ox	ca, ep, q
115	Cu	Zulema	25°49'30"	70°26'30"	Vein	cp, ox	ca
116	Cu	Radoslava	25°50'	70°25'	Veins	ox	aq, ca, ep, hem
117	Cu	Los Pepes	25°51'	70°27'30"	Veins	ox, cp	q, ca, ep, hem
118	Cu	S. Antonio	25°57'	70°26'	Vein	ox	q, ca, ch, hem
119	Cu	Escondida	25°45'00"	70°09'30"	Vein	cp, ox	q, lim, ca, hem, py

Number*	Element**	Mine	Location		Form	Mineralogy***	Gangue****
			Lat. S	Long. W			
120	Cu		25°45'30"	70°25'30"	Manto	cp, ox	ca, ch
121	Cu		25°45'30"	70°22'30"	Manto	cc, ox	ca, ch, ep
122	Fe		25°46'10"	70°16'45"	Vein	ox, mag	q
123	Cu		25°46'00"	70°08'30"	Vein	ox	hem, ca, lim, sc
124	Cu		25°49'00"	70°00'45"	Irreg. body	ox	q, ca
125	Fe		25°50'45"	70°04'25"	mass- ive	mag	ep, q, ap
126			25°50'25"	70°22'50"	Manto	ox	hem, ch, ca, py
127			25°50'48"	70°29'00"	Vein	ox	ca, lim
128	Fe	Mateo	25°52'	70°06'	Veins	ak, hem, magn	q, ep
129	Mn	Soledad	25°56'	70°03'	Veins	psil, bran	hem, pied
130	Cu		25°30'30"	70°34'46"	Manto	cp, ox	py, lim, hem
131	Cu		25°35'50"	70°31'16"	Veins	ox	q, lim, hem
132	Cu		25°38'40"	70°31'20"	Vein	ox, cc	ca, ch
133	Cu	Corpus Christi	25°38'43"	70°31'20"	Vein	ox, bo	ca, ch
134	Cu		25°39'30"	70°31'50"	Manto	ox, bo, cc, cp	ca, ch
135	Cu	Llampera	25°41'45"	70°31'30"	Veins	ox, cp	py, q, ca, ch
136	Cu		25°42'30"	70°31'20"	Veins	ox, cp	ca, ch
137	Cu		25°42'50"	70°30'15"	Vein	ox, cc	ca, ch
138	Cu		25°41'20"	70°31'05"	Vein	ox, cp	q, ch
139	Au Cu		25°41'04"	70°35'30"	Vein	cp, Au	q, ca, py, lim
140	Cu		25°43'20"	70°30'15"	Vein	ox	ca, q
141	Cu		25°44'00"	70°31'41"	Vein	ox	ca, q
142	Pb		25°45'00"	70°34'45"	Vein	gn, sp	hm, q
143			25°45'40"	70°33'15"	Vein	mag	py, q
144	Pb		25°45'30"	70°33'45"	Vein	gn, sp	hm, q
145	Pb		25°46'15"	70°33'45"	Vein	gn, sp	q
146	Cu		25°46'50"	70°30'16"	Manto	ox, cc	ca
147	Cu		25°49'30"	70°29'35"	Vein	ox, cp	py, q, ca, lim

Number*	Element**	Mine	Location		Form	Mineralogy***	Gangue****
			Lat. S	Long. W			
148	Cu		25°50'00"	70°30'10"	Vein	ox, cp	py, ca
149	Cu		25°50'20"	70°34'30"	Veins	cp, ox, bo	py, ca, q, hem
150	Ag Au	Paula	25°51'25"	70°31'45"	Veins	Cu, Au, Ag	ep, q
151	Au	Carlota Vieja	25°51'40"	70°30'40"	Veins	Cu, Au	lim, q
152	Cu		25°52'00"	70°32'38"	Veins	ox	lim, q
153	Ag	Blanca Torres	25°52'15"	70°33'00"	Veins	Ag	
154	Co	Rigoberto	25°51'17"	70°30'00"	Veins	cp, ox, cv, saff, gersd nicc., brthp- skut, asp ramm	py, ca
155	Cu		25°52'30"	70°31'45"	Veins	cp, ox	lim, hem, ca
156	Cu		25°52'30"	70°30'17"	Veins	ox	q, ca
157	Cu		25°55'30"	70°32'15"	Veins	ox	lim, q
158	Cu	Clementina	25°33'40"	70°32'45"	Manto	ox, cp, cc	ca, q
159	Cu	Carñota	25°52'	70°30'15"	Vein	ox	ca, hem
160	Cu	Guanillos	25°55'15"	70°34'00"	Vein	cp, ox	hem, lim
161	Cu	S. Luis	25°42'	70°31'	Vein	ox	ca
162	Cu	Luzbel	25°32'	70°11'	Vein	ox	q, ca
163	Cu	Nueva Estrella	25°37'30"	70°29'30"	Veins	ox, cs	q, ca, ch, hem
164	Au	Flor	25°52'	70°32'	Veins	hem, py, an	b, ca, q, tl.
165	Cu	Esmeralda	25°51'	70°32'	Veins	py, cp, bo	q, lim, ba

**FIGURE 4.1** Distribution of mineral  
occurrences and mines.

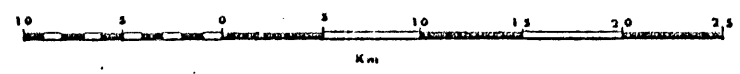
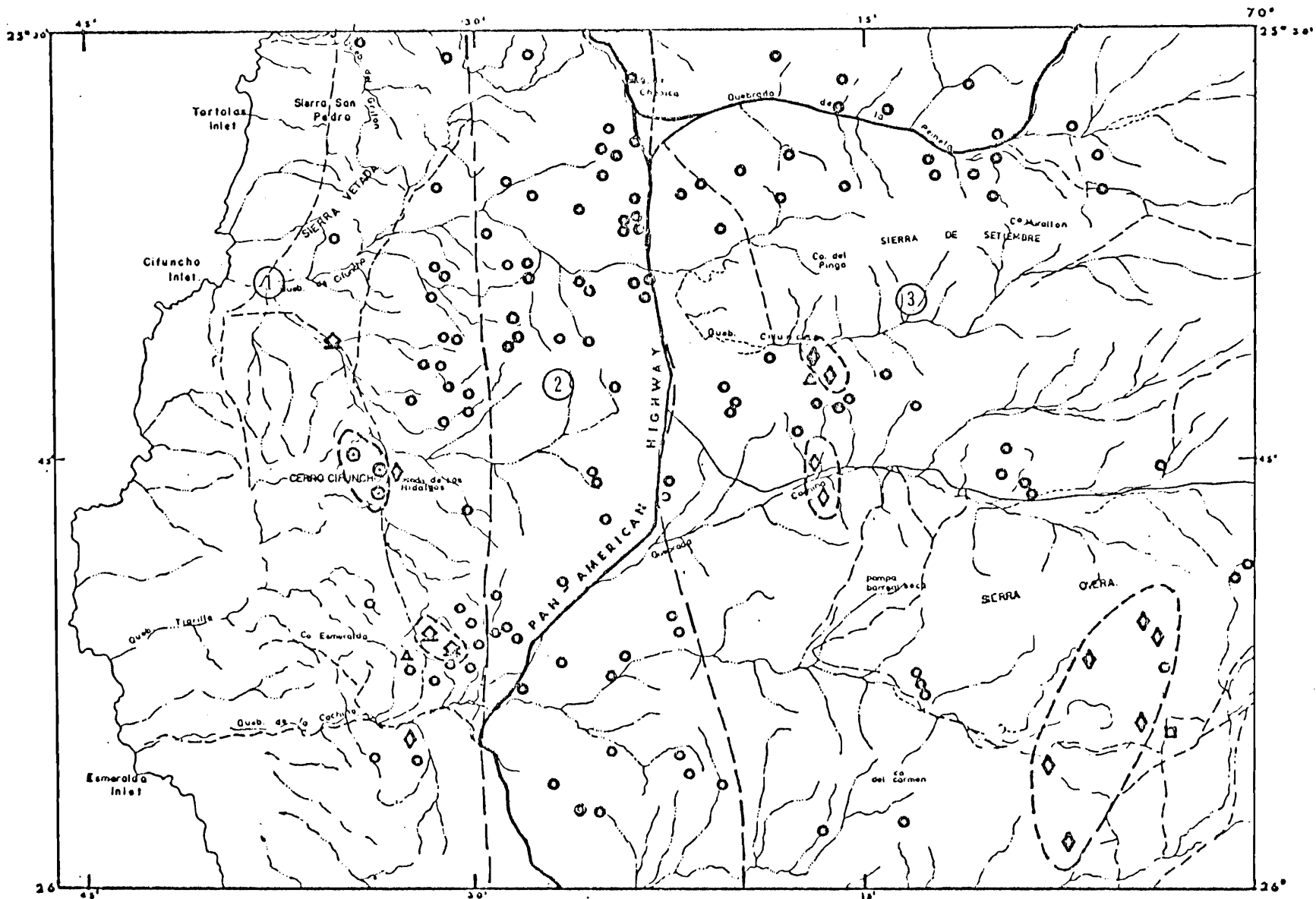


FIGURE 4.2 Distribution of mineral occurrences  
and mines; metallogenic subprovinces  
(in pocket).

○ Cu   ◇ Fe   △ Ag   □ Mn   ⬠ Au   ⊙ Pb-Zn

① Lower Jurassic      JURASSIC SUB-PROVINCE  
② Middle Jurassic

③ CRETACEOUS SUB-PROVINCE





It consists of small quartz veins with galena and sphalerite in metamorphic rocks of the Las Tortolas Formation and gold-quartz veins and pyrite in granitic rocks of Permian age (e.g. 142, 144, Figure 4.1). The mineralization is in the proximity of, and probably genetically associated with the Sierra Esmeralda Pluton north of Sierra del Pingo. Cu mineralization has been observed in quartzites and schists of Paleozoic Las Tortolas Formation and in Mesozoic granite. It consists in quartz veins mineralized with chalcopyrite, and copper oxides. The mineralization, despite being in Paleozoic host rocks, has the mineral association that is typically associated with the Lower Cretaceous magmatic activity (Cerro del Pingo Batholith).

#### Jurassic Metallogenic Subprovince (Figure 4.2)

No mineralization that can be ascribed to a Triassic, metallogenic epoch has been recognized in the area. However, a small number of significant ore deposits and mineral occurrences exist within and in the vicinity of the Sierra Esmeralda Pluton (Figure 2.3). One representative mining district is Sierra Esmeralda (Lat.  $25^{\circ}54'S$ ) (150, 151, 152, 153, 154, 165, 166, Figure 4.1), located north of La Cachina gully. Several small, copper, gold, silver and cobalt mines worked a series of veins in Lower Jurassic sediments and in the Sierra Esmeralda Pluton that has intruded them. The copper-cobalt ores at the Don Rigoberto mine (154, Figure 4.1) consist of chalcopyrite, cobaltian arsenopyrite and pyrite, accompanied by small amounts

of niccolite, safflorite-rammelsbergite, gersdorffite, breithauptite and skutterudite (Serrano and Ortiz, 1962). The Flor (152, 164, Figure 4.1) mine is a vein in quartz-monzonite and contains hematite, pyrite and gold. Chalcopyrite-specularite-calcite veins are abundant in the contact zone of the Sierra Esmeralda Pluton (K/Ar biotite age  $186 \pm 6$  Ma).

Andesites and volcanoclastic sediments of the Jurassic La Negra Formation contain several manto-type (i.e. a flat-lying, bedded deposit) and occasional vein-type mineralizations of bornite, chalcopyrite and chalcocite (e.g. 106, 107, 108, 109, 111, Figure 4.1). For example, at the Las Luces mine (111, Figure 4.1) flows of porphyritic andesite are mineralized in the form of irregular disseminations and in veins as well.

The manto-type deposits occur mainly in the upper vesicular or brecciated part of each individual flow. This type of deposit shows a great distribution along the coastal cordillera.

The genesis of this type of deposit elsewhere in Chile is a matter of discussion; they have been considered epigenetic (Ruiz and Ericksen, 1962), syngenetic and volcanic-exhalative (Stoll, 1965; Ruiz et al., 1965). Later Losert (1972) indicated that the copper mineralization post-dated the regional metamorphism (prehnite-pumpellyite facies) and would more probably be related to the porphyry dioritic plutons that intrude the volcanic formations.

West of Cerros Buena Esperanza there are a group of deposits localized along a fault separating the Posada Hidalgos Formation from the La Negra Formation (e.g. 135, 136, 137, 158, Figures 2.3 and 4.1). They have been intensively mined and at the present they are abandoned. For example, at the Clementina mine (158, Figure 4.1) the mineralization consists of chalcopyrite, bornite, pyrite and copper oxides contained in silicified limestone and sandstone. The mineralization is related with andesitic dykes intruding the Lower Jurassic formations and it is post-faulting.

#### Cretaceous Metallogenic Subprovince (Figure 4.2)

One of the most important metallogenic provinces corresponds to the Cerro del Pingo Batholith which is mineralized at the margins and in roof pendants. Numerous veins of copper, iron, silver, gold and apatite are emplaced within or in the surrounding rocks. Several deposits located along the Atacama Fault are related to this batholith (Figure 2.3).

Contact metasomatic iron deposits are present in the metamorphosed host rocks (andesites - Aeropuerto Formation) and in veins of the intrusive body (e.g. 93, 128, Figure 4.1). For example, at the Mateo mine (128, Figure 4.1) the mineralization consists of massive magnetite veins emplaced in the Cerro del Pingo Batholith. The intruded andesite rock has been transformed to a meta-andesite with abundant actinolite, scapolite, chlorite, hematite and disseminated magnetite. These deposits form a belt extending from Latitude  $30^{\circ}\text{S}$  to beyond the boundary of the study

area (farther north). Generally associated with the Fe mineralization, there are several parallel apatite veins ( $25^{\circ}54'15''\text{S}$  -  $70^{\circ}03'45''\text{W}$ ).

Numerous aeromagnetic anomalies were found close to the contact between intrusive rocks and andesites of the Aeropuerto Formation, member 2, which can be correlated with magnetite concentrations. The origin of the iron deposits has been much disputed. They have been considered a magmatic injection of magnetite-apatite-amphibole melt (Geijer, 1961, 1967), a hypothesis adopted by Park (1972) for the Circum-Pacific belt of deposits; or a contact-metamorphic (metasomatic) origin has been proposed (Ruiz, 1959; Flores, 1959; Ruiz *et al.*, 1965). Recently Bookstrom (1977) suggests that the magnetite ore deposition was hydrothermal and accompanied by actinolitization. Although there is probably evidence for the presence of melts, the discussion is not yet settled and is beyond the scope of this thesis. Together with the iron mineralization, numerous veins carry chalcopyrite, specularite and pyrite (e.g. 94, 95, 96, 97, 100, 101, Figure 4.1). They are located in the Cerro del Pingo Batholith close to the contact with andesites of member 1 of the Aeropuerto Formation.

South of the Taltal Airport, limestones of the Aeropuerto Formation (member 1) contain several veins mineralized with copper, gold and silver (Figure 2.3). For example, at the Union mine (105, Figure 4.1) the mineralization consists of chalcopyrite, bornite, chalcocite, pyrite, gold and silver. The wall

rock shows a slight disseminated mineralization. Gold and silver are in different proportions but when the gold content increases, the copper grade increases; when silver content increases, the copper content decreases.

A set of silver veins occur in andesites of the Aeropuerto Formation (member 1) close to the Islena Fault (Figure 2.3). For example, at the Islena mine (30, Figure 4.1) the quartz veins contain chalcopyrite, bornite, pyrite, gold and silver with quartz, calcite and hematite-actinolite as accessory minerals. The San Jose del Pingo mine (62, Figure 4.1) consists of veins mineralized with chalcopyrite, pyrite and silver minerals. It is located close to the contact between the Paleozoic metamorphic rocks and the Cerro del Pingo granodiorite Batholith.

Several barite vein deposits in the La Negra Formation and in the Aeropuerto Formation have been recognized. They are probably related to the hydrothermal activity during the Early Cretaceous.

Most of the deposits of this metallogenetic subprovince are located within or close to the contact aureoles between plutons and sedimentary and/or volcanic rocks. There is no doubt that the mineralization is related to the extensive magmatic activity of Cretaceous time.

The distribution of magmatogenic ore types described above, shows a rough metal zonation in the study area. From west to east, the zonation is characterized by subparallel belts of Ag,

Au (Cu, Pb, Zn), Cu; Cu (Au, Ag); Fe; Cu, Au (Fe); Figure 4.2, whose age appears to be oldest in the west (Lower Jurassic) and becomes progressively younger towards the east.

It is difficult to assess here the importance of the depth of erosion in the patterns of mineral distribution. All the plutons are probably epizonal, and in most localities the plutons still preserve some of their almost coeval volcanic cover. One cannot suggest that the older plutons are more deeply eroded than the younger ones; in fact, plutons affecting the thick Jurassic La Negra Formation are not unroofed, whereas the Cretaceous Cerro del Pingo Batholith, due to its tectonic position with respect to the Atacama Fault System, is more deeply eroded and deeper zones of the intrusion are exposed at the surface. However, the predominantly volcanic Cretaceous Aeropuerto Formation is better preserved in the east and in the vicinity of Altamira, the plutonic rocks exposed correspond to (very shallow?) porphyries.

The general zonation pattern which is ascribed to the Andes (e.g. Petersen, 1970; Sillitoe, 1972; 1976; Mitchell and Garson, 1972) is not clearly represented in the study area. Phenomena of supergene enrichment appear to be less important in the study area than further east, but it is clear that most ores show the effects of oxidation and weathering near the surface.

In summary, the author concludes that the mineralization in the Cifuncho-Cerro del Pingo area is genetically associated with

the plutonic rocks, and accordingly, the age of the ore deposits follows the same pattern of eastward younging displayed by the plutons. The zonation of metals can only be understood when considering the whole array of sedimentary, magmatic and tectonic processes that have affected this part of the continental margin.

### Geological Evolution

A summary of the geological evolution of the study area is presented in chart form in Figure 4.3. During the Paleozoic times a thick sequence of paralic (?) marine sediments of the Los Tortolas Formation were deposited. A Devonian plant fossil attests to the age. In post-Devonian times the rocks were deformed, accompanied by metamorphism of low (Abukurna-type) greenschist facies (Miller, 1972). At some time in the Early Permian, a post-tectonic granitoid batholith (Cifuncho Batholith) was intruded.

Uplift and erosion followed until the event possibly in Late Permian-Early Triassic times when rhyolites were extruded and conglomerates were deposited (red conglomerate unit). Later Triassic conglomerates and sandstones were deposited on a rather flat surface. In lowermost Jurassic, a marine transgression deposited limestone, shales, sandstone with a rich fauna of ammonites (Pan de Azucar Formation) defining the base of the Hettangian zone; and accumulation of up to 1000 m of marine sediments culminated in Late Sinemurian-Early Pliensbachian with some andesitic volcanism and instability (Posada Hidalgos

Formation). At this time the Sierra Esmeralda Pluton was intruded (Pliensbachian?). This magmatic phase is associated with Co, Au and Ag mineralization, and veins of Pb-Zn, although they occur locally in Paleozoic granitoids and metamorphic sediments are clearly related to this Lower Jurassic episode.

Major tilting and erosion ensued and in Bajocian times the accumulation of the volcanic La Negra Formation started. In Late Jurassic times (Portlandian?) dyke swarms affected the area. Copper mineralization is common in disseminations in vesicular tops of flows and in veins. At some time in Late Jurassic times, a major structural feature developed: the Atacama Fault. It seems that the western block went down and the eastern one went up at least 3000 m and possibly as much as 5000 m, exposing the crystalline basement. The Aeropuerto Formation deposited marine sediments directly onto Paleozoic metamorphic sediments.

At some time in the Early Cretaceous (Valanginian-Aptian) the huge multiphase Cretaceous batholith was intruded (Cerro del Pingo Batholith) followed by hydrothermal alteration related to the iron mineralization, which to some extent has been emplaced into branches of the Atacama Fault System.

Tertiary and younger rocks are well developed to the east, but outside the study area gravels and saline encrustations were developed in valleys and depressions. Tectonic movements have affected the Atacama Fault System during the Tertiary and even to the Holocene.



FIGURE 4.3 Stratigraphic column of the study area.  
(synoptic chart).

...	Sandstone
---	Shale
ooo	Conglomerate
III	Limestone
vv	Andesites
TT	Tuff
ΔΔ	Breccia
~	Quartzites



## CONCLUSIONS

Among the significant conclusions of this thesis are the following:

1. A pluton dated by the K/Ar method at  $186 \pm 6$  Ma intrudes fossiliferous Hettangian and Sinemurian (possibly Lowermost Pliensbachian) rocks, and is unconformably overlain by Bajocian rocks. This not only confirms the much disputed existence of an Early Jurassic magmatism at these latitudes, but also provides a useful constraint for the correlation between the stratigraphic and absolute time scales.
2. This work has demonstrated that the eastward migration of the magmatic front with time proposed by Farrar et al. (1970) for a transect of the Andes near Latitude  $27^{\circ}$ S, is also valid between  $25^{\circ}30'$  and  $26^{\circ}$ S.
3. Each of the above discrete volcano-plutonic cycles of Early Jurassic, Middle Jurassic and Early Cretaceous age has given rise to characteristic metallogenic sub-provinces which, accordingly, become younger from west to east.

4. This thesis has put forward evidence for a pre-Early Cretaceous displacement of the Atacama Fault Zone, a major longitudinal structure recognized along 900 km of the continental margin and that is probably active. Probably as much as 5000 m of Jurassic and Triassic strata were eroded from the uplifted eastern block of the fault, to enable an Early Cretaceous transgression to deposit sediments directly onto Paleozoic basement.
5. The Andean type of plate margin is usually referred to as "compressive"; however, little evidence of compression can be found in the Cifuncho-Cerro del Pingo area after the Paleozoic. Both the existence of Jurassic dyke swarms and block faulting in the area are more indicative of an extensional regime during Mesozoic times.

## REFERENCES

- Aguirre, L., Charrier, R., Davidson, J., Mpodozis, A., Rivano, S., Thiele, R., Tidy, E., Vergara, M. and Vicente, J.C. (1974). Andean magmatism: Its paleogeographic and structural setting in the central part ( $30^{\circ}$ - $35^{\circ}$ S) of the Southern Andes. *Pacific Geology* 8, 1-38.
- Aguirre, L., Levi, B., and Offler, R. (1978). Unconformities as mineralogical breaks in the burial metamorphism of the Andes. *Contrib. Mineral. Petrol.* 66, 361-366.
- Alvarez, O. (1967). Prospeccion del Yacimiento de hierro Mahuilque, Arauco. *Inst. Inv. Geol. Santiago, Resumenes Jornadas de Trabajo*, 42-44.
- Arabasz, W.J. (1970). Geological and geophysical studies of the Atacama fault zone in northern Chile. Ph.D. Diss., Calif. Inst. Technol.
- Aubouin, J., Borrello, A.V. (1970). Regard sur la geologie de la Cordillere des Andes: relais paleogeographiques et cycles orogeniques superposes; le nord argentin. *Bull. Soc. Geol. de France* (7), XII, 1970, No. 2, 246-260.
- Audebaud, E., Capdevila, R., Dalmayrac, B., Debelmas, J., Laubacher, G., Lefevre, C., Marocco, R., Martinez, C., Mattauer, M., Megard, J., Paredes, J. and Tomasi, P. (1973). Les traits geologiques essentials des Andes Centrales (Peru-Bolivie). *Rev. Geogr. Phys. Geol. Dyn.* 15, 73-114.
- Beckinsale, R.D. and Gale, N.H. (1969).  $^{40}\text{Ar}$  reappraisal of the decay constants and branching ratio of  $^{40}\text{K}$ . *Earth Planet. Sci. Lett.*, 6, 289.
- Bowes, W.A., Knowles, P.H., Serrano, M., Klohn, E., Moraga, A.A. and Gruenwald, R. (1966). Exploracion de Minerales Radioactivos en Chile. *Inst. Inv. Geologicas Chile, Bol.* 22.
- Brereton, N.R. (1970). Corrections for interfering isotopes in the  $^{40}\text{Ar}$ - $^{39}\text{Ar}$  dating method. *Earth Planet. Sci. Lett.* 8, 427-433.
- Brereton, N.R. (1972). A reappraisal of the  $^{40}\text{Ar}$ - $^{39}\text{Ar}$  stepwise degassing technique. *Geophys. J. R. astr. Soc.* 27, 449.
- Brüggen, J. (1950). *Fundamentos de la Geología de Chile*. Instituto Geográfico Militar, Santiago, 374 p.

- Bryner, L. (1969). Ore deposits of the Philippines - An introduction to their geology. *Econ. Geol.* 64, 644-666.
- Baksi, A.K., York, D., and Watkins, N.D. (1967). Age of the Steens Mountain geomagnetic polarity transition. *Jour. Geophys. Research*, 72, 6299-6308.
- Barazangi, M. and Isacks, B.L. (1976). Spatial distribution of earthquakes and subduction of the Nazca plate beneath South America. *Geology* 4, 686-692.
- Bilibin, Y.A. (1968). *Metallogenic Provinces and metallogenic Epochs*, translation. Queen's College Press, Flushing, New York.
- Bird, J.M. and Dewey, J.F. (1970). Lithosphere plate continental margin tectonics and the evolution of the Appalachian orogen. *Geol. Soc. Amer. Bull.* 81, 1031-1060.
- Bonatti, E. (1975). Metallogenesis at oceanic spreading centers. *Ann. Rev. Earth Planet. Sci.* 3, 401-431.
- Bookstrom, A.A. (1977). The magnetite deposits of El Romeral, Chile. *Econ. Geol.* 72, 1101-1130.
- Cecioni, G. (1960). La zona con *Psiloceras planorbis* en Chile. *U. Chile, Esc. Geol., Comunicaciones*, Año 1, No. 1, 19.
- Cecioni, G. (1970). Esquema de paleogeografía Chilena - 144 p. Edit. Universitaria, Santiago de Chile.
- Charrier, R. and Vicente, J.C. (1970). Liminary and geosynclinal Andes: Major orogenic phases and synchronical evolutions of the Central and Magellan Sectors of the Argentine-Chilean Andes. *Solid Earth Probl. Conf., Upper Mantle Project*, Buenos Aires, 2, 451-470.
- Charrier, R. (1973). Interruptions of spreading and the compressive tectonic phases of the Meridional Andes. *Earth Planet. Sci. Lett.* 20, 243-249.
- Chong, D.G. (1977). Contribution to the knowledge of the Domeyko Range in the Andes of Northern Chile. *Geol. Rundsch.* 66, 374-404.
- Clark, A.H., Farrar, E., Caelles, J.C., Haynes, S.J., Lortie, R.B., McBride, S.L., Quirt, G.S., Robertson, R.C.R. and Zentilli, M. (1976). Longitudinal variations in the metallogenic evolution of the Central Andes: A Progress Report. *Geol. Assoc. Canada, Spec. Pap.* 14, 25-58.

- Coleman, P.J. (1975). On island Arcs. *Earth Sci. Rev.* 11, 47-80.
- Coney, P. (1970). The tectonic cycle and the new global tectonics. *Geol. Soc. Amer. Bull.* 81, 739-748.
- Corvalán, J. (1960). Occurrence of the genus Psiloceras in Chile. Stanford Univ., unpubl. Ph.D. Thesis.
- Corvalán, J. (1965). Geología. IN Geografía Económica de Chile, CORFO, 35-82.
- Cox, A. (1973). Plate tectonics and geomagnetic reversals. W.H. Freeman and Co. (San Francisco) 702 pp.
- Cox, A. and Dalrymple, G.B. (1967). Statistical analysis of geomagnetic reversal data and the precision of potassium-argon dating. *Jour. Geophys. Research*, 72, No. 10, 2603-2614.
- Dalrymple, G.B. and Lanphere, M.A. (1971). Ar<sup>40</sup>-Ar<sup>39</sup> technique of K-Ar dating: a comparison with the conventional technique. *Earth Planet. Sci. Lett.* 12, 300-308.
- Dalrymple, G.B. and Lanphere, M.A. (1974). <sup>40</sup>Ar-<sup>39</sup>Ar age spectra of some undisturbed terrestrial samples. *Geochim. Cosmochim. Acta*, 38, 715-738.
- Darapsky, L. (1900). Das Departament Taltal (Chile). Seine Bodenbildung und Schatze, Berlin, 229 p.
- Dediós, P. (1967). Cuadrángulo Vicuña, Provincia de Coquimbo. IIG, Carta Geol. 16, 65 p.
- Dewey, J.F. (1969). Continental margins: a model for conversion of Atlantic-type to Andean-type. *Earth Planet. Sci. Lett.* 6, 189-197.
- Dewey, J.F. and Bird, J.M. (1970). Mountain belts and the new global tectonics. *J. Geophys. Res.*, 75, 2625-2647.
- Dickinson, W.R. (1971). Plate tectonic models of geosynclines. *Earth and Planet. Sci. Lett.* 10, 165-174.
- Dickinson, W.R. (1977). Tectono-stratigraphic evolution of subduction-controlled sedimentary assemblages. IN Island arc deep sea trenches and back-arc basins, p. 33-41, Talwani, M. and Pitman III, W.C. (ed.) *Amer. Geophys. Union.*

- Dietz, R.S. (1961). Continent and ocean basin evolution by spreading of the sea floor. *Nature*, 190, 854-857.
- Dietz, R.S. and Holden, J.C. (1966). Microgeosynclines in space and time. *J. Geol.* 74, 566-583.
- Engels, J.C. (1971). Effects of sample purity on discordant mineral ages found in K-Ar dating. *Jour. Geol.* 79, 609-615.
- Engels, J.C. (1972). Determination of purity of mineral separates used in K-Ar dating - an interpretative review. *Can. Miner.* 11, 743-759.
- Ewing, J. and Ewing, M. (1967). Sediment distribution on the mid-ocean ridges with respect to spreading of the sea floor. *Science* 156, 1590-1592.
- Farrar, E., Clark, A.H., Haynes, S.J., Quirt, G.S., Cohn, H., and Zentilli, M. (1970). K-Ar evidence for the post-Paleozoic migration of granitic intrusion foci in the Andes of northern Chile. *Earth Planet. Sci. Lett.* 9, 17-28.
- Faure, G. (1977). Principles of isotope geology (J. Wiley and Sons) 464 p.
- Fitch, J.G., Miller, J.A. and Mitchell, J.G. (1969). A new approach to radio-isotopic dating in orogenic belts. IN Time and Place in orogeny (editors P.E. Kent, G.E. Satterthwaite, and A.M. Spencer), pp. 157-195, Geol. Soc. London Spec. Publ. 3.
- Fleck, R.J., Sutter, J.F., and Elliot, D.H. (1977). Interpretation of discordant  $^{40}\text{Ar}$ - $^{39}\text{Ar}$  age-spectra of Mesozoic tholeiites from Antarctica. *Geochim. Cosmochim. Acta* 41, 15-32.
- Frutos, J. (1970). Ciclos tectónicos sucesivos y direcciones estructurales super-impuestas en los Andes del Norte Grande de Chile. *Solid Earth Probl. Conf.*, Buenos Aires, 473.
- Frutos, J. and Tobar, A. (1975). Evolution of the southwestern continental margin of South America. *Proc. Gondwana Symp.*, Canberra, Australia, 567-578.
- Fuenzalida, H. (1965). Clima. IN Geografía Economica de Chile, CORFO, Santiago, 99-155.
- Fullagar, P.D. (1971). Age and origin of plutonic intrusions in the Piedmont of the southeastern Appalachians. *Bull. Geol. Am.*, 82, 2845-2862.



- García, F. (1959). Informe geológico sobre viaje de reconocimiento a la parte norte de la provincia de Atacama y sur de la provincia de Antofagasta. IIG, unpub. report, 13.
- García, F. (1960). Notas geológicas sobre estratigrafía en la parte sur de la provincia de Antofagasta y norte de Atacama. IIG, unpub. report, 12.
- García, F. (1967). Geología del Norte Grande de Chile (1964), ENAP (ed.). Soc. Geol. Chile, Symposium Geosinclinal Andino 3, 138 pp.
- Garson, M.S. and Krs, M. (1976). Geophysical and geological evidence of the relationship of Red Sea transverse tectonics to ancient fractures. Geol. Soc. Amer. Bull. 87, 169-181.
- Garson, M.S. and Mitchell, A.H.G. (1977). Mineralization at destructive plate boundaries: a brief review. IN Volcanic Processes in ore genesis. Inst. Min. and Metall., Geol. Soc. London, 81-97.
- Gass, I.G., Smith, A.G. and Vine, F.J. (1975). Origin and emplacement of ophiolites. Geodynamics today, 54-64.
- Geijer, P. (1931). The iron ores of the Kiruna type. Sveriges Geologiska Undersokning, ser. C., Arhandlingar och uppsater, No. 367, Arsbok 24, No. 4.
- Geijer, P. (1960). The Kiruna iron ores, 21st. Inst. Geol. Congr. Guide Excursions A25-C20, 3-17.
- Geijer, P. (1967). Internal features of the apatite-bearing magnetite ores. Sveriges Geol. Undersokning, ser. C., NR 624, Arsbok 61, NRg, 32 pp.
- González-Bonorino, F. and Aguirre, L. (1970). Metamorphic facies series of the crystalline basement of Chile. Geol. Rundsch., 59, 979-994.
- Grasty, R.L. and Mitchell, J.G. (1966). Single sample potassium-argon ages using the omegatron. Earth Planet. Sci. Lett. 1, 121-122.
- Groeber, P. (1963). La Cordillera entre las latitudes 22°20' y 40° S. Bol. Acad. Nac. Cienc. (Cordoba), 43.
- Halpern, M. (1972). Geochronological evolution of southern South America. IN Simp. Intern. Sistemas Carbonifero e Permiano ma America do sul, Amm. Acad. Brasil Cienc (Suplemento) 44.

- Halpern, M. (1978). Geological significance of Rb-Sr isotopic data of northern Chile crystalline rocks of the Andean orogen between latitudes 23° and 27° south. *Bull. Geol. Soc. Am.*, 89, 522-532.
- Hanus, V. and Venek, J. (1978). Morphology of the Andean Wadati-Benioff zone, andesitic volcanism, and tectonic feature of the Nazca plate. *Tectonophysics*, 44, 65-77.
- Harper, C.T. (1970). Graphical solution to the problem of radiogenic argon-40 loss from metamorphic minerals. *Eclogae, Geol. Helv.* 63, 119-140.
- Harrington, J.J. (1961). Geology of parts of Antofagasta and Atacama Provinces, northern Chile. *Amer. Assoc. Petrol. Geol. Bull.*, 45, 169-197.
- Harris, P.M., Hollick, C.T. and Wright, R. (1967). Mineral separation for age determination. *Inst. Mining Met., Trans.*, 76, B181-B189.
- Hayatsu, A. and Carmichael, C.M. (1970). K-Ar isochron method and initial argon ratios. *Earth Planet. Sci. Lett.* 8, 71-76.
- Hayatsu, A. (1972). On the basic assumptions in K-Ar dating method. *Comm. Earth Sci. Geophys.* 3, 69-75.
- Hayatsu, A. and Carmichael, C.M. (1977). Removal of atmospheric argon contamination and the use and misuse of the K-Ar isochron method. *Can. Jour. Earth Sci.* 14, 337-345.
- Haynes, S.J. (1976). Relation of metallogeny to granitoid plutonism and the new global tectonics in the Atacama Province, Chile (Abstr.) *Int. Geol. Congr. Abstr.* 25, 3, 739.
- Heirtzler, J.R., Dickson, G.O., Herron, E.M., Pitman, W.C. III and LePichon, X. (1968). Marine magnetic anomalies, geomagnetic field reversals, and motions of the ocean floor and continents. *J. Geophys. Res.*, 73, 2119-2136.
- Hess, H.H. (1962). History of the ocean basins. *IN Petrological studies*, A.J.G. Engel, *et al.* (eds.). *Geol. Soc. Amer.*, 599-620.
- Hillebrandt, A.V. (1973). Neue Ergebnisse über den Jura in Chile und Argentinien.-Munster. *Forsch. Geol. Palaont.*, 31/32, 167-199.

- James, D.E. (1971). Plate tectonic model for the evolution of the Central Andes. *Geol. Soc. Amer. Bull.* 82, 3325-3346.
- James, D.E. (1973). The evolution of the Andes. *Sci. American* 229, No. 2, 60-69.
- James, D.E. (1978). Subduction of the Nazca plate beneath central Peru. *Geology*, 6, 174-178.
- Jensen, I.O. (1976). Geología de la cordillera de las nacientes del río Copiapo entre los 27°53' y 28°20' de latitud sur; provincia de Atacama, Chile. Thesis, Dep. Geol., Fac. Cien Fis. Mat. Univ. Chile.
- Kistler, R.W. (1974). Phanerozoic batholiths in western North America: a summary of some recent work on variations in time, space, chemistry and isotopic composition. *Ann. Rev. Earth. Plan. Sci.* 2, 404-418.
- Klohn, E. and Peebles, F. (1965). Geología y Yacimientos sedimentarios de manganeso entre los ríos ELQUI y HURTADO, prov. de Coquimbo, IIG Report.
- Knowles, P.H., Bowes, W.A., Serrano, M.C., Klohn, E., Gruenwald, R.S. (1959). U.S. Atomic Energy Comm., report RME-4535.
- Krummenacher, D. (1970). Isotopic composition of argon in modern surface volcanic rocks. *Earth Planet. Sci. Lett.* 8, 109-117.
- Krynine, P.D. (1943). Diastrophism and the evolution of sedimentary rocks. *Amer. Assoc. Petrol. Geol.*, (Distinguished Lecture Series).
- Kulm, L.D., Schweller, W.J. and Masias, A. (1977). A preliminary analysis of the subduction processes along the Andean continental margin, 6° to 45° S. p. 285-302. IN Island arcs, deep sea trenches and back-arc basins, Talwani, M. and Pitman, W.C. (eds.) Amer. Geophys. Union.
- Kutina, J. (1976). Relationship between the distribution of big endogenic ore deposits and the basement fracture pattern - examples from continents. *Proced. 1st. Intern. Conf. New Basement Tectonics*, Utah Geol. Assoc. Pub. 5, 565-593.
- Lanphere, M.A. and Reed, B.L. (1973). Timing of Mesozoic and Cenozoic plutonic events in circum-Pacific North America. *Bull. Geol. Soc. Am.* 84, 3773-3782.

- Lanphere, M.A. and Dalrymple, G.B. (1978). The use of  $^{40}\text{Ar}$ - $^{39}\text{Ar}$  data in evaluation of disturbed K-Ar systems. Geol. Survey open-file report 78-701.
- Levi, B., Mehech, S. and Munizaga, F. (1963). Edades radiométricas y petrografía de granitos Chilenos. IIG Bol. 12, 42 pp.
- Losert, J. (1972). Alterations and associated copper mineralizations in the Jurassic andesites of the Formacion La Negra in the area of Buena Esperanza Mine (Prov. Antof. N. Chile). Colloquium, Dept. Geol. Univ. Chile, 11 April.
- Mapa geológico de Chile (1968). Instituto de Investigaciones Geológicas, Scale 1:1,000,000.
- McBride, S.L., Caelles, J.C., Clark, A.H. and Farrar, E. (1976). Paleozoic radiometric age provinces in the Andean basement latitudes  $25^{\circ}$ - $30^{\circ}$  S. Earth Planet. Sci. Lett. 29, 373-383.
- McDougall, I., Polach, H.A., and Stipp, J.J. (1969). Excess radiogenic argon in young subaerial basalts from the Auckland volcanic field, New Zealand. Geochim. Cosmochim. Acta 33, 1484-1520.
- McNutt, R.H., Crockett, J.H., Clark, A.M., Caelles, J.C., Farrar, E., Haynes, S.J. and Zentilli, M. (1975). Initial  $\text{Sr}^{87}/\text{Sr}^{86}$  ratios of plutonic and volcanic rocks of the Central Andes between latitudes  $26^{\circ}$  and  $29^{\circ}$  S. Earth Planet. Sci. Lett. 27, 305-313.
- Mercado, E.M.W. (1977). Geología de la Cordillera de la costa entre Chanaral y Caldera 73 p. Santiago (Fac. Cien. Fis. Mat., Univ. Chile) Unpubl. Thesis.
- Merrihue, C.M. (1964). Trace-element determinations and potassium-argon dating by mass spectroscopy of neutron-irradiated samples. Trans. Amer. Geophys. Union 46, 125.
- Merrihue, C.M. and Turner, G. (1966). Potassium-argon dating by activation with fast neutrons. J. Geophys. Res. 71, 2852.
- Miller, H. (1970). Vergleichende Studieren an pramesozoischen Gesteinen Chiles unter besonderer Berücksichtigung ihrer Kleintektonik. Geotektonische Forschungen, Heft 36, II, 1-64.
- Miller, H. (1973). Neues zur Geologie von Chile. Zbl. Geol. Palaont. Teil I, 76-142.

- Mitchell, A.H. and Reading, H.G. (1969). Continental margin, geosynclines and ocean floor spreading. *J. Geol.*, 77, 629-646.
- Mitchell, A.H.G. and Bell, J.D. (1973). Island-arc evolution and related mineral deposits. *J. Geol.* 81, 381-405.
- Mitchell, A.H.G. and Garson, M.S. (1976). Mineralization at plate boundaries. *Minerals Sci. Engng.* 8, No. 2, 129-169.
- Mitchell, A.H.G. (1976). Tectonic settings for emplacement of subduction related magmas and associated mineral deposits. *Geol. Assoc. Can. Spec. Pap.* 14, 3-21.
- Mitchell, J.G. (1968). The  $^{40}\text{Ar}$ - $^{39}\text{Ar}$  method for potassium-argon age determination. *Geochim. Cosmochim. Acta* 32, 781-790.
- Muñoz, J. (1956). Chile. *IN* W.F. Jenks (ed.), Handbook of South America Geology. GSA Memoir 65, 187-214.
- Naranjo, S.J.A. (1978). Geología del Cuadrangulo las Bombas y Sector Septentrional del cuadrangulo EL SALADO, Region de Atacama. 117 p. Unpub. Thesis, Dept. de Geología, Fac. Cien. Fis. Mat., Univ. Chile.
- Nier, A.O. (1950). A redetermination of the relative abundances of the isotopes of carbon, nitrogen, oxygen, argon and potassium. *Phys. Rev.* 77, 789-793.
- Nikolaev, V.A. (1959). Some structural characteristics of mobile tectonic belts. *Intern. Geol. Rev.* 1, 50-64.
- Ortiz, F.J. (1960). Descripción litológica de la Formación Pan de Azúcar y de las rocas volcánicas subyacentes, Posada de los tres Hidalgos, Taltal. IIG, Unpubl. Report, 12 pp.
- Parrot, R.J.E. (1976).  $^{40}\text{Ar}$ - $^{39}\text{Ar}$  dating of the Labrador Sea volcanics and their relation to sea-floor spreading. M.Sc. thesis, Dalhousie University, Halifax (N.S.).
- Pitcher, W.S. (1974). The Mesozoic and Cenozoic batholiths of Peru. *Pac. Geol.* 8, 51-62.
- Pitcher, W.S. (1978). The anatomy of a batholith. *J. Geol. Soc. London*, 135, 157-182.
- Pitcher, W.S. and Bussell, M.A. (1977). Structural control of Batholith emplacement in Peru: a review. *J. Geol. Soc. London*, 133, 294-256.

- Pitman, W.C., Herron, E.M. and Heirtzler, J.R. (1968). Magnetic anomalies and sea-floor spreading. *J. Geophys. Res.* 73, 2069-2085.
- Quirt, G.S. (1972). A potassium-argon geochronological investigation of the Andean mobile belt of north-central Chile. Ph.D. thesis, Dept. of Geol. Sci., Queen's Univ., Kingston, Ontario.
- Reineck, H.E. and Singh, I.B. (1975). Depositional sedimentary environments. p. 253-263. Springer-Verlag, New York-Heidelberg-Berlin.
- Reutter, K.J. (1974). Entwicklung und Bauplan der Chilenischen Hochkordillere im Bereich 29° Sudlicher Breite. *N. Jb. Geol. Palaont. Abh.*, 146, 2, 153-178.
- Reynolds, P.H., Muecke, G.K. and Kublick, E.E. (1973). Potassium-argon dating of slates from the Meguma Group, Nova Scotia. *Can. J. Earth Sci.* 10, 7, 1059-1067.
- Ruiz, C. (1943). Los yacimientos de hierro de Copiapo. *Soc. Nac. Min. Bol. Minero*, No. 522, 820-887, No. 523, 906-915.
- Ruiz, C. and Ericksen, G.E. (1962). Metallogenetic provinces of Chile. *S. A. Econ. Geol.*, 57, 91-106.
- Ruiz, C., Corvalan, J., Klohn, E. and Levi, B. (1965). *Geologia y Yacimientos metaliferos de Chile*. IIG, 360 pp.
- Schweller, W.J. and Kulm, L.D. (1978). Extensional rupture of oceanic crust in the Chile trench. *Marine Geology* 28, 271-291.
- Segerstrom, K. (1959). Cuadrangulo Los Loros, Prov. de Atacama. IIG, Carta Geol. 1, 33 pp.
- Serrano, M. and Ortiz, F. (1962). Antecedentes geologicos sobre algunas minas del Dept. de Taltal. IIG, unpubl. report.
- Shafiqullah, M. and Damon, P.E. (1974). Evaluation of K-Ar isochron methods. *Geochim. Cosmochim. Acta*, 38, 1341-1358.
- Sigurgeirsson, T. (1962). Age dating of young basalts with the potassium-argon method. Physics Lab. Report, Univ. Iceland, p. 9.
- Sillitoe, R.H. (1972). Relation of metal provinces in western America to subduction of oceanic lithosphere. *Bull. Geol. Soc. Amer.*, 83, 813-818.

- Sillitoe, R.H. (1976). Andean mineralization: A model for the metallogeny of convergent plate margins. *Geol. Assoc. Can., Spec. Pap.*, 14, 59-100.
- St. Amand, P. and Allen, C.R. (1960). Strike-slip faulting in northern Chile (abstr.). *Geol. Soc. Amer. Bull.*, 71, 1965.
- Steiger, R.H. and Jaeger, E. (1977). Subcommittee on geochronology: Convention on the use of decay constants in geo- and cosmochronology. *Earth Planet. Sci. Lett.* 36, 359-362.
- Stewart, J.W., Evernden, T.F. and Snelling, N.J. (1974). Age determinations from Andean Peru: A reconnaissance survey. *Geol. Soc. Amer. Bull.* 85, 1107-1116.
- Stoll, W.C. (1965). Metallogenic provinces of South America. *Mining Mag.* 112, 22-33, 90-99.
- Strong, D.F. (1974). Plate tectonic setting of Newfoundland mineral deposits. *Geoscience Canada*, 1, No. 2, 20-30.
- Stukas, V. (1974).  $^{40}\text{Ar}$ - $^{39}\text{Ar}$  dating of the Long Range Dykes, Newfoundland. *Earth Planet. Sci. Lett.* 22, 256.
- Stukas, V. (1977). Plagioclase release patterns: a high resolution  $^{40}\text{Ar}$ - $^{39}\text{Ar}$  study. Ph.D. Thesis, Dalhousie Univ., Halifax (N.S.).
- Tobar, B.A. (1977). Stratigraphy and structure of the El Salvador-Potrerrillos Region, Atacama, Chile. Ph.D. Thesis, Grad. Div. Univ. Calif., Berkeley.
- Thayer, T.P. (1964). Principal features and origin of podiform chromite deposits and some observations on the Gulerman-Soriday district, Turkey. *Econ. Geol.* 59, 1497-1524.
- Thayer, T.P. (1969). Peridotite-gabbro complexes as keys to petrology of mid-oceanic ridges. *Geol. Soc. Amer.* 80, 1515-1522.
- Turner, G. (1968). The distribution of potassium and argon in chondrites. *IN* *Origin and Distribution of the elements* (ed. L.H. Alvens) 387-389, Pergamon.
- Turner, G. (1969). Thermal histories of meteorites by the  $\text{Ar}^{39}$ - $\text{Ar}^{40}$  method. *IN* *Meteorite Research* (ed. P.M. Millman) 407-417, D. Reidel.
- Turner, G. (1971).  $^{40}\text{Ar}$ - $^{39}\text{Ar}$  dating: the optimization of irradiation parameters. *Earth Planet. Sci. Lett.* 10, 227.

- Uyeda, S. (1978). The new view of the earth. W.H. Freeman and Co. (San Francisco), 217 pp.
- Vicente, J.C. (1975). Essai d'organisation paleogeographique et structurale du Paleozoique des Andes Meridionales. Geol. Rundsch. 64, 343-394.
- Vine, F.J. and Matthews, D.H. (1963). Magnetic anomalies over oceanic ridges. Nature 199, 947-949.
- Vine, F.J. (1966). Spreading of the ocean floor: new evidence. Science 154, 1405.
- Wetzell, W. (1927). Zur Erdgeschichte der mittleren Atacama. N. Jb. Min. Geol. Pal., Beil-Bd. 58, 511-520.
- White, D.E. (1968). Environments of generation of some base metal ore deposits. Econ. Geol. 63, 301-335.
- Wilson, J.T. (1965). A new class of faults and their bearing on continental drift. Nature 207, 343-347.
- Zagruzina, I.A. and Yakovleva, L.V. (1978). The main epochs of Mesozoic plutonism in the circum-Pacific Area. 4th Int. Conf. Geochron. Cosmochron., Isot, Geol. Geol. Survey Open-file report 78-701.
- Zeil, W. (1960). Zur geologie der Nordchilenischen Kordilleren. Geol. Rundsch. 50, 639-673.
- Zentilli, M. (1974). Geological evolution and metallogenetic relationships in the Andes of Northern Chile between 26° and 29° South. Ph.D. thesis, Queen's University, Kingston, Ontario, 394 pp.



## APPENDIX I

The K/Ar and  $^{40}\text{Ar}/^{39}\text{Ar}$  Method

## The Potassium-Argon Method of Age Determination

The potassium-argon technique has advantages over other methods such as the relatively low cost of the equipment required, compared with rubidium-strontium and uranium-lead methods, and its inherent simplicity. Potassium-argon dating methods are based upon the natural decay of the isotope  $^{40}\text{K}$  to  $^{40}\text{Ar}$ . The isotopic abundances of potassium and argon are compiled in Table 1. The branching nature of  $^{40}\text{K}$  decay is shown in Figure 1. Beckinsale and Gale (1969) have reviewed the decay of  $^{40}\text{K}$  and have urged the use of decay constants based on recent direct counting measurements. The IUGHS subcommission on Geochronology (1976) further recommended the adoption of a standard set of decay constants and isotopic abundances. The recommended values after Steiger and Jaeger (1977), which are relevant to the present study are given in Table 2.

### Assumptions and Limitations of the Method

In order that the potassium-argon equations give the time of formation of an igneous rock, the following assumptions must be satisfied (Hayatsu, 1972; Farn, 1977).

1. The rock unit cooled to argon retention temperatures ( $300^{\circ}\text{C}$  for micas) soon after crystallization.
2. The minerals selected for dating purposes have subsequently remained closed systems with respect to potassium and argon.

FIGURE 1 Decay scheme diagram for the branched decay of  $^{40}\text{K}$  to  $^{40}\text{Ar}$  by electron capture and by positron emission and to  $^{40}\text{Ca}$  by emission of negative beta particles.

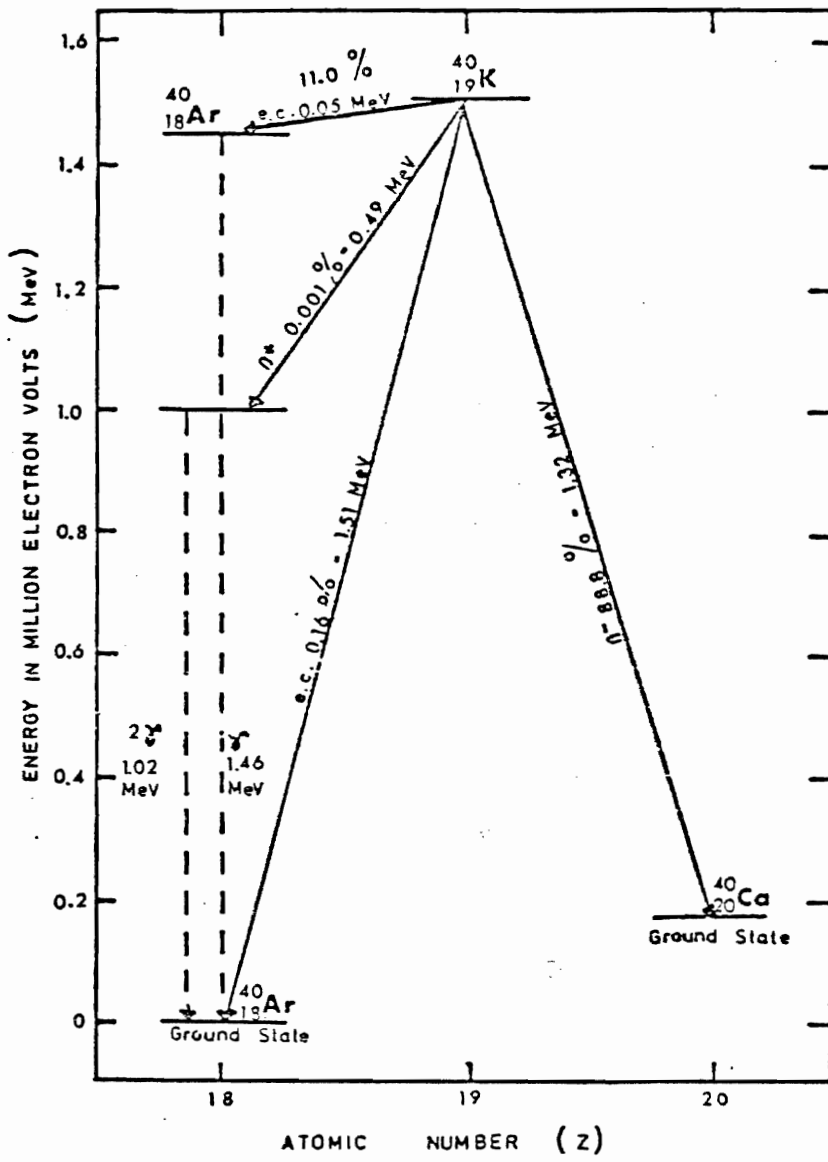


TABLE 1. Isotopic abundances of naturally occurring isotopes of argon and potassium.

ISOTOPE	ISOTOPE ABUNDANCE %
(1) Ar <sup>40</sup>	99.60
Ar <sup>38</sup>	0.063
Ar <sup>36</sup>	0.337
(2) K <sup>41</sup>	6.7302
K <sup>40</sup>	0.01167
K <sup>39</sup>	93.2581

(1) After Nier (1950);

(2) After Steiger and Jaeger (1977).

TABLE 2. The decays constants of K<sup>40</sup>.

PARAMETER	Beckinsale and Gale (1968)	Steiger and Jaeger (1977)
$\lambda\beta$	4.963 x 10 <sup>-10</sup> yr.	4.952 x 10 <sup>-10</sup> yr.
$\lambda e'$	0.5724 x 10 <sup>-10</sup> yr.	--
$\lambda e'$	8.778 x 10 <sup>-10</sup> yr.	--
$\lambda e + \lambda e'$	0.581 x 10 <sup>-10</sup> yr.	0.581 x 10 <sup>-10</sup> yr.

3. Non radiogenic argon in the samples has an isotopic composition identical to that of present-day atmospheric argon.
4. The decays constants of  $^{40}\text{K}$  are known accurately and have not been affected by the physical or chemical conditions of the environment in which the potassium has existed since it was incorporated into the rock.

Although many minerals contain detectable amounts of potassium, not one is totally retentive of argon and only a few retain argon sufficiently well to be used in potassium-argon geochronology.

#### The $^{40}\text{Ar}/^{39}\text{Ar}$ Method of Dating

The  $^{40}\text{Ar}/^{39}\text{Ar}$  method of age determination is based on the formation of  $^{39}\text{Ar}$  by the irradiation of K-bearing samples with fast neutrons in a nuclear reactor. Due to the irradiation some of the  $^{39}\text{K}$  atoms are transmuted to  $^{39}\text{Ar}$  atoms by an (n,p) reaction ( $\text{K}(n,p)\text{Ar}$ ) (Sigurgeirson, 1962; Merrihue, 1965; Grasty and Mitchell, 1966). The age of the sample is calculated from the  $^{40}\text{Ar}(\text{radiogenic})/^{39}\text{Ar}$  ratio.

If the sample is totally fused after irradiation (that is, all the argon is released in one step) then the total-gas age results. Alternatively, release of argon in a stepwise manner (by step-heating), results in a series of apparent ages for one sample (Turner, 1968; Fitch et al., 1969; Dalrymple and Lanphere, 1971, 1974, 1979; Brereton, 1972). Merrihue and Turner (1966) suggested the use of a mineral of known age as a fast neutron flux monitor. The  $^{40}\text{Ar}(\text{rad.})/^{39}\text{Ar}$  ratio of the

flux monitor is used in conjunction with the  $^{40}\text{Ar}$  radiogenic/ $^{39}\text{Ar}$  ratio of the unknown to obtain the age later.

This technique has been used widely for dating lunar rocks, meteorites, metamorphic, volcanic and plutonic rocks.

#### Experimental Procedures

The argon extraction system (Figure 2) is divided into three sections. The first section contains the extraction furnace, as internal resistance furnace with a tantalum ribbon heating coil. Gases released from the sample are collected in an activated charcoal cold trap. In the middle section on the line, a titanium getter along with a copper-copper oxide oxidizer remove the chemically active gases.

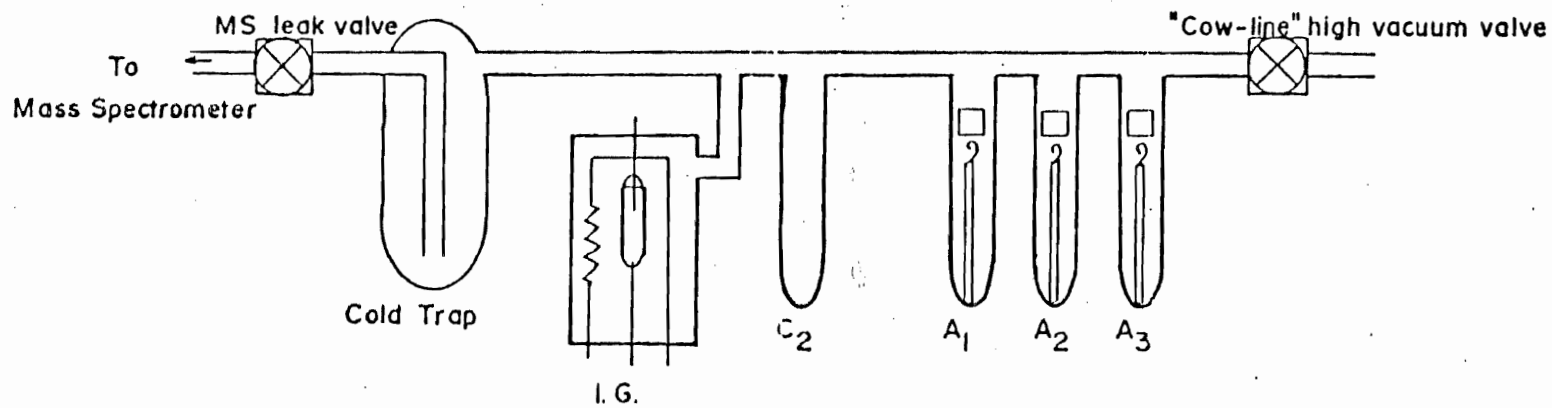
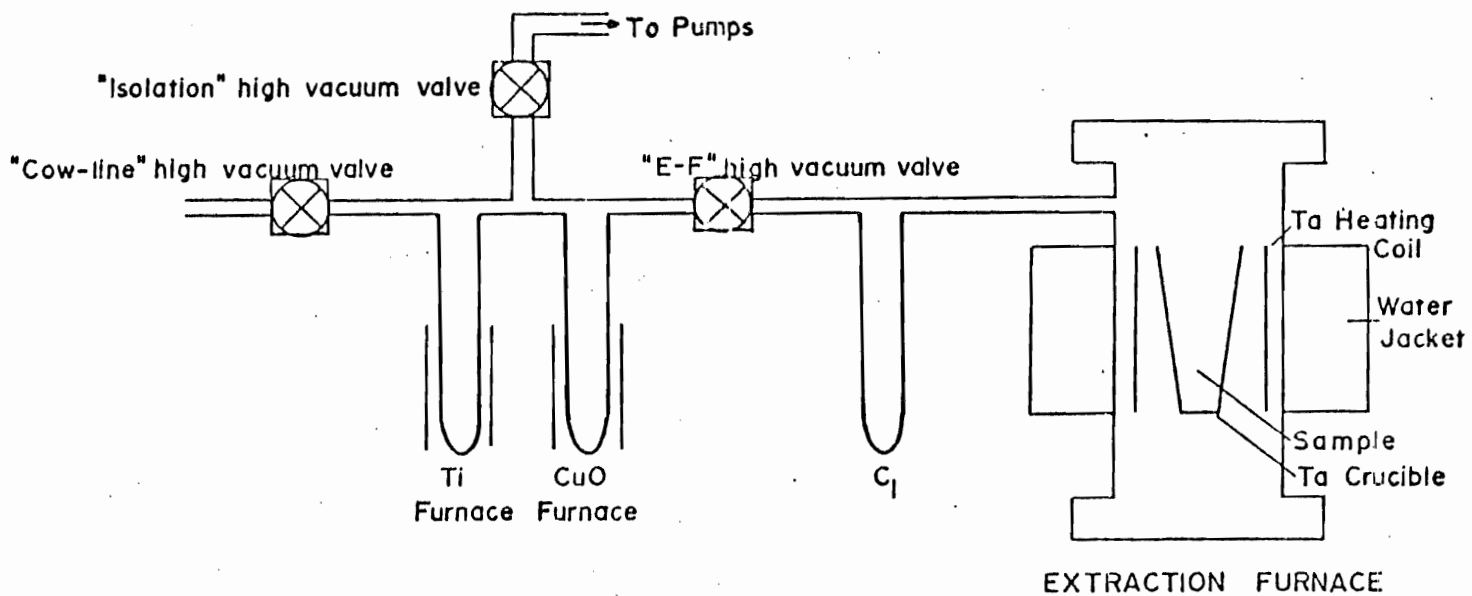
The third and last section serves as an inlet system to the mass spectrometer. A final purification of the argon is carried out here by means of a cold trap with liquid nitrogen.

The mass spectrometer, a substantially modified AEI MS10 is operated in the static mode. Samples were irradiated in the McMaster University reactor, with a total flux density of  $1.1\text{-}2.0 \times 10^{13} \text{ m cm}^{-2} \text{ sec}^{-1}$ ; the standard sample (i.e. the flux monitor) was a biotite mica No. 71-232 (Reynolds et al., 1973) which has an age of 366 ± 4 m.a. Detailed descriptions of the equipment and the irradiation requirements can be found in Stukas (1973, 1977) and Parrott (1976).

FIGURE 2 Schematic diagram of the argon extraction system.

$C_1, C_2$	Cold Fingers
$A_1, A_2, A_3$	Air Sample Tubes
I.G.	Iron Gauge





### Sample Preparation

The determination of the purity of separated minerals used for potassium and argon analyses may be critical to the interpretation of the ages obtained (Engels, 1972). Usually purity of at least 99% is attempted in mineral extraction in order to ensure sample homogeneity and the absence of unsuitable minerals.

In analysing a mineral or rock, the amounts of argon and potassium are measured on separated portions of the materials; for argon it is necessary to extract all the argon from the sample; argon loss during extraction and atmospheric contamination must be prevented.

Samples are fused in vacuo, thus releasing argon. Other volatiles contained in the specimen are also liberated, in order that only a pure inert gas mixture is admitted to the mass spectrometer.

### Mineral and whole rock separation

Rock samples containing mica or hornblende were broken with a splitter into cubes, were ground to pea-sized fragments in a jaw-crusher and then reduced to a workable mesh size by successive passes through a disc-mill grinder.

Usually for mica separation, size fractions of from 40 to 60 and 60 to 80 mesh were used. The portions were washed with water to remove dust adhering to the grains. When more than about 3% mica was present

in the sample, it could be poured off with the water and trapped in a sieve. For samples with less than 3% mica, or in the case of small samples, froth flotation was employed following the method of Harris et al. (1967). This approach also yielded a concentrate of 70-75% mica. Magnetite, very common and abundant mineral, was removed previously with a hand magnet. Following this, several passes through the Prantz isodynamic separator usually sufficed to give a separate of 90% purity or better.

Some samples containing feldspar and quartz grains with finely divided magnetite were further purified through a heavy liquid separation with acetylene tetrabromide (s.g. = 2.96 gr/cc). However, in order to get a concentrate of 99% mica, it was necessary to separate the finely hornblende grains from the biotite by hand-picking.

Hornblende preparation was carried out on sample fractions 60 to 80 mesh and 80-100 mesh. Smaller grain sizes were used to ensure purity. After the magnetite was removed with a hand magnet the fractions were passed through the magnetic separator in order to concentrate the pure hornblende. Acetylene tetrabromide was used to float unwanted quartz and feldspar grains. Small biotite grains were removed by hand-washing.

Whole rock samples were ground in the same way previously described and the fractions 40 to 60 mesh was retained for analyses.

After each step of preparation of each sample tending to get a mineral concentrate, the equipment was carefully cleaned. The concentrates produced by using heavy liquid were rinsed thoroughly in acetone and dried under a heat lamp.

#### The $^{40}\text{Ar}/^{39}\text{Ar}$ Method

In the  $^{40}\text{Ar}/^{39}\text{Ar}$  method a known fraction of the  $^{39}\text{K}$  in a rock or mineral sample is converted through an (n,p) reaction to  $^{39}\text{Ar}$  by irradiation with fast neutrons and the age is calculated from the ratio  $^{40}\text{Ar}/^{39}\text{Ar}$ . Because the  $^{40}\text{K}/^{39}\text{K}$  ratio is virtually constant, the measurement of the  $^{39}\text{Ar}$  content after irradiation provides an indirect measurement of the  $^{40}\text{K}$  content.

The method has two variations: the total fusion technique (conventional analysis), in which the sample is totally fused after irradiation and all the argon is analyzed in a single experiment. After correcting the  $^{40}\text{Ar}$  for any atmospheric Ar present the  $\text{Ar}^{40} \text{ rad.}/^{39}\text{Ar}$  ratio is equivalent to the  $^{40}\text{Ar} \text{ rad.}/^{40}\text{K}$  ratio and thus proportional to the age of the sample. The other technique is the incremental heating or age spectrum or step-heating technique, in which the argon is released by stepwise heating and which results in a series of apparent ages for one sample.

## 1. Total fusion technique.

When a rock is irradiated with thermal and fast neutrons, the production of isotopes of argon from a K-bearing sample is shown by the reaction  $^{39}\text{K} (n,p) ^{39}\text{Ar}$ . The  $^{39}\text{Ar}$  is unstable and decays to  $^{39}\text{K}$  by beta emission with a half-life of 269 years. The number of  $^{39}\text{Ar}$  atoms formed in the sample is

$$^{39}\text{Ar} = ^{39}\text{K} \Delta T \int \phi(\epsilon) \sigma(\epsilon) d\epsilon \quad (1)$$

where:  $^{39}\text{K}$  = number of atoms of this isotope in the sample.

$^{39}\text{Ar}$  = number of atoms produced by irradiation

T = length of the irradiation

$\phi(\epsilon)$  = neutron flux density at energy

$\sigma(\epsilon)$  = neutron capture cross section of  $^{39}\text{K}$  for neutrons having energy

The number of radiogenic  $^{40}\text{Ar}$  atoms present in the sample due to decay of  $^{40}\text{K}$  is:

$$^{40}\text{Ar} = \frac{\lambda_e}{\lambda} ^{40}\text{K} (e^{\lambda t} - 1) \quad (2)$$

where:  $\lambda_e$  = decay constant of  $^{40}\text{K}$

$\lambda$  = total decay constant of  $^{40}\text{K}$  ( $\lambda = \lambda_e + \lambda_\beta$ )

The ratio of  $^{40}\text{Ar}$  rad./ $^{39}\text{Ar}$  after irradiation is given by:

$$\frac{{}^{40}\text{Ar}^*}{{}^{39}\text{Ar}} = \frac{\lambda e}{\lambda} \frac{{}^{40}\text{K}}{{}^{39}\text{K}} \cdot \frac{1}{\Delta T} \left[ \frac{e^{\lambda t} - 1}{\phi(\epsilon) \sigma(\epsilon) d\epsilon} \right] \quad (3)$$

$$\text{let } J = \frac{\lambda}{\lambda e} \frac{{}^{40}\text{K}}{{}^{39}\text{K}} \cdot \frac{1}{\Delta T} \int \rho(\epsilon) \sigma(\epsilon) d(\epsilon) \quad (4)$$

then, the irradiation parameters, J, becomes:

$$J = \frac{e^{\lambda t} - 1}{{}^{40}\text{Ar}^*/{}^{39}\text{Ar}} \quad (5)$$

If a standard sample of known age,  $t_m$ , is irradiated along with an unknown of age t, then:

$$({}^{40}\text{Ar}^*/{}^{39}\text{Ar})_{\text{atm}} = ({}^{40}\text{Ar}^*/{}^{39}\text{Ar})_t \cdot \left( \frac{e^{\lambda t m} - 1}{e^{\lambda t} - 1} \right) \quad (6)$$

The  ${}^{40}\text{Ar}$  rad./ ${}^{39}\text{K}$  ratio of the unknown sample is used to calculate dates from:

$$t = \frac{1}{\lambda} \ln \left( \frac{{}^{40}\text{Ar}^*}{{}^{39}\text{Ar}} \cdot J + 1 \right) \quad (7)$$

A number of standard samples are irradiated together with the unknowns in a single sample holder, because the energy spectrum of neutron flux (H) to which a particular sample is exposed during the irradiation depends on its position in the sample holder. The J values are calculated using eq. (5) and are plotted as a function of position in the sample holder. Interpolation of the resulting graph from their known positions in the holder let to calculate the respective J values of the unknown samples.

The advantage of the  $^{40}\text{Ar}/^{39}\text{Ar}$  total fusion technique is that K and Ar rad. are measured on the same sample aliquot, thus eliminating possible sampling error. However, the accuracy of the technique is affected by any errors in monitoring the neutron flux.

## 2. The step-heating or incremental technique.

The principle of the method has been discussed in detail by Turner (1968, 1969), Fitch et al. (1969), Dalrymple and Lanphere (1971), Brereton (1972), and is identical to total fusion technique; the difference is that instead of melting the sample, and analysing all the released argon, the sample is heated in stages for fixed period of time and the released gas is analyzed at each stage. The process is repeated for increased temperature until the melting point is reached. Such an experiment gives a series of apparent K-Ar ages for a single sample.

If the sample has been closed to argon and potassium since the time of initial cooling, the ages calculated at each step should be constant. However, commonly some loss of  $^{40}\text{Ar}$  rad. has occurred by diffusion; in such a case the gas released at different temperatures may vary, and a spectrum of dates will then result.

### Correction Factors

In applying the  $^{40}\text{Ar}/^{39}\text{Ar}$  technique is necessary to correct for Ar isotopes produced or removed during irradiation by reactions other than the  $^{39}\text{K} (n,p) ^{39}\text{Ar}$  reaction.

### 1. The correction for atmospheric argon

The naturally occurring isotopes  $^{40}\text{Ar}$ ,  $^{38}\text{Ar}$  and  $^{36}\text{Ar}$  occur in the atmosphere in the relative proportions  $^{40}\text{Ar}/^{36}\text{Ar} = 295.5$ ,  $^{38}\text{Ar}/^{36}\text{Ar} = 0.187$  (Nier, 1950). The total amount of  $^{40}\text{Ar}$  present is either radiogenic or atmospheric. The amount of atmospheric argon is determined by monitoring  $^{36}\text{Ar}$  which is assumed to be only atmospheric in origin. Thus

$$^{40}\text{Ar}^*/^{39}\text{Ar} = ^{40}\text{Ar}/^{39}\text{Ar} - 295.5 \quad ^{30}\text{Ar}/^{39}\text{Ar} \quad (8)$$

### 2. Neutron interactions

Argon isotopes are also produced by several interfering reactions caused by interaction of neutrons with the isotopes of calcium, potassium and chlorine in the sample.

Detailed discussions of the corrections have been given by Mitchell (1968), Brereton (1970), Turner (1971) and Dalrymple and Lanphere (1971).

The main interfering reactions are those involving the isotopes of calcium (Table A.4). Calcium derived  $^{36}\text{Ar}$  ( $^{36}\text{Ar}_{\text{NCa}}$ ) and  $^{39}\text{Ar}$  ( $^{39}\text{Ar}_{\text{NCa}}$ ), potassium derived  $^{40}\text{Ar}$  ( $^{40}\text{Ar}_{\text{NK}}$ ); chlorine derived  $^{38}\text{Ar}$ .

In order to correct for interference effects it is assumed that all  $^{37}\text{Ar}$  is derived from calcium. The  $^{37}\text{Ar}$  produced from potassium is small.

The measured volumes of  $^{36}\text{Ar}$ ,  $^{37}\text{Ar}$ ,  $^{38}\text{Ar}$ ,  $^{39}\text{Ar}$  and  $^{40}\text{Ar}$ , after the irradiation can be written:



$$\begin{aligned}
 {}^{40}\text{Ar} &= {}^{40}\text{Ar}_{\text{atm}} + {}^{40}\text{Ar}^* + {}^{40}\text{Ar}_{\text{NK}} + {}^{40}\text{Ar}_{\text{NCa}} - {}^{40}\text{Ar}_{\text{RR}} \\
 {}^{39}\text{Ar} &= {}^{39}\text{Ar}_{\text{NK}} + {}^{39}\text{Ar}_{\text{NCa}} \\
 {}^{38}\text{Ar} &= {}^{38}\text{Ar}_{\text{at}} + {}^{38}\text{Ar}_{\text{NK}} + {}^{38}\text{Ar}_{\text{NCa}} - {}^{38}\text{Ar}_{\text{RR}} \\
 {}^{37}\text{Ar} &= {}^{37}\text{Ar}_{\text{NCa}} \\
 {}^{36}\text{Ar} &= {}^{36}\text{Ar}_{\text{at}} + {}^{36}\text{Ar}_{\text{NCa}} - {}^{36}\text{Ar}_{\text{RR}}
 \end{aligned} \tag{9}$$

where the superscripts denote the components of the measured volumes:

At = atmospheric

NCa = neutron induced from calcium

NK = neutron induced from potassium

RR = removed by neutron reaction.

\* = radiogenic

Substituting the values for Ca and K at zero age and forming the ratios calculate the correction  
factors required (see Brereton, 1972 for detailed explanation).

The expression for  ${}^{40}\text{Ar}^*/{}^{39}\text{Ar}_{\text{NK}}$  is written:

$$\frac{{}^{40}\text{Ar}_{\text{K}}}{{}^{39}\text{Ar}_{\text{NK}}} = \frac{{}^{40}\text{Ar}/{}^{39}\text{Ar} - {}^{36}\text{Ar}/{}^{39}\text{Ar} \cdot {}^{40}\text{Ar}_{\text{atm}}/{}^{36}\text{Ar}_{\text{atm}} + {}^{37}\text{Ar}/{}^{39}\text{Ar} \cdot \text{fe}^{\lambda t} (bx + ac) - c}{1 - \frac{{}^{37}\text{Ar}}{39}\text{Ar} \cdot \text{fe}^{\lambda t} \cdot a}$$

where:

$$\begin{aligned}
 a &= \frac{{}^{39}\text{Ar}_{\text{NCa}}}{{}^{37}\text{Ar}_{\text{NCa}}} \\
 b &= \frac{{}^{36}\text{Ar}_{\text{NCa}}}{{}^{37}\text{Ar}_{\text{NCa}}}
 \end{aligned}$$

$$c = \frac{{}^{40}\text{Ar}_{\text{NK}}}{{}^{39}\text{Ar}_{\text{NK}}}$$

$$\lambda = \frac{\ln Z}{35.1} \text{ days}^{-1}$$

t = time interval between irradiation and isotopic analysis of the sample

$$f = \lambda \Delta t (1 - e^{-\lambda \Delta t})^{-1}$$

$\Delta t$  = duration of irradiation.

For samples that are old and have high K/Ca ratios, Dalrymple and Lanphere (1971) developed a more general expression:

$$F = \frac{A - C_1 B + C_1 C_2 D - C_3}{1 - C_4 D}$$

where:

$$F = {}^{40}\text{Ar}^*/{}^{39}\text{Ar}$$

A = measured value of  ${}^{40}\text{Ar}/{}^{39}\text{Ar}$  ratio

B = measured value of  ${}^{36}\text{Ar}/{}^{39}\text{Ar}$  ratio

$C_1$  =  ${}^{40}\text{Ar}/{}^{36}\text{Ar}$  ratio in the atmosphere (= 295.5)

$C_2$  =  ${}^{36}\text{Ar}/{}^{37}\text{Ar}$  ratio produced by interfering reactions with Ca (=  $2.72 \pm 0.014 \times 10^{-4}$ )

$C_3$  =  ${}^{40}\text{Ar}/{}^{39}\text{Ar}$  produced by interfering reactions with K (0.0059  $\pm$  0.00042)

$C_4$  =  ${}^{39}\text{Ar}/{}^{37}\text{Ar}$  ratio produced by interfering reactions Ca (=  $6.33 \pm 0.043 \times 10^{-4}$ )

D =  ${}^{37}\text{Ar}/{}^{39}\text{Ar}$  ratio in the sample after correcting for decay of  ${}^{37}\text{Ar}$ .

## Precision of age calculations

Systematic methods for estimating the analytical precision of conventional K-Ar ages have been developed (Cox and Dalrymple, 1967; Baksi et al., 1967; Dalrymple and Lanphere, 1971). The estimated analytical error in K-Ar ages obtained by the  $^{40}\text{Ar}/^{39}\text{Ar}$  technique that takes into account the errors by the different interfering isotopes correction is obtained from the following expression (Dalrymple and Lanphere, 1971):

$$\sigma_t = \left[ \frac{J^2 F^2 (\sigma_F^2 + \sigma_J^2)}{J^2 (1 + FJ)^2} \right]^{1/2}$$

where  $F = \frac{^{40}\text{Ar}^*_{\text{rad.}}}{^{39}\text{Ar}}$

$\sigma_F^2$  and  $\frac{\sigma_J^2}{J}$  are the variances of F and J, respectively, expressed in percent

t = age of the sample

$\lambda$  = total decay constant of  $^{40}\text{K}$

The precision of an individual K-Ar age determination is estimated by the quadratic summation of the uncertainties associated with the measurement of  $^{40}\text{Ar}$  rad., the  $^{38}\text{Ar}$  spike calibration and the potassium determination.

The error associated with measuring the  $^{40}\text{Ar}$  rad./ $^{39}\text{Ar}$  ratio is given by (Dalrymple and Lanphere, 1971):

$$\sigma_F^2 = A^2 \sigma_Z^2 + C_1^2 B^2 \sigma_B^2 + [C_4 A - C_1 C_4 B + C_1 C_2] \Delta D$$

where  $F = \frac{^{40}\text{Ar}^* \text{ rad.}}{^{39}\text{Ar}}$  ratio and  $B, C_1, C_2, C_4, D$  are estimated coefficients of variations of the isotope ratios.

### The Isochron Technique

The Rb-Sr isochron method (Faure and Powell, 1972) was derived to measure the  $^{87}\text{Sr}/^{86}\text{Sr}$  ratio of the non-radiogenic strontium component; by analogy, this technique has been applied to K-Ar data to evaluate excess radiogenic argon or argon loss in a suite of cogenetic rocks (McDougall et al., 1969; Hayatsu and Charnichael, 1970, 1977).

An isochron plot is obtained for a suite of samples by plotting the radioactive parent as the independent coordinate vs the radiogenic daughter as the dependent coordinate.

Several types of isochron are commonly used, among them:

1. The  $^{40}\text{Ar}/^{36}\text{Ar}$  vs  $^{39}\text{Ar}/^{36}\text{Ar}$  isochron.

Basically the method consists of converting a measured fraction of  $^{39}\text{K}$  in a sample to  $^{39}\text{Ar}$  by fast neutron irradiation. The age is a function of the  $^{40}\text{Ar}/^{39}\text{Ar}$  ratio, corrected for atmospheric and neutron generated argon isotopes.

The method was described by Merrihue and Turner (1966), Brereton (1972), Dalrymple and Lanphere (1974), Fleck et al. (1977), Dalrymple and Lanphere (1978). Briefly, in the plots  $^{40}\text{Ar}/^{36}\text{Ar}$  is the ordinate and  $^{39}\text{Ar}/^{36}\text{Ar}$  is the abscissa, for the individual steps of a

stepwise heating or total fussion. Ideally, for an undisturbed system, the data points lie on a straight line, the slope of which is proportional to the age of the sample.

The advantage of this method is that no correction for or assumption about the isotopic composition of atmospheric argon need be made.

## 2. The $^{40}\text{Ar}/^{36}\text{Ar}$ vs $^{40}\text{K}/^{36}\text{Ar}$ isochron

It is based in the same principle as the Rb-Sr isochron (McDougall et al., 1969) and it is plotted  $^{40}\text{Ar}/^{36}\text{Ar}$  (measured) as the ordinate and  $^{40}\text{K}/^{36}\text{Ar}$  (measured) as the abscissa. The slope of the isochron line is proportional to the age and the intercept on the  $^{40}\text{Ar}/^{36}\text{Ar}$  axis gives the extraneous ratio of the suite of samples. In an ideal case, the value of the interception is 295.5, the atmospheric ratio.

The isochron equation is (Shafigullah and Damon, 1974):

$$^{40}\text{Ar}_m / ^{36}\text{Ar}_m = ^{40}\text{K}_m \frac{\lambda e}{\lambda} (e^{\lambda t} - 1) / ^{36}\text{Ar}_m + ^{40}\text{Ar}_a / ^{36}\text{Ar}_m + ^{40}\text{Ar}_e / ^{36}\text{Ar}_m - ^{40}\text{Ar}_d / ^{36}\text{Ar}_m$$

where:

$^{40}\text{Ar}_m$  and  $^{40}\text{K}_m$  = measured argon 40 and measured K-40

$^{40}\text{Ar}_d$  = Ar-40 lost by diffusion

$^{40}\text{Ar}_e$  = extraneous Ar-40, except the atmospheric component

$^{40}\text{Ar}_a$  = atmospheric Ar-40

The isochron is valid only if (op. cit.):

- a. -  $^{40}\text{Ar}_e / ^{36}\text{Ar}_m - ^{40}\text{Ar}_d / ^{36}\text{Ar}_m = 0$   
 b. -  $^{40}\text{Ar}_a / ^{35}\text{Ar}_m + ^{40}\text{Ar}_e / ^{36}\text{Ar}_m - ^{40}\text{Ar}_d / ^{36}\text{Ar}_m = \text{a constant}$

The amount and composition of the non-radiogenic Ar-40 component is seldom constant for a suite of coeval samples (Shafigullah and Damon, 1974). Biotite usually contains more atmospheric argon than cogenetic sanidine and hornblende.

### 3. $^{40}\text{Ar}$ vs $^{40}\text{K}$ isochron

It is a plot of apparent radiogenic  $^{40}\text{Ar}$  content against  $^{40}\text{K}$  content. In the ideal case, the isochron is a straight line through the origin. The slope is proportional to the age, the time of closure of the system.

The isochron is represented by the equation (Harper, 1970)

$$(^{40}\text{Ar}_m - ^{40}\text{Ar}_a) = ^{40}\text{Ar}_0 + \frac{\lambda e}{\lambda} ^{40}\text{K} (e^{\lambda t} - 1)$$

The age calculated depends on the  $^{40}\text{Ar}_0$  value; positive means excess of argon in the sample, negative the sample lost argon and if it is constant from sample to sample, the isochron age dates a geological event (Shafigullah and Damon, 1974).

APPENDIX II  
The Geological Time Scale  
Used in this Thesis

## The Geological Time Scale\*

ERA	PERIOD	EPOCH	AGE	AGE IN MILLIONS OF YEARS		
				1	2	3
Cenozoic				65	64	64-65
Mesozoic	Cretaceous	Late				
			Turonian	94	-	89-90
			Cenomanian	100	102	94
		Early	Albian	106		
			Aptian	112		
			Barremian	118		
			Hauterivian	124		
			Valanginian	130		
			Berriasian	136	140	
	Jurassic	Malm	Portlandian	146		
		(Late)	Kimmeridgian	151		
			Oxfordian	157		
		Dogger	Callovian	162		
		(Middle)	Bathonian	167		
			Bajocian	172		
			Aalenian	-	-	-
		Lias	Toarcian	178		
		(Early)	Pliensbachian	183		
			Sinemurian	188		
			Hettangian	190-195	208	
	Triassic	Late		205?		
		Middle		215?		
		Early		225	7242	
Paleozoic	Permian	Late		240		
		Early		280	284	
	Carboni-ferous	Late		325	335	
		Early		345	360	
	Devonian	Late		359		
		Middle		370		
		Early				

\*After Faure, G. (1977)

1. Harland et al. (1964) in Faure (1977).
2. Armstrong and McDowal (1974) in Faure (1977).
3. Obradovich and Cobban (1975) in Faure (1977).